

## 10. SITE 751<sup>1</sup>

### Shipboard Scientific Party<sup>2</sup>

#### HOLE 751A

**Date occupied:** 18 April 1988  
**Date departed:** 19 April 1988  
**Time on hole:** 1 day, 3 hr, 30 min  
**Position:** 57°43.56'S, 79°48.89'E,  
**Bottom felt (rig floor; m, drill pipe measurement):** 1644.30  
**Distance between rig floor and sea level (m):** 10.50  
**Water depth (drill pipe measurement from sea level, m):** 1633.80  
**Total depth (rig floor; m):** 1810.50  
**Penetration (m):** 166.20  
**Number of cores (including cores with no recovery):** 18  
**Total length of cored section (m):** 166.20  
**Total core recovered (m):** 162.92  
**Core recovery (%):** 98  
**Oldest sediment cored:**  
Depth (mbsf): 166.20  
Nature: nannofossil ooze with diatoms  
Age: early Miocene  
Velocity (km/s): 1.563

**Principal results:** Site 751 (proposed Site SKP-2C) is located in the central part of the Raggatt Basin on the Southern Kerguelen Plateau (57°43.56'S, 79°48.89'E; water depth, 1633.8 m) and was intended to recover a high-resolution Neogene and Paleogene stratigraphic section deposited above the calcium carbonate compensation depth and well south of the present-day Polar Front, which lies 900 km to the north.

Site 751 is a key component of a latitudinal paleoceanographic transect across the plateau. The *Marion Dufresne* MCS line MD47-05 shows a thick sedimentary cover of at least 2500 m at this locality. Due to time constraints imposed by an unexpected mid-cruise round-trip between the Kerguelen Plateau and Fremantle, Australia, drilling at Site 751 was limited to the Neogene objective, which comprises a seismic sequence of 0.24 s two-way traveltime (TWT).

A 166.2-m section of upper Pleistocene through middle lower Miocene mixed biosiliceous and calcareous ooze was cored with the advanced hydraulic piston corer (APC) with 98% recovery. An unusual finding was an exceptionally young (early Pliocene age) porcellanite bed encountered in Core 120-751A-2H. Operations in high seas ended when the APC piston rod failed during pullout, leaving the core barrel and the last core stuck in the hole.

The following lithologic units were recognized at Site 751:

Unit I (0–40.1 mbsf): upper Pleistocene (>0.2 Ma) to lower Pliocene diatom ooze with minor ice-rafted debris, foraminifers, volcanic ash, and porcellanite.

The carbonate content ranges from 0% to 70%, whereas foraminifers range from ~3%–25% near the top to rare near the bottom of the unit. Ice-rafted debris is scattered in minor abundance throughout the unit, mostly as sand-size specks. The predominantly milky-

white porcellanite, disturbed by drilling, fills the top 44 cm of Core 120-751-3H and contains some burrowlike casts. Two vitric ash layers are present in the lower Pliocene sediments.

Unit II (40.1–166.2 mbsf): upper Miocene to lower Miocene diatom nannofossil ooze.

Although nannofossils predominate, diatoms occur in equal or greater abundance in many intervals; foraminifers, radiolarians, and silicoflagellates are rare or appear in trace amounts. Faint green centimeter-scale laminae enriched in diatoms occur between 88 and 104 mbsf.

The lower Pliocene through lower Miocene represents an expanded section with sedimentation rates from 15 to 20 m/m.y., whereas much lower rates of ~3 m/m.y. characterize the abbreviated upper Pliocene–Pleistocene section. We were able to detect as many as four hiatuses. The most extensive of these was correlated across the Raggatt Basin and spans the interval from ~12.5 to 16 Ma in the middle Miocene. A second represents ~3.5 m.y. between 9.5 and 6 Ma in the late Miocene. A third short hiatus represents ~0.4 m.y. between 4.8 and 5.2 Ma, whereas a fourth spans an interval of ~0.3 m.y. between 1.9 and 2.2 Ma in the late Pliocene. Magnetostratigraphic data are of mixed quality, but key polarity reversals are identified in the early Pliocene to late Miocene (Anomaly Correlatives 3, 3A, 4, and 5) and early Miocene (Anomaly Correlatives 5C through 6).

High biogenic silica contents in lithologic Unit I yielded low bulk densities and high porosity values relative to Unit II. Compressional wave velocity values, however, were generally higher above 45 mbsf than below this level in the nannofossil ooze (1560 m/s above vs. 1505 m/s below). The corresponding seismic data do not indicate a correlation of lithologic subdivisions or identified hiatuses with specific reflectors. From the compressional wave velocity measurements, however, we anticipated that the first reflector at 0.24 s TWT would lay just below the bottom of the hole at about 185 m and would correspond to the Oligocene/Miocene contact. If so, sedimentation rates would then suggest that a disconformity could be expected at this point.

The relatively high carbonate contents and high sedimentation rates for the Miocene at this site, plus the co-occurrence of siliceous and calcareous microfossil groups, is unique for these high southern latitudes and will make this and other Leg 120 sites on the Kerguelen Plateau important reference sections for stable isotope and biomagnetostratigraphic studies. Changing microfossil assemblage compositions within each group indicate repeated fluctuations of major water mass properties over the site and should provide important paleobiogeographic and paleoceanographic records for this region. The most striking feature of this record is the rapid meter-scale alternations in microfossil assemblage characteristics and in physical and sedimentologic properties, which indicate that this site may be capturing some of the high-frequency paleoclimatic variability observed in other parts of the world ocean.

#### BACKGROUND AND OBJECTIVES

The Kerguelen Plateau extends between 46°S and 64°S and can be divided into two distinct domains: the Kerguelen-Heard Plateau to the north and the Southern Kerguelen Plateau to the south (Schlich, 1975, 1982; Houtz et al., 1977). Site 751 (57°43.56'S, 79°48.89'E) is located on the Southern Kerguelen Plateau in the central part of the Raggatt Basin, approximately 900 km south of the present-day Antarctic Convergence at a water depth of about 1630 m (see "Introduction" chapter, this volume).

<sup>1</sup> Schlich, R., Wise, S. W., Jr., et al., 1989. *Proc. ODP, Init. Repts.*, 120: College Station, TX (Ocean Drilling Program).

<sup>2</sup> Shipboard Scientific Party is as given in the list of participants preceding the contents.

Three northeast-trending multichannel seismic reflection lines (RS02-22, RS02-24, and RS02-27), separated by approximately 50 km, one north-trending line (MD47-16), and two northwest-trending lines (MD47-05 and MD47-15) in the central part of the Raggatt Basin provide good regional control for the area close to Site 751 (Fig. 1). To the west the Raggatt Basin ends abruptly against the 77°E Graben. The eastern edge of the Raggatt Basin is a scarp or slope merging into the deep Labuan Basin. To the north and to the south the sedimentary section thins

gradually, but a lack of seismic reflection data prevents precise delineation of the basin.

In the central part of the Raggatt Basin, close to Site 751, normal north-trending faults with small throw affect the lower part of the sedimentary section. The sediment cover reaches 2500–3000 m in the central part of the basin and rests upon a weakly defined basement reflector. Schlich et al. (1988) and Colwell et al. (1988) independently identified six seismic sequences in the basin. Joint interpretation of Australian and

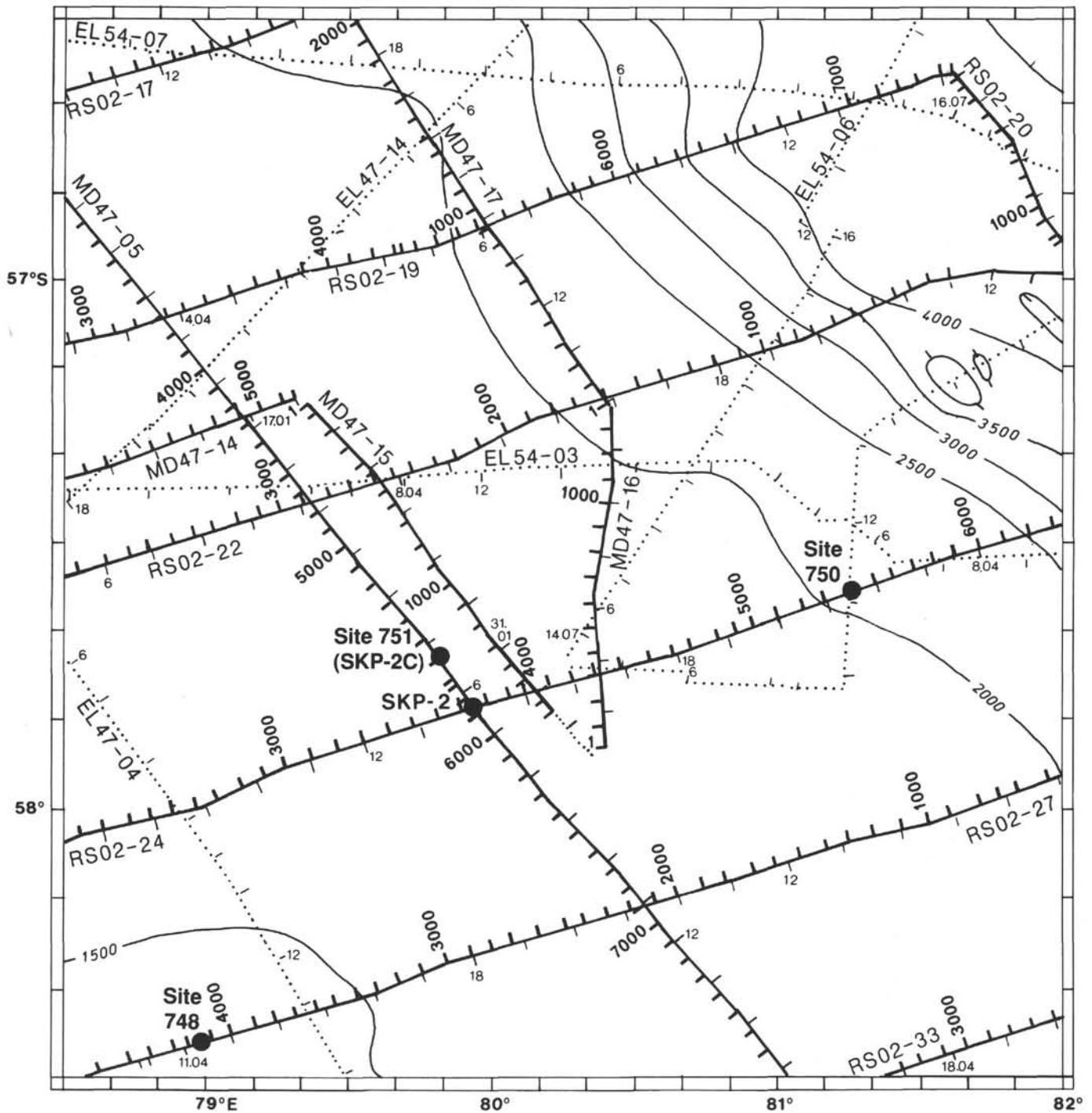


Figure 1. Track lines in the vicinity of Site 751. Bold lines denote *Rig Seismic* (RS02) and *Marion Dufresne* (MD47) multichannel seismic reflection profiles. The bathymetry is from Schlich et al. (1987).

French multichannel seismic reflection data (Coffin et al., in press) distinguished seven seismic sequences that can be grouped into two megasequences. The upper megasequence is divided into three sequences (NQ1, PN1, and P2) and the lower megasequence into four sequences (P2, K3, K2, and K1). Piston cores taken across the Raggatt Basin provided for sediment ages that ranged between the Holocene and Maestrichtian (Leclaire et al., 1987a, 1987b).

Site 751 (target site SKP-2C) is on the French multichannel seismic reflection line MD47-05 (shot point 5600) trending northwest across the Raggatt Basin, where the sedimentary cover reaches its maximum thickness and where the Neogene section appears to be the thickest. Target site SKP-2C (Site 751) lies about 12 km to the northwest of the original proposed site SKP-2 (shot point 5838) at the intersection of the *Rig Seismic* RS02-24 and *Marion Dufresne* MD47-05 multichannel seismic reflection lines. The location of these two sites on *Marion Dufresne* profile MD47-05 is given in Figure 2.

### Objectives

The objective of drilling Site 751 on the Southern Kerguelen Plateau was to recover a high-resolution Neogene and Paleogene stratigraphic section deposited above the calcium carbonate compensation depth and well south of the present-day Polar Front. This site represents a key component of the meridional paleoceanography transect, combined with the other Neogene sites drilled on Legs 119 and 120.

Due to severe time constraints related to the unexpected additional transit between the Kerguelen Plateau and Fremantle, we decided to limit drilling to the upper Neogene objectives.

### Drilling Strategy

The drilling strategy planned at Site 751 called for advanced hydraulic piston coring (APC) followed by the extended core barrel (XCB) until refusal.

### SITE GEOPHYSICS

*JOIDES Resolution* departed Site 750 on 18 April 1988 in the early afternoon (0600 hr UTC) heading west toward Site 751 (proposed Site SKP-2C). Site 751, the third site to be drilled in the Raggatt Basin on the Southern Kerguelen Plateau, is about 46 nmi west of Site 750 on *Marion Dufresne* line MD47-05, shot point 5600 (Fig. 1). The site lies in the central part of the Raggatt Basin where the sedimentary coverage is extremely thick and where the seismic sequences are flat lying in all directions over large distances.

Since drilling was restricted to the upper Neogene section, the site was located only by its coordinates without a presite survey. *JOIDES Resolution* approached the site at reduced speeds with global positioning system (GPS) satellite navigation, and a beacon was dropped at 1157 hr (UTC) on 18 April 1988 on our passage over the proposed site (Fig. 3). The final coordinates of Site 751 are 57°43.56'S and 79°48.89'E; the water depth as measured from the drill pipe (DPM) and corrected for the height of the rig floor above sea level is 1633.8 m.

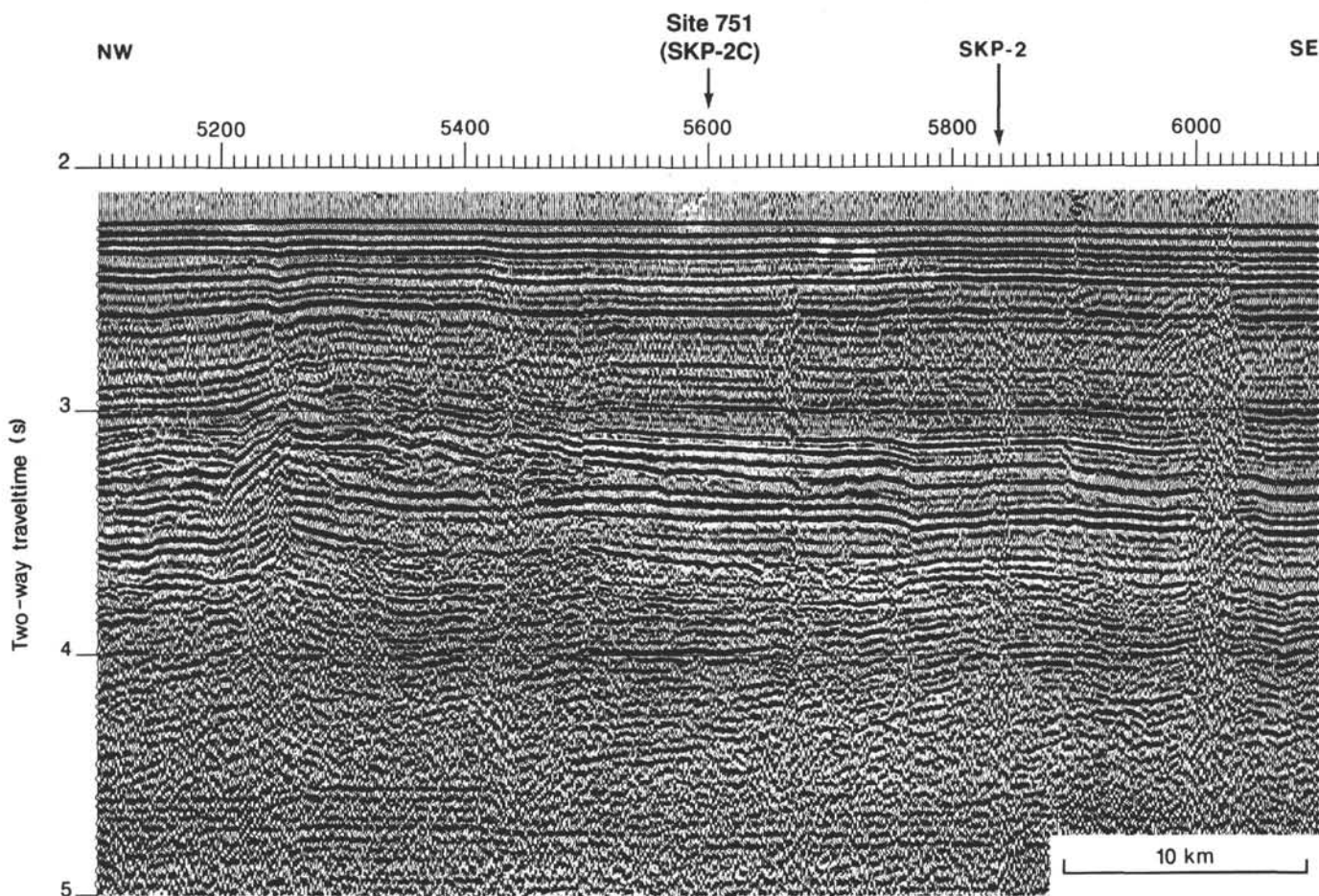


Figure 2. Seismic section MD47-05 (shot points 5100–6100) and location of sites SKP-2 and SKP-2C (Site 751).

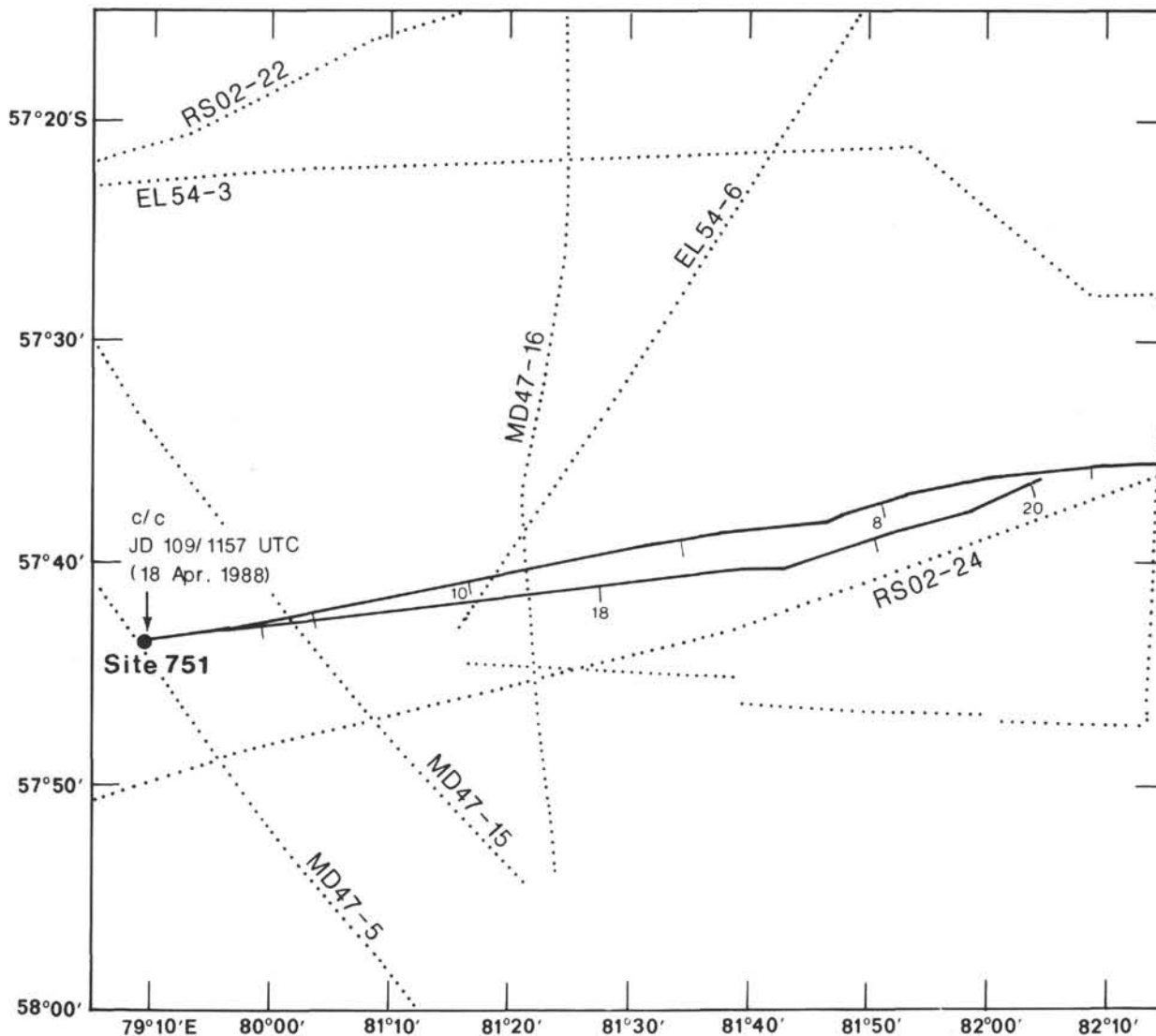


Figure 3. JOIDES Resolution site approach and Site 751 location.

The sediment cover in the Raggatt Basin reaches 2500–3000 m and rests upon a weakly defined basement reflector. Interpretation of the Australian and French multichannel seismic reflection profiles acquired in 1985 and 1986 over the Raggatt Basin identified seven distinct seismic sequences that can be grouped into two megasequences. The upper megasequence is divided into three sequences (NQ1, PN1, and P2). Sequences NQ1 and PN1 are only observed in the central part of the Raggatt Basin and are truncated in all directions by toplap. Sequence P2 filled the relief of the lower megasequence by onlap.

The lower megasequence is divided into four sequences (P1, K3, K2, and K1). Sequences P1 and K3 are characterized by mounds that appear as isolated features or in association with normal faults. The thickness of Sequence P1 remains fairly uniform in the basin, whereas Sequence K3 shows significant variations in thickness. Sequences K2 and K1 filled up the center of the basin and disappeared in all directions by onlap. A major tectonic episode corresponding to normal faulting occurred at the boundary between Sequences K3 and P1; this event is related to the shift of the depocenter, which moves from west (K1, K2, and K3) to east (P1, P2, PN1, and NQ1).

Using all the available seismic data, an isochron map of the top of the acoustic basement (Fig. 4) and two isopach maps, one for the total sedimentary cover (Fig. 5) and one for upper

Sequences NQ1 and PN1 (Fig. 6), were drawn for the area close to the drill site. Site 751 is located in the central part of the Raggatt Basin where the upper megasequence almost reaches its maximum thickness (Fig. 6). To the north and to the west of the site, normal north-trending faults with a small throw affect the lower megasequence.

At Site 751 the basement reflector lies at about 1.76 s TWT below seafloor, and a major reflector corresponding to the boundary between Sequences P2 and P1 can be traced at 0.88 s TWT below seafloor on the *Marion Dufresne* multichannel seismic reflection profile (Fig. 7). From seismic stratigraphy studies, it is possible at this site to scale several other reflectors at 0.24, 0.37, 0.99, 1.11, and 1.52 s TWT below seafloor. These reflectors define the boundaries between the different seismic sequences.

The first two reflectors at 0.24 and 0.37 s TWT correspond to the base of Sequences NQ1 and PN1, respectively. The vertical velocity distribution was estimated from sonobuoy experiments carried out in the Raggatt Basin during *Marion Dufresne* cruise 47 (1986) and from seismic reflection stack velocities. Considering these results, the bases of Seismic Sequences NQ1 and PN1 were expected at about 220 and 320 mbsf, respectively.

Site 751 was cored to a depth of 166.2 mbsf, at which point the APC piston rod failed during pullout, leaving the core bar-

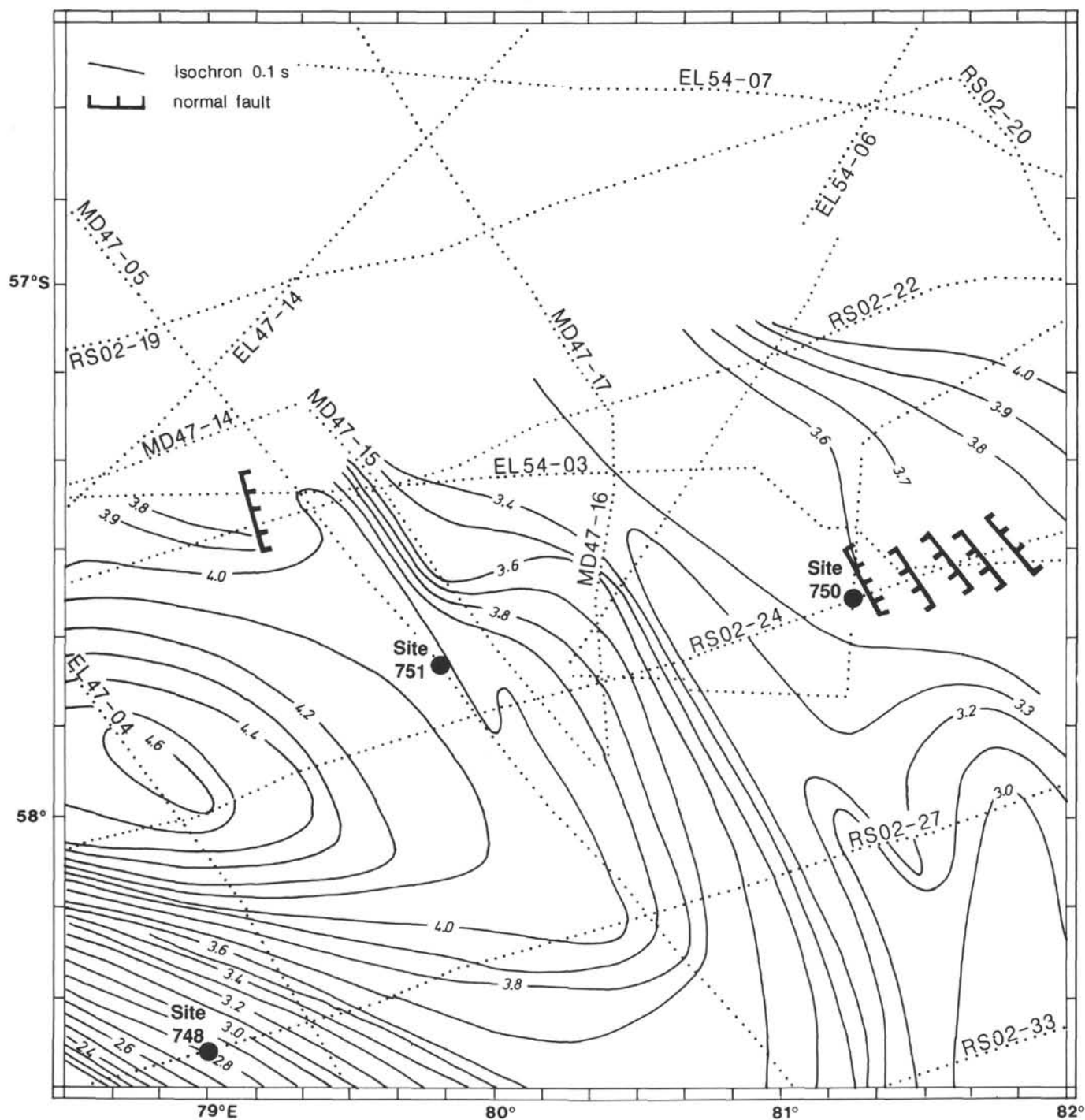


Figure 4. Isochron map of the top of the acoustic basement contoured in seconds (TWT).

rel and the last core stuck in the hole (see "Operations" section, this chapter). *JOIDES Resolution* departed Site 751 at 1530 hr (UTC) on 19 April 1988 to return to Site 750.

## OPERATIONS

### Site 751 (SKP-2C)

#### Hole 751A

No profiling gear was streamed on the approach to Site 751, and the 46-nmi transit to the west was direct, with our arrival

coinciding with the GPS window. The beacon was dropped at 2000 hr, 18 April 1988, and the ship took station without delay.

The relatively good weather of the transit deteriorated as the pipe was run. The temperature dropped to  $-2.5^{\circ}\text{C}$ , and gusts to 60 kt caused the chill factor to plummet. We discovered that a control valve for the top drive tilt system was frozen, which resulted in a 1-hr delay in spudding. The strong and shifting wind gave the automatic station-keeping (ASK) system problems in maintaining station within acceptable limits. A "mud line" APC core was taken, but spudding of the bit was delayed an additional hour until positioning could be stabilized. Continuous

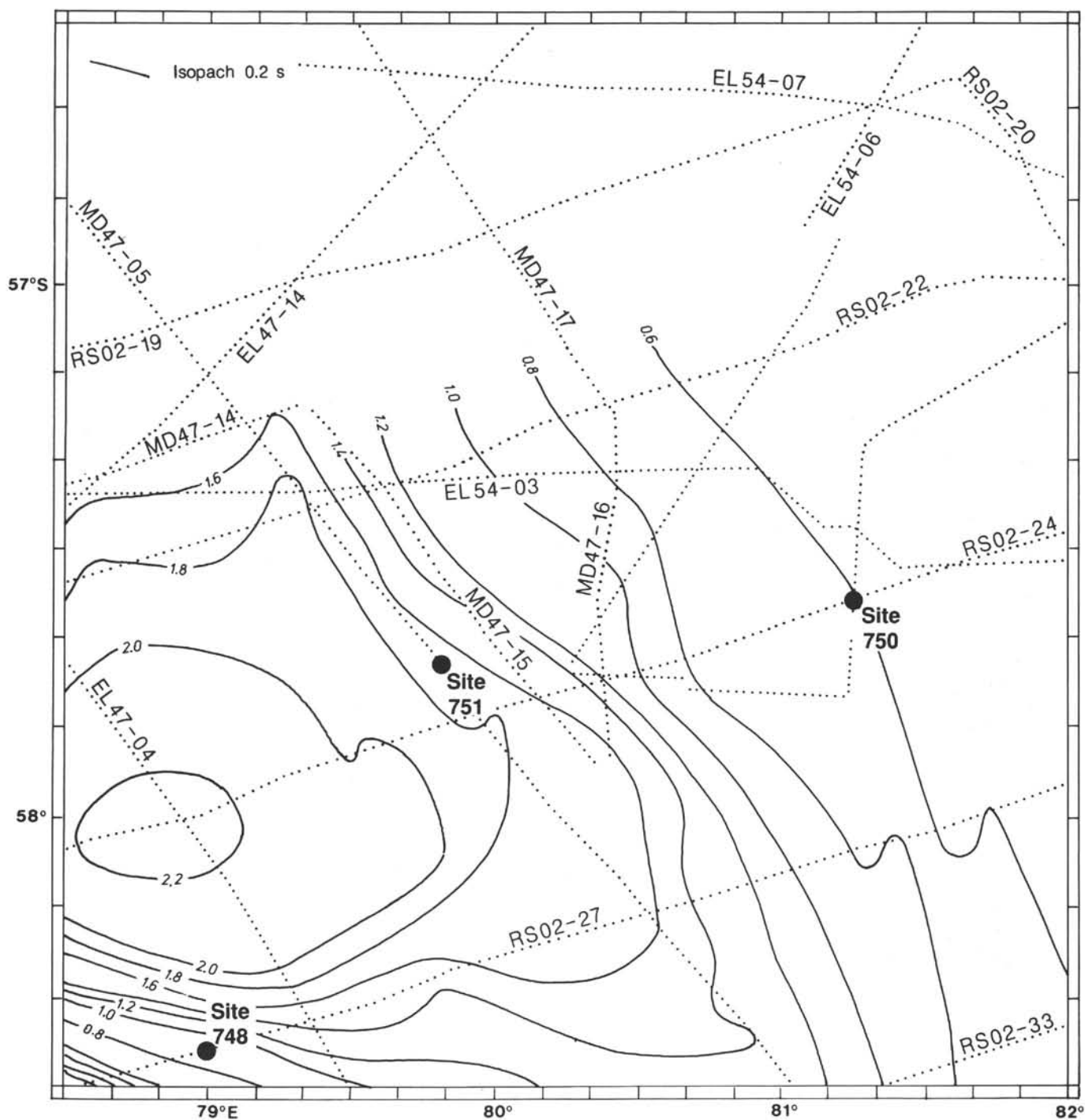


Figure 5. Total sediment isopach map contoured in seconds of reflection time.

APC coring was quite successful, considering the adverse motion conditions and the penetration of a porcellanite concentration at shallow depth. After the weather delay, 161.5 m were cored with 98% recovery in just 9 hr. The good recovery and rapid coring under adverse conditions were the direct result of an experienced and well-trained crew.

Following a 50,000-lb. pullout force on Core 120-751A-18H, Core 120-751A-19H gave incomplete stroke indication. When withdrawal from the sediment was attempted, a sudden heave caused overpull to hit 120,000 lb. The piston rod failed, leaving

the core barrel and core at total depth and junking the hole just short of the Oligocene objective.

After a quick assessment of the remaining time and scientific objectives, we decided to return to Site 750 and spend the remainder of our operating time coring the Cretaceous section beyond the depth reached in Hole 750A. An expeditious departure from Site 751 would also allow us to arrive at Site 750 within a GPS window, which in heavy seas would ensure acquisition of the beacon left there during our previous occupation of the site.

The coring summary for Site 751 appears in Table 1.

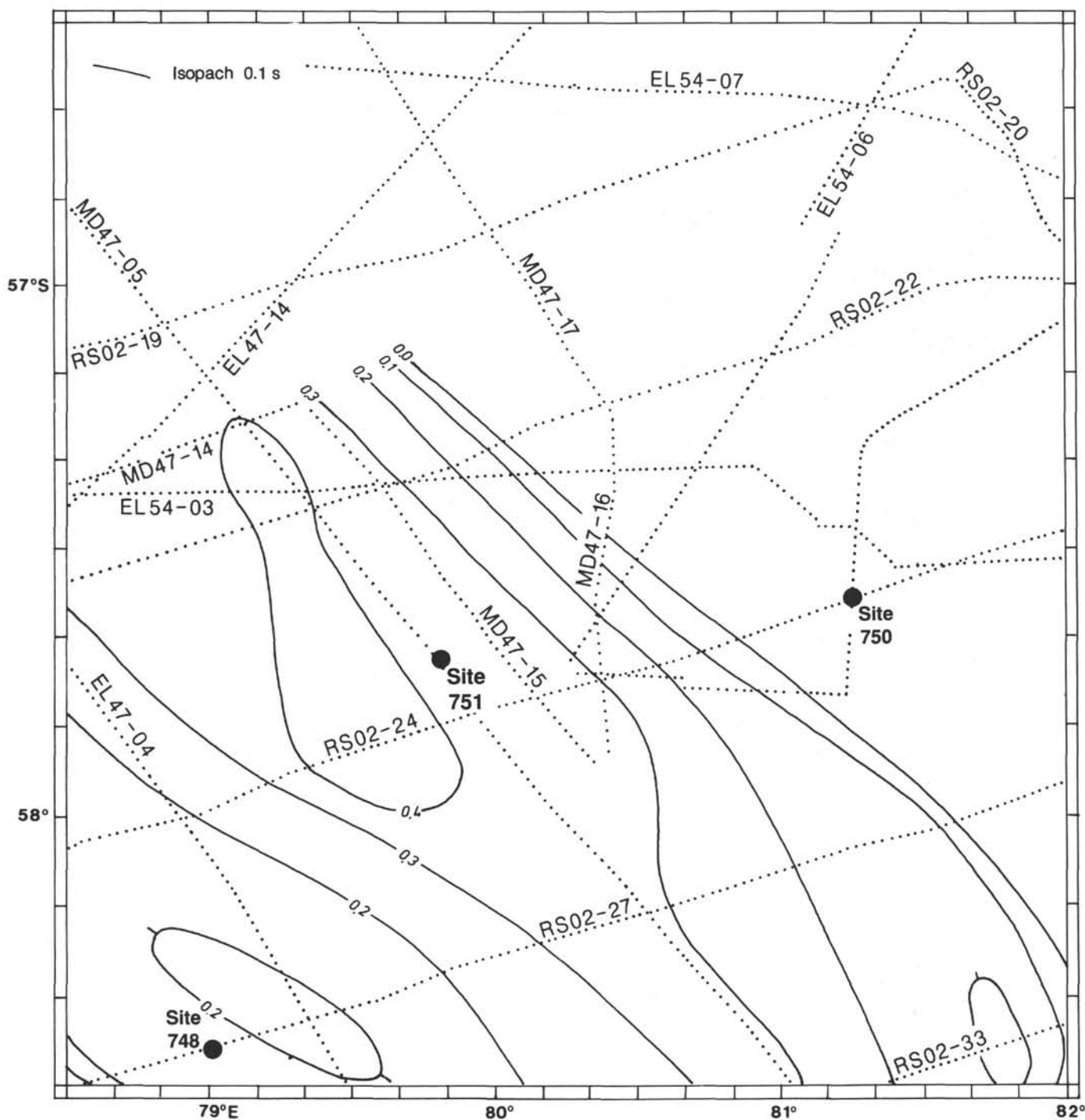


Figure 6. NQI and PN1 isopach map contoured in seconds of reflection time.

## LITHOSTRATIGRAPHY AND SEDIMENTOLOGY

### Introduction

Site 751 is located in 1633.8 m of water at 57°43.56'S, 79°48.89'E. The site lies in the central Raggatt Basin on the Southern Kerguelen Plateau. The primary site objective was to obtain a high-resolution record of Neogene sedimentation and paleoceanography for the high-latitude Southern Indian Ocean. A single hole was drilled, using the APC to core to 166.2 mbsf, and 162.92 m of upper Pleistocene to lower Miocene pelagic biogenic oozes were recovered (98% recovery). We stopped coring Hole 751A after the APC core barrel failed on pullout.

We distinguished two lithologic units at this site (Table 2 and Fig. 8). Unit I consists of 40.1 m of upper Pleistocene to lower Pliocene diatom ooze, with minor components of ice-rafted debris (IRD), volcanic ash, foraminifers and foraminifer fragments, and intervals of porcellanitic chert. Unit II consists of 126.1 m of upper to lower Miocene diatom nannofossil ooze. The units are distinguished mainly by the dominance of nannofossils as a sedimentary component in Unit II and the near absence of nannofossils in Unit I (Fig. 9).

Volcanic ash and IRD, minor components in Unit I, are virtually absent in Unit II (Fig. 9). The distinct change in nannofossil abundance at this lithologic boundary is reflected by an

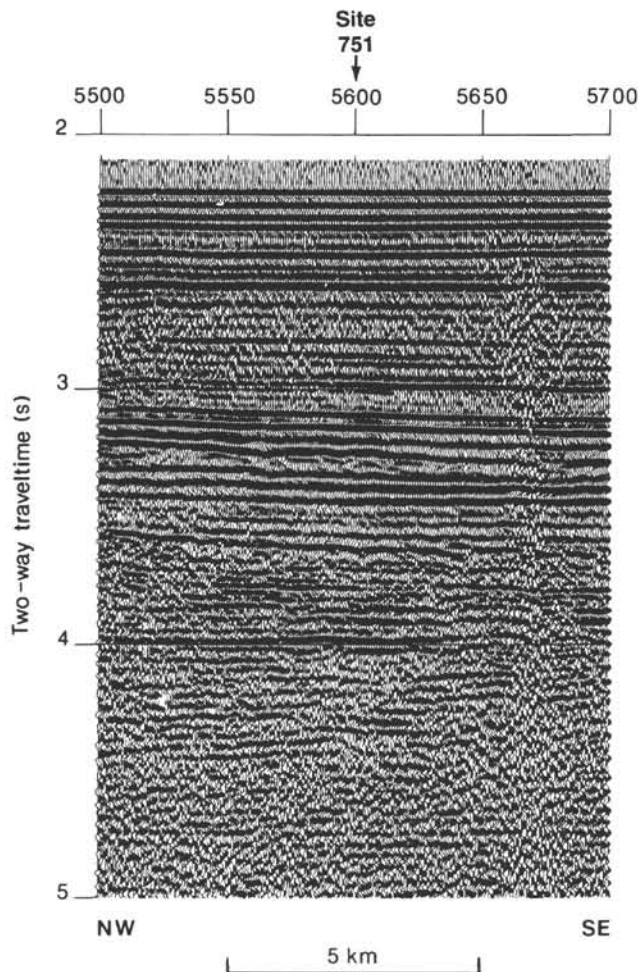


Figure 7. *Marion Dufresne* (MD47-05) multichannel seismic reflection line in the vicinity of Site 751.

Table 1. Coring summary, Site 751.

Core no.	Date (April 1988)	Time (local)	Depth (mbsf)	Cored (m)	Recovered (m)	Recovery (m)
1H	19	0520	0-4.7	4.7	4.68	99.6
2H	19	0740	4.7-14.2	9.5	5.38	56.6
3H	19	0820	14.2-23.7	9.5	7.83	82.4
4H	19	0855	23.7-33.2	9.5	10.07	106.0
5H	19	0925	33.2-42.7	9.5	8.30	87.3
6H	19	0955	42.7-52.2	9.5	9.71	102.0
7H	19	1015	52.2-61.7	9.5	9.92	104.0
8H	19	1045	61.7-71.2	9.5	8.33	87.7
9H	19	1110	71.2-80.7	9.5	10.13	106.6
10H	19	1140	80.7-90.2	9.5	9.83	103.0
11H	19	1225	90.2-99.7	9.5	9.70	102.0
12H	19	1305	99.7-109.2	9.5	9.66	101.0
13H	19	1340	109.2-118.7	9.5	9.95	105.0
14H	19	1415	118.7-128.2	9.5	10.16	106.9
15H	19	1450	128.2-137.7	9.5	9.63	101.0
16H	19	1535	137.7-147.2	9.5	9.99	105.0
17H	19	1610	147.2-156.7	9.5	9.68	102.0
18H	19	1640	156.7-166.2	9.5	9.97	105.0
Coring totals				166.2	162.92	98.0

equally sharp change in calcium carbonate percentage (See “Organic Geochemistry” section, this chapter) and by a distinct shift in bulk density at the depth at which calcite replaces opaline silica as the dominant mineralogy (See “Physical Properties” section, this chapter).

#### Unit I: Diatom Ooze

Interval: Core 120-751A-1H-1, 0 cm (0 mbsf) to Core 120-751A-5H-5, 90 cm (40.1 mbsf).

Depth: 0-40.1 mbsf.

Thickness: 40.1 m.

Age: late Pleistocene to early Pliocene.

Lithologic Unit I is composed of diatom ooze with minor components of IRD, foraminifers and foraminifer fragments, volcanic ash, and porcellanitic chert (Fig. 9). Grain-size analyses (Fig. 9 and Table 3) show the presence of IRD and foraminifers as enrichments in sand ( $>63 \mu\text{m}$ ) and consequent increases in mean grain size. These oozes are mostly tan or pale brown (2.4Y 6/4) to cream white (10YR 8/1) and light grey (10YR 7/2). Color changes indicate sedimentologic variability on scales of less than 1 m in this unit.

Drilling disturbance is generally slight to moderate; cores are distorted mainly where the sediment has a high water content and is adjacent to chert occurrences in soft sediment (e.g., Cores 120-751A-4H-1, 0-150 cm, and 120-751A-4H-2, 0-65 cm). Flow-in occurs in Sections 120-751A-1H-2, 120-751A-1H-3, and 120-751A-4H-7. Core 120-751A-1H is highly disturbed; the bottom 1.5-2 m are flow-in, the result of incomplete stroke-out/penetration possibly due to ship heave while the mud line core was taken. Although the top of Core 120-751A-1H has not been unambiguously identified as the mud line, the diatom species present indicate an age for the top of less than 0.7 Ma (see “Sedimentation Rates” and “Biostratigraphy” sections, this chapter). Bioturbation is slight to moderate throughout this unit. Motting is expressed by distinct color changes and the presence of ash or IRD.

Porcellanitic chert occurs in Cores 120-751A-2H-CC, 120-751A-3H-1, 0-44 cm, and 120-751A-3H-3, 28-46 cm, as well as in Cores 120-751A-4H-1, 0-70 cm, 120-751A-4H-2, 0-5 cm, and 120-751A-6H-1, 0-50 cm. Cherts are dark gray to milky white. All of these except the first occurrence are probably cavings. This chert is unusual for its shallow burial depth and young Pliocene age (see “Biostratigraphy” section, this chapter). Porcellanitic cherts of Pliocene age were also found on the Kerguelen Plateau in *Eltanin* Core 47-15 (Weaver and Wise, 1973). Similar to the *Eltanin* core, Site 751 porcellanite consists mainly of lepispheres, which are further evidence for the early diagenesis of biogenic silica.

The uppermost occurrence of porcellanite in this section from Core 120-751A-2H-CC is composed of a breccia of highly angular, low-density fragments, ~1 cm in diameter. In Core 120-751A-4H porcellanitic chert occurs as irregularly shaped nodules, with burrowlike features preserved internally; in addition, the shape of many of the nodules suggests burrow casts (Fig. 10). Drilling records indicate that after Core 120-751A-2H was taken, the lower 4.12 m of the core was lost. We then had to rotate the drill bit in order to penetrate the section of the column corresponding to the porcellanite, which suggests that this lithology occurred as a discrete, coherent layer about 0.3 m thick rather than as isolated nodules.

The IRD is scattered in minor abundance throughout Unit I and is seen mainly as sand-size specks. The IRD grains are scattered through Cores 120-751A-2H-1, 28-150 cm, 120-751A-2H-2, 0-150 cm, 120-751A-2H-3, 0-150 cm, 120-751A-3H-4, 39-56 cm, 120-751A-3H-5, 0-150 cm, 120-751A-3H-CC, 120-751A-5H-1, 80-150 cm, and 120-751A-5H-2, 72-150 cm, and in a slightly

**Table 2. Summary of dominant lithologic units at Site 751, central Raggatt Basin on the Southern Kerguelen Plateau.**

Unit	Lithology	Features	Depth (mbsf)	Core, section, interval (cm)	Thickness (m)	Age
I	Diatom ooze	Minor IRD, ash, and chert	0-40.1	120-751A-1H-1, 0 cm, to 120-751A-5H-5, 90 cm	40.1	late Pleistocene to early Pliocene
II	Diatom nannofossil ooze	High variance in diatom/nannofossil ratio on meter scale	40.1-166.2 (TD)	120-751A-5H-5, 90 cm, to 120-751A-18H-CC	126.1	late Miocene to early Miocene

Note: IRD = ice-rafted debris and TD = total depth.

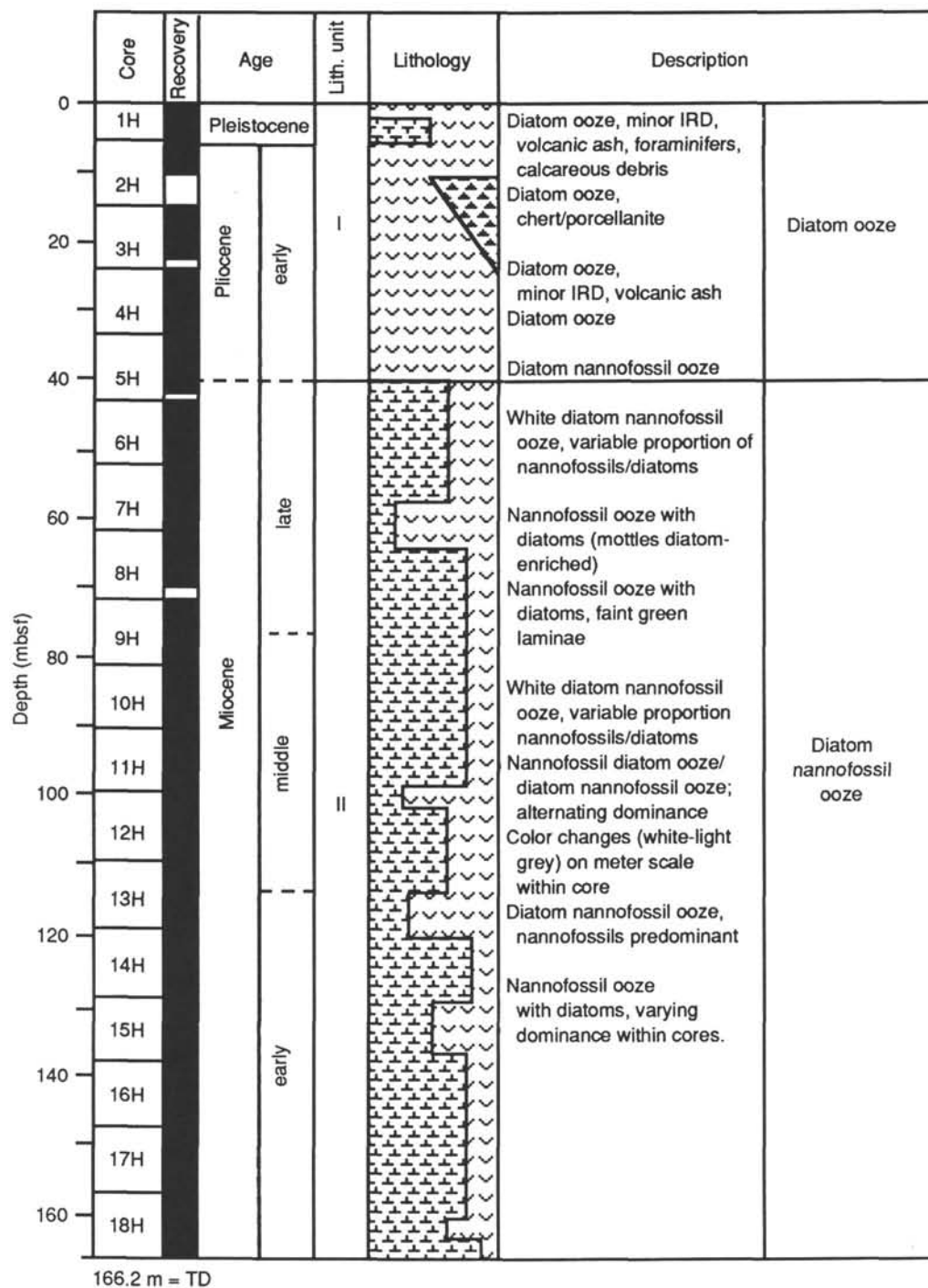


Figure 8. Lithostratigraphy of Site 751, Raggatt Basin, Southern Kerguelen Plateau. Recovered intervals indicated by shading in recovery column. For key to patterns in lithology column, see "Explanatory Notes" chapter (this volume). IRD = ice-rafted debris and TD = total depth.

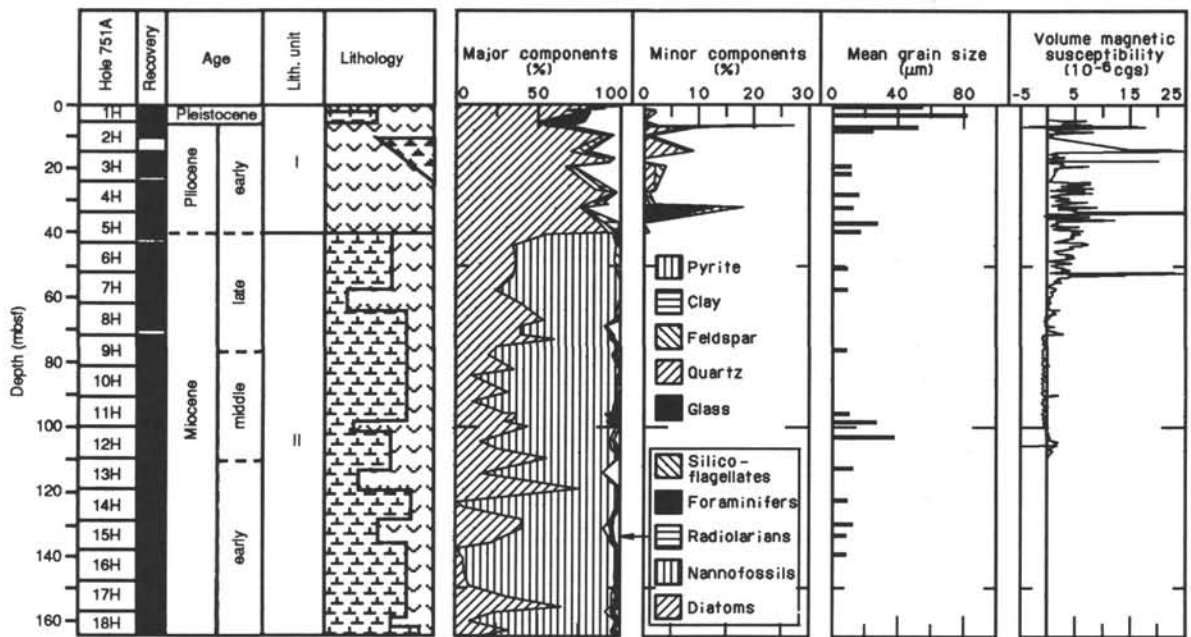


Figure 9. Lithologic summary, Site 751, including plots of percentages of major (biogenic) and minor (nonbiogenic) components as estimated from smear slides, grain size and percent coarse fraction (as estimated by laser optical grain-size analyzer) vs. depth, and whole-core volume magnetic susceptibility vs. depth.

Table 3. Mean grain size and percentages of sand, silt, and clay fractions of Site 751 shipboard samples.

Core, section, interval (cm)	Depth (mbsf)	Mean grain size (µm)	Sand (%)	Silt (%)	Clay (%)
120-751A-					
1H-1, 30-32	0.30	54.8	26	68	6
1H-3, 30-32	3.30	81.9	68	31	1
2H-2, 70-72	6.90	50.9	38	58	4
2H-3, 70-72	8.40	23.8	11	83	6
3H-4, 70-72	19.00	11.1	1	85	14
3H-5, 115-116	21.35	10.7	2	84	14
4H-3, 114-115	27.84	15.5	3	95	2
4H-6, 71-72	31.91	12.4	1	95	4
5H-2, 115-116	36.85	26.8	16	76	8
5H-5, 30-32	39.52	16.7	5	84	11
6H-6, 70-71	50.90	9.5	2	81	17
7H-4, 70-71	57.40	9.1	1	90	9
9H-4, 70-71	76.40	8.6	0	96	4
11H-4, 135-136	96.05	9.9	2	86	12
11H-6, 115-117	98.85	26.2	15	80	5
12H-3, 70-72	103.40	37.0	25	73	2
13H-3, 70-72	112.90	12.3	2	90	8
14H-3, 130-131	123.00	9.3	0	89	11
15H-2, 87-89	130.57	11.6	2	90	8
15H-4, 115-117	133.85	8.2	0	71	29
16H-2, 30-32	139.50	8.2	0	95	5

concentrated layer in Core 120-751A-2H-2, 90-107 cm. In addition, isolated dropstones were seen in Cores 120-751A-3H-5, 117 cm, 120-751A-4H-2, 92 cm, 120-751A-4H-7, 80 cm, 120-751A-5H-1, 59 cm, and 120-751A-5H-4, 9 cm. Dropstones represent a variety of lithologies, including gneiss, red sandstone, granite, and quartzite.

Intervals of mixed vitric volcanic ash and diatom ooze occur in Cores 120-751A-2H-2, 49-59 cm, and 120-751A-4H-6, 85-90 cm. The presence of ash and IRD at Site 751 is seen as increases in the magnetic susceptibility of the sediment (Fig. 9). These values drop to near-zero levels below about 55 mbsf (Core 120-

751A-7H). Although no IRD or ash was described in Cores 120-751A-6H or the upper part of Core 120-751A-7H, the relatively high magnetic susceptibility values in these cores suggest the presence of some type of terrigenous material in low abundance.

The biogenic components of this unit are overwhelmingly diatom frustules, which make up about 90% of the sediment throughout Unit I. Short intervals appear to be nearly pure diatom "cotton." Foraminifers are extremely rare in the bottom of this unit (Cores 120-751A-3H through -5H), but they are present in greater abundance in Cores 120-751A-1H and 120-751A-2H (from ~3% to as high as 25%). Nannofossils are noted for their near absence. Foraminifers are common as calcareous debris. Radiolarians are present in abundances of 2%-12%, and silicoflagellate abundance is estimated as 1%-10%.

**Unit II: Diatom Nannofossil Ooze**

Interval: Core 120-751A-5H-5, 90 cm, to 120-751A-18H-CC.  
 Depth: 40.1-166.2 mbsf (TD).  
 Thickness: 126.1 m.  
 Age: late Miocene to early Miocene.

Unit II consists of diatom nannofossil ooze (Fig. 8), although diatoms are present in greater abundance than nannofossils in several intervals (Fig. 9). The sediment is nearly a uniform white to light grey color (N8 to 10YR 8/2). Drilling disturbance is slight throughout most of the unit. Flow-in occurs in the bottom meter of Core 120-751A-8H. Disturbed intervals occur where chert cavings were driven into soft sediment, such as in Cores 120-751A-6H-1, 0-50 cm, and 120-751A-7H-1, 0-150 cm.

Bioturbation appears to be moderate throughout the unit, with very faint mottles mixing the usually subtle color changes. Centimeter-scale laminae with a faint green tint occur in Cores 120-751A-10H-6, 50-150 cm, 120-751A-11H-3, 100 cm, 120-751A-11H-4, 120-751A-11H-6, and 120-751A-12H-3. The laminae are enriched in diatoms relative to the surrounding sediment. Foraminifers are rare (from trace amounts to 7%) as are radiolarians (from trace amounts to 4%). Silicoflagellates are present throughout this unit in trace amounts.

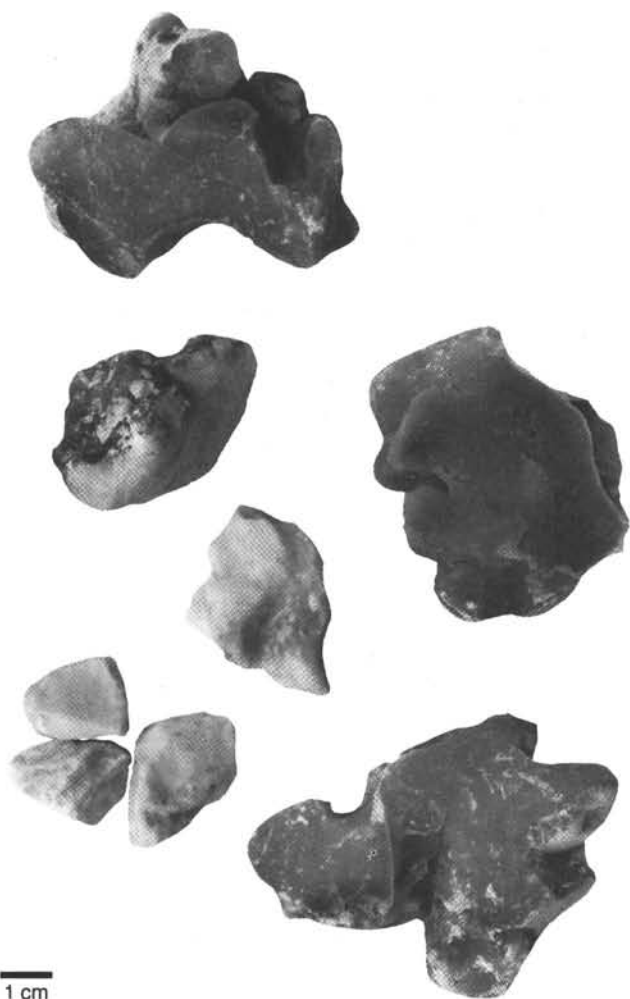


Figure 10. Pliocene chert nodules occurring in Section 120-751A-6H-1.

### Summary

The most striking feature of the sedimentology at Site 751 is the depth-dependent variability in the relative proportions of calcareous and siliceous microfossils. In particular, diatoms abruptly change in abundance on a scale of 1 m or less. At the ~20 m/m.y. sedimentation rates estimated for the Miocene of Site 751 (see "Sedimentation Rates" section, this chapter), this depth scale corresponds to a time scale from  $10^4$  to  $10^5$  yr. Thus, this site may be capturing some of the high-frequency paleoclimatic variability observed in other parts of the Neogene ocean.

## BIOSTRATIGRAPHY

### Introduction

Site 751 in the central Raggatt Basin was drilled with the objective of recovering an expanded section of Neogene biogenic sediments south of the present Polar Front and above the carbonate compensation depth (CCD), for high-resolution biostratigraphic, isotopic, paleoceanographic, and sedimentologic analysis. Hole 751A, the only hole drilled at this site, penetrated 166.2 m of sediment including portions of the upper Pleistocene through the middle lower Miocene (<20 Ma). The entire sequence was cored by the APC with 98% recovery.

The Pliocene-Pleistocene interval is largely biosiliceous with isolated occurrences of carbonate (see "Lithostratigraphy and

Sedimentology" section, this chapter). The Miocene is represented by a mixed carbonate and siliceous facies with diatoms and nannofossils alternating as the dominant sediment constituents. Two lithologic units are recognized at this site. Pliocene and Pleistocene lithologic Unit I (0–40.1 mbsf) consists of diatom ooze with minor IRD, foraminifers, volcanic ash, and porcellanite. Middle lower Miocene to upper Miocene lithologic Unit II (40.1–166.2 mbsf) consists of diatom nannofossil ooze.

Two hiatuses in the middle Miocene and late Miocene and two minor ones in the latest Miocene–earliest Pliocene and late Pliocene are identified on biostratigraphic evidence (see "Sedimentation Rates" section, this chapter). These interrupt Miocene sedimentation rates of between 15 and 20 m/m.y. and late Pliocene–Pleistocene rates of ~3 m/m.y. The length of several paleomagnetic reversals suggests that sedimentation rates in the Miocene may vary between ~10 and 30 m/m.y., but give the above averaged rate. Approximately 65% of the last 20 m.y. is represented by sediment in Hole 751A; the rest is missing due to unconformities.

Biostratigraphic dating of the Pliocene and Pleistocene is based primarily on diatoms and radiolarians. Biostratigraphic control for the Miocene is based primarily on diatoms, radiolarians, and planktonic foraminifers. A summary of the biostratigraphy and zonal assignments is presented in Figure 11 and discussed below. Refer to the "Explanatory Notes" chapter (this volume) for further discussion of the biostratigraphic procedures employed at this site.

### Planktonic Foraminifers

Hole 751A was drilled to a total depth of 166.2 m and recovered 18 cores that span a stratigraphic interval of lower Miocene to Pleistocene. Although diatoms and radiolarians are the dominant components of most core-catcher samples, planktonic foraminifers occur together with these biosiliceous elements in some cores and dominate the assemblages in others, attesting to the repeated changes in paleoceanographic conditions at this site during the Neogene.

Samples 120-751A-1H-CC through 120-751A-3H-CC contain virtually monospecific *Neogloboquadrina pachyderma* (sinistral) assemblages over a stratigraphic interval spanning the Pleistocene to the lower Pliocene, according to siliceous microfossils. Sample 120-751A-4H-CC is barren of planktonic foraminifers, whereas Sample 120-751A-5H-CC contains *Neogloboquadrina pachyderma*, *N. nympa* (*acostaensis* sensu Tjalsma, 1974), *Globorotalia scitula*, and *Globigerina woodi*. Sample 120-751A-6H-CC is essentially barren; only three specimens of *G. woodi* were found.

Sample 120-751A-7H-CC contains *Globorotalia scitula*, *Globigerina bulloides* (sensu Tjalsma, 1974; = *G. woodi*), and *Globorotalia infracta*. This association suggests a late Miocene age by comparison with Sites 747 and 748. Samples 120-751A-8H-CC and 120-751A-9H-CC contain a globigerinid fauna with *G. falconensis* and *G. woodi*. Low diversity continues to characterize the planktonic foraminifer assemblage in Sample 120-751A-10H-CC with *Globigerina woodi* essentially the sole taxon present, together with rare *Neogloboquadrina nympa*.

Samples 120-751A-11H-CC and 120-751A-12H-CC (diatomaceous ooze) contain *N. nympa*, *N. continua*, and small, indeterminate globigerinids and are suggestive of a late middle to early late Miocene age. The first occurrence of *N. nympa* is found in Sample 120-751A-12H-CC; this taxon is not present in Section 120-751A-13H-1. In Sample 120-751A-12H-CC, reworked specimens of *Globorotalia zealandica* (late early Miocene) occur, presaging the unconformity that occurs between this level and Sample 120-751A-13H-CC.

In Sample 120-751A-13H-CC, *Globorotalia zealandica*, *G. miozea*, and *G. praescitula* occur together with *Globigerina*

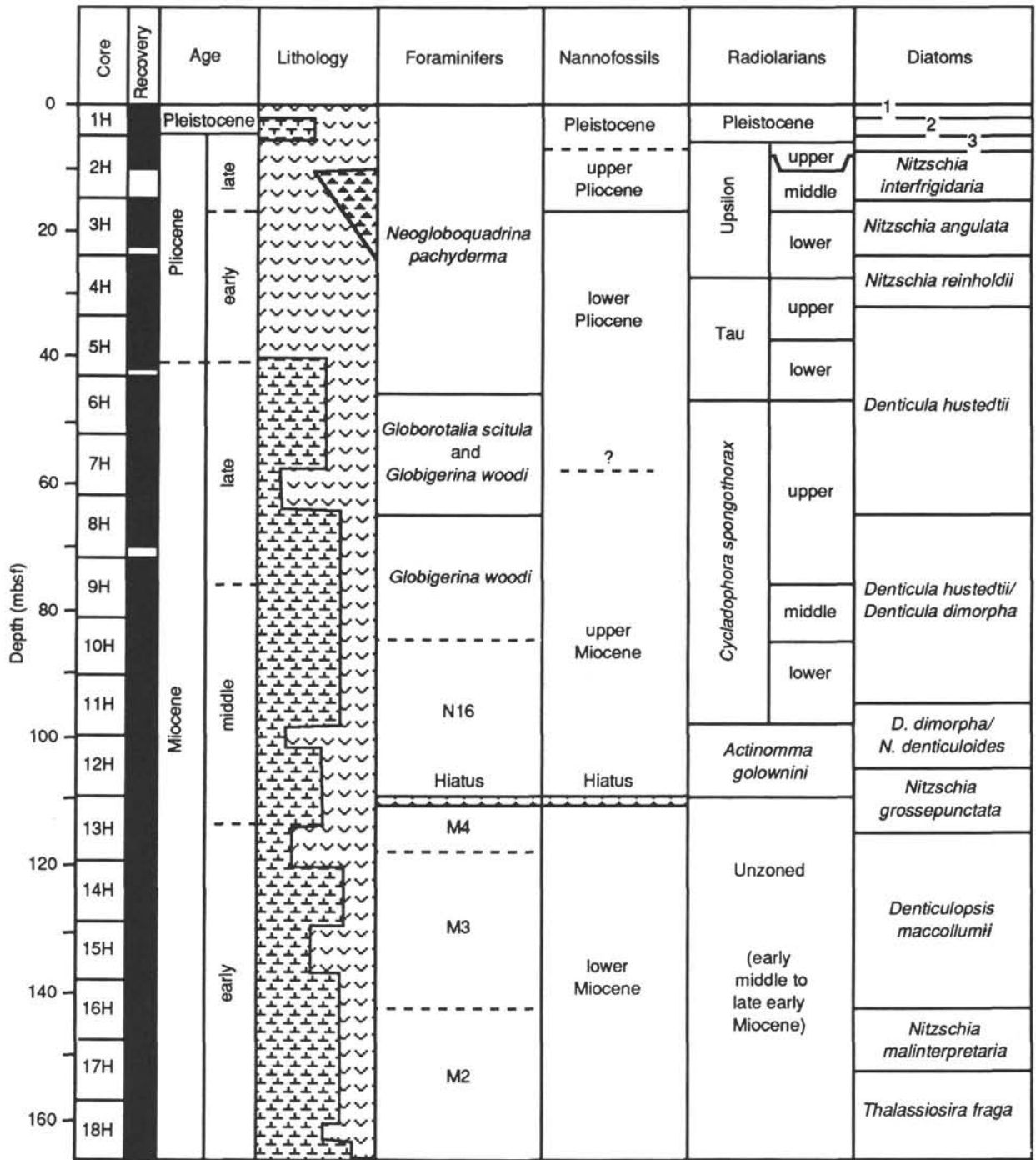


Figure 11. Summary of biostratigraphic age assignments and zonal stratigraphy for Neogene sediments recovered in Hole 751A. Key to diatom zones: 1 = *Thalassiosira lentiginosa*; 2 = *Coscinodiscus elliptopora*/*Actinocyclus ingens*; and 3 = *Coscinodiscus vulnificus* to *Nitzschia interfrigidaria*/*Coscinodiscus vulnificus*.

*woodi* in a calcareous ooze biofacies similar to that seen at Site 748. The presence of *G. miozea* in the lower half of Core 120-751A-13H indicates that this interval can be assigned to Zone M4 (Berggren et al., 1983) of latest early Miocene (Burdigalian) age. A detailed study of Core 120-751A-13H was made in order to determine its biostratigraphy and to confirm the presence of Zone M4 in Hole 751A. Core 120-751A-13H is a mixed calcareous and diatomaceous ooze in which planktonic foraminifers are alternately rare (and exhibit evidence of dissolution) and abundant, although of low diversity. *Globorotalia zealandica*

and *Globigerina woodi* range throughout Core 120-751A-13H; *G. praescitula* occurs in Sections 2 to 6 of this core; and *Globorotalia miozea* and *Globigerina brazieri* occur within Sections 120-751A-13H-3 to 120-751A-13H-CC.

Sample 120-751A-14H-CC contains an essentially monospecific assemblage of *Globorotalia zealandica*, indicating a late Zone M3 age. Sample 120-751A-15H-CC contains *Globorotalia zealandica*, *G. praescitula*, *Catapsydrax dissimilis*, *Globigerina brazieri*, and *G. woodi*. The overlap in range of *G. zealandica* and *G. dissimilis* indicates placement in the lower part of Zone

M3; a similar overlap was observed in Hole 748A. Sample 120-751A-16H-CC contains *Globorotalia praescitula* and *Catapsydrax dissimilis* and is of early Miocene age. The presence of *G. praescitula* suggests an age no older than the Otaian Stage of New Zealand, which is correlative with a level equivalent to Zone N6 of the standard low latitude zonation (early to middle Burdigalian).

Sample 120-751A-17H-CC contains an assemblage dominated by *Paragloborotalia incognita* with rare specimens of *P. semivera* and *C. dissimilis* and is of Zone M2 (early Miocene) age. The oldest sample at Site 751 is Sample 120-751A-18H-CC, and the fauna consists of relatively large globigerinid forms referable to *Globigerina brazieri* as well as *G. woodi*, *Paragloborotalia incognita*, and *Catapsydrax dissimilis*, suggesting an early Miocene (M2) age.

Although there are no dramatic conclusions that can be drawn at this time as a result of the preliminary examination of the 18 core-catcher samples of Hole 751A, we can draw attention to the potential this material holds for future studies:

1. Site 751 lies near the southern end of a latitudinal transect that also includes Sites 747 and 748. Although biosiliceous oozes predominate in the Neogene sequence obtained at Site 751, the sporadic occurrence of carbonate oozes with planktonic foraminifer faunas attests to the repeated changes in paleoceanographic conditions over this site during the past 20 m.y.

2. It should be possible to map the biogeographic distribution and migration patterns of the faunal assemblage through the several degrees of latitude represented by the Site 747, 748, and 751 transects and to place this within a relatively precise chronologic framework thanks to the integrated magnetobiostratigraphic studies that will be conducted on shore.

### Benthic Foraminifers

All core-catcher samples from Site 751 and a sample from the base of Section 120-751A-1H-1 were investigated for their benthic foraminifer content. Benthic foraminifers in core-catcher samples down to the lower upper Miocene (Sample 120-751A-12H-CC) are generally very rare and poorly preserved. However, Sample 120-751A-1H-CC (< 1.9 Ma, 4.68 mbsf) yielded an abundant and diverse benthic foraminifer fauna, and most of the other post-middle Miocene core-catcher samples include a sufficient number of benthic foraminifers for qualitative analysis. Benthic foraminifers of early and middle Miocene age (Samples 120-751A-13H-CC through 120-751A-18H-CC) are abundant and well preserved. About 100 specimens were counted from the > 125- $\mu$ m fraction of each sample whenever possible.

The following benthic foraminifer assemblages were recognized in the Neogene sedimentary sequence of Hole 751A (the assemblages are defined and numbered according to the criteria and stratigraphic boundaries established for Sites 747 through 750).

#### Assemblage 1a: Pleistocene

This assemblage is represented by a sample from the base of Section 120-751A-1H-1. Its benthic foraminifer fauna is characterized by the dominance of *Trifarina earlandi* and its co-occurrence with *Bulimina aculeata*. Common accessory constituents include *Pullenia subcarinata*, *Fursenkoina* sp., and *Oridorsalis umbonatus*. *Ehrenbergina glabra*, *Melonis zaandami*, *Pullenia bulloides*, *Fissurina* sp., and *Cibicidoides* sp. are rare components.

#### Assemblage 1b: Early Pleistocene–Late Pliocene

At Site 748 this assemblage was defined on the stratigraphic interval between the FO of *Trifarina earlandi* and the FO of *Bulimina aculeata*. In Hole 751A, this foraminifer assemblage is present in Samples 120-751A-1H-CC and 120-751A-2H-CC. How-

ever, the composition of the fauna is slightly different than at Site 748. *Trifarina earlandi* still dominates this assemblage in Hole 751A. Common constituents are *Eggerella bradyi* and *Cibicidoides* sp. Frequent accessory species include *Oridorsalis umbonatus*, *Melonis pompilioides*, and *M. zaandami*. Rare components are *Pyrgo murrhina*, *P. serrata*, *Pullenia bulloides*, *P. subcarinata*, *Astronion pusillum*, *Globocassidulina subglobosa*, *Fursenkoina texturata*, *Fissurina laevigata*, *Lenticulina* sp., and *Lagena* sp.

#### Assemblage 2: Early Pliocene–Late Miocene

This assemblage constitutes Samples 120-751A-3H-CC through 120-751A-7H-CC. It is characterized by the occurrence of *Epi-stominella exigua*, *Laticarinina pauperata*, and *Oridorsalis umbonatus*. The characteristic taxa of Assemblages 1a and 1b (*T. earlandi* and *B. aculeata*) are absent from this fauna.

As at Sites 747 and 748, the diversity and number of specimens are low in Assemblage 2. However, common accessory species are *Pyrgo murrhina*, *Gyroidina* spp., *Astronion pusillum*, *Pullenia bulloides*, *P. subcarinata*, *Cibicidoides* sp., *Uvigerina hispidocostata*, and *Eggerella bradyi*. *Cibicidoides wuellerstorfi* and *Karrerella bradyi* are very rare.

#### Assemblage 3: Middle Miocene–Early Miocene

The upper boundary of this assemblage is defined by the LO of *Nuttallides umbonifera*. It comprises Samples 120-751A-8H-CC through 120-751A-18H-CC. In most of these samples, *Nuttallides umbonifera* is the dominant or one of the most common species. Below Sample 120-751A-12H-CC the preservation improves; consequently, the number of specimens and the diversity dramatically increases. However, no major benthic faunal change or overturn could be detected between the older and the younger part of this assemblage.

We suggest, therefore, that the benthic foraminifer faunas of Samples 120-751A-8H-CC through 120-751A-12H represent the most resistant species of an originally diverse and abundant fauna represented by the older Samples 120-751A-13H-CC through 120-751A-18H-CC (solution-residue fauna). The enhanced CCD could have coincided with the glacially forced middle Miocene cooling event. However, the abundance of *N. umbonifera* in early Miocene sediments indicates a cool and corrosive bottom water mass already in the early Neogene.

The common components of the solution-residue fauna include, besides *N. umbonifera*, *Astronion pusillum*, *Gyroidina soldanii*, *Cibicidoides mundulus*, and *Cibicidoides* spp., *Pullenia bulloides*, *Oridorsalis umbonatus*, as well as *Eggerella bradyi*, *Karrerella bradyi*, and *K. novangliae*. The latter agglutinated species are reported to use siliceous cement in highly aggressive water masses instead of their usual calcareous cement (Schroder, 1986). Rare components of this fauna are *Hanzawaia* sp., *Uvigerina proboscidea*, *Pullenia subcarinata*, *Stilostomella* spp., *Pyrgo* sp., *Gyroidina lamarckiana*, *Quinqueloculina* spp., *Bolivina* spp., and *Melonis pompilioides*.

The highly diverse early Miocene fauna is clearly dominated by *N. umbonifera*. The most common and frequent characteristic components are *Astronion pusillum*, *Cibicidoides mundulus*, *Pullenia bulloides*, *Gyroidina umbonata*, *G. soldanii*, *G. lamarckiana*, *Anomalina* sp., *Globocassidulina subglobosa*, *Oridorsalis umbonatus*, *Stilostomella* spp., *Laticarinina pauperata*, *Ehrenbergina carinata*, *Bolivina subspinescens*, *Karrerella bradyi*, *Uvigerina proboscidea*, *U. graciliformis*, *Bulimina mexicana*, *Fursenkoina texturata*, *Alabamina* sp., and *Melonis affinis*.

### Calcareous Nannoplankton

A thick biogenic sequence (166.2 m) of mixed carbonate and siliceous oozes was recovered at Site 751. Calcareous nannofossil assemblages have been examined from the 18 APC core-catcher samples obtained from Hole 751A.

Calcareous nannofossils are extremely rare in the upper 25 m of this sequence (Core 120-751A-1H-CC to 120-751A-3H-CC), common in the underlying 10 m (Core 120-751A-4H-CC), and abundant throughout the remaining part of the sequence. Preservation is generally good, except at some levels (e.g., in Samples 120-751A-3H-CC and 120-751A-5H-CC) where there is high fragmentation as a result of strong dissolution. The indigenous (Neogene) calcareous nannofossils only show effects of dissolution, whereas reworked ones (mainly Oligocene) show slight overgrowth.

Extreme low diversity characterizes assemblages above Core 120-751A-12H-CC. Monospecific assemblages occur in Samples 120-751A-9H-CC and 120-751A-10H-CC. Diversity increases below Core 120-751A-12H-CC but remains low. This low diversity reflects the geographic position of Site 751 close to the Polar Front. Substantial amounts (over 50% of the large species) of reworked Oligocene taxa (all slightly overgrown) are observed at almost all levels, except in the upper part of the sequence (Cores 120-751A-1H through -4H).

Calcareous nannofossils have restricted usefulness for establishing the stratigraphy of most of the Neogene oozes recovered at Site 751. The presence of small forms of the genus *Gephyrocapsa* indicate a probable Pleistocene age for Core 120-751A-1H. The highest occurrence of *Reticulofenestra* spp. group *R. pseudombilica* in Sample 120-751A-3H-CC suggests that the lower/upper Pliocene contact may lie between Cores 120-751A-2H-CC and 120-751A-3H-CC. No stratigraphic marker was found between Cores 120-751A-3H-CC and 120-751A-12H-CC. The few overgrown placoliths of *Reticulofenestra floridana* that occur in Core 120-751A-12H are interpreted as reworked.

Reworking of Oligocene taxa is intensive in Core 120-751A-12H, and all reworked specimens are slightly overgrown in contrast with the indigenous coccoliths, which show the effects of dissolution (this results in the former having stronger birefringence than the latter). As it has been shown that the LAD of *R. floridana*, a species which ranges from late middle Eocene through late middle Miocene, occurs within Zone NN7 with an estimated age of 11.6 Ma (Miller et al., 1985), the stratigraphic position of Core 120-751A-12H-CC correlates with the upper part of Zone NN7 (upper middle Miocene) or younger.

Assemblages in Core 120-751A-13H-CC strongly differ from those in Core 120-751A-12H-CC in being more diversified. *Reticulofenestra floridana* is common, and reworked Oligocene coccoliths occur in lower numbers than they do above. The occurrence of *Helicosphaera ampliaperta* in Core 120-751A-13H-CC indicates an early Miocene age (older than 16.2 Ma). Because marker species of the genus *Sphenolithus* are absent in the sediments recovered from the Kerguelen Plateau (see "Biostratigraphy" sections, Sites 747 and 748 chapters, and Barron, Larson, et al., 1989), it is not possible to subdivide precisely the interval between Cores 120-751A-13H and -18H. Discoasters are relatively common in Cores 120-751A-17H where the occurrence of *Discoaster* sp. cf. *D. druggi* suggests a stratigraphic position no older than NN2 (younger than 23.2 Ma).

The most interesting observation resulting from an examination of the calcareous nannofossil assemblages recovered at this site is the alternation of two types of assemblages, one dominated by *Reticulofenestra* spp., the other by *Coccolithus pelagicus* (s.l.). Such alternations were also observed at Sites 747 and 748. Their significance will be part of an ongoing global study of similar fluctuations already recorded at all latitudes in the Atlantic, Caribbean, and Mediterranean areas. Hole 751A is particularly suited for such a study because of the high sedimentation rates and excellent stratigraphic control (provided by radiolarians, diatoms, and, at certain levels, planktonic foraminifers and magnetostratigraphy).

In summary, calcareous nannofossil biostratigraphy at Hole 751A supports the presence of an unconformity between Cores 120-751A-12H and -13H (see "Planktonic Foraminifers" section above). The duration of this unconformity cannot be precisely determined, however, based solely on calcareous nannofossil biostratigraphy (see "Sedimentation Rates" section, this chapter). In addition, Hole 751A will provide the opportunity to study calcareous nannofossil fluctuations in diversity in relation to climatic variations through integration with sedimentologic and isotopic studies (see "Lithostratigraphy and Sedimentology" section, this chapter).

### Radiolarians

Radiolarians are abundant throughout Hole 751A, the single hole cored at Site 751. Radiolarians are well preserved in middle Miocene and younger sediments, whereas preservation is moderate in lower Miocene sediments. All late Pliocene to middle Miocene radiolarian zones and subzones were recognized in this hole between the lower upper Pliocene-middle Upsilon Subzone and the middle Miocene *Actinomma golownini* Zone (see "Explanatory Notes" chapter, this volume; Fig. 11).

As at Site 748, no zonal markers were seen in the uppermost Pliocene to Holocene interval (Samples 120-751A-2H-2, 98-102 cm, to the top of the hole), and no zonal assignments are given for this interval. *Cycladophora davisiana* is present throughout this interval, indicating an age of less than 2.6 Ma throughout.

Radiolarian assemblages from Cores 120-751A-13H through -18H at the bottom of the hole are equivalent to lower middle Miocene to lower Miocene assemblages recovered at Sites 747 and 748 and at Deep Sea Drilling Project (DSDP) Site 266 (Leg 28; Chen, 1975). Species include *Thyrsoecyrtis clausa*, *Cycladophora gollii*, *Lithactis timmsi*, *Cyrtocapsella tetrapera*, *Amphistylus angelinus*, *Eucyrtidium cienkowskii*, *E. punctatum*, and *Cyrtocapsella longithorax*. No subdivision of this lower interval is attempted at present, although shore-based work should be able to identify and propose additional radiolarian zones.

### Diatoms

Diatoms are common in all core-catcher samples (Cores 120-751A-1H through -18H). These samples represent the basis for the following biostratigraphic analysis of Miocene diatoms. Pliocene and Pleistocene diatom biostratigraphy is based on the study of core-catcher samples and smear slides used by sedimentologists to describe Hole 751A. Sample spacing for the Pliocene-Pleistocene is generally less than 2 m and for the Miocene is every 9.5 m. Preservation is good in all samples except for the intervals between Cores 120-751A-7H to -10H, where it is poor, and between Cores 120-751A-13H to -18H, where it is fair to poor. In most cases, the poor preservation is due to dissolution, and a rough correlation exists between poor silica preservation and association with calcareous-nannofossil-rich intervals.

Most assemblages are dominated by two to four species of diatoms. The composition of these dominant members changes downhole, and in some instances dramatic changes are noted between adjacent core-catcher samples. Some of these variations resulted from changing compositions due to evolution and extinction, whereas others most likely reflect changes in productivity regime and physical characteristics of surface waters. The frequency of these assemblage variations is unknown due to broad sample spacing. Shore-based studies will determine whether there is a correspondence between these assemblage changes and the variance noted in carbonate content, porosity, and density values (see "Physical Properties" and "Organic Geochemistry" sections, this chapter).

Lower Pliocene and lower Pleistocene intervals in Hole 751A are dominated by diatoms *Nitzschia kerguelensis*, *Thalassiosira*

*lentiginosa*, *Actinocyclus ingens*, and *Eucampia antarctica*. The assemblage in the upper three sections of Core 120-751A-2H contains a relatively diverse assemblage. Below this level, lower Pliocene assemblages in Core 120-751A-2H are dominated by *Thalassiothrix* sp., *Eucampia antarctica*, and *Nitzschia "angulata"*. Some intervals contain a near monospecific ooze of *Thalassiothrix*, the high concentration of which is responsible for the "diatom cotton" texture of much of the sediment in Core 120-751A-2H. Core 120-751A-3H is dominated by *Thalassiothrix*, followed by *N. "angulata"* and *Nitzschia praeinterfrigidaria*.

Sample 120-751A-4H-CC is similar to the above assemblage but differs by the absence of *N. "angulata"* and the presence of common *Actinocyclus octonarius*. Several samples within Core 120-751A-5H contain a high-diversity assemblage with common *Coscinodiscus insignis*, *C. insignis f. triangularis*, *Neobrunia mirabilis*, *Stellarima microtrias*, and a lower number of *Thalassiothrix* than was present in the overlying lower Pliocene. Samples 120-751A-6H-CC and 120-751A-7H-CC are dominated by *Coscinodiscus marginatus*, *Denticulopsis* spp., *Thalassiothrix* sp., and *Azpeitia tabularis*. Sample 120-751A-8H-CC is similar to the above assemblage but differs in the replacement of *A. tabularis* by *Actinocyclus ingens* as a common element.

Samples 120-751A-9H-CC and 120-751A-10H-CC are dominated by *Denticulopsis dimorpha* and *Thalassiothrix* sp. in an assemblage that is poor in centric diatoms. Sample 120-751A-11H-CC differs from the above two samples only by the abundance of *C. marginatus*. Sample 120-751A-12H-CC is dominated by *Denticulopsis* spp. and *Actinocyclus ingens v. nodus*. Sample 120-751A-13H-CC is dominated by centric diatoms *Actinocyclus ingens* and *A. ingens v. nodus*. Samples 120-751A-14H-CC to 120-751A-16H-CC are poorly preserved but contain common *Denticulopsis* sp., *Thalassiothrix* sp., and *Thalassionema* spp., all of which are pennate diatoms. Samples 120-751A-17H-CC and 120-751A-18H-CC are dominated by centric diatoms *Coscinodiscus marginatus* and *Thalassiosira fraga*.

It is unclear what these abundance changes reflect, what is the duration of any given assemblage's dominance, and whether there is a relationship between the size and shape of the biogenic sediment particles in a particular sample and the fluctuating signals observed in the physical property data (see "Physical Properties" section, this chapter). These are questions to be addressed with shore-based analysis at closer sample spacing.

#### Pliocene-Pleistocene

The upper Pleistocene *Thalassiosira lentiginosa* Zone (Fig. 11) is identified from the top of Hole 751A down to the interval between Samples 120-751A-1H-1, 82–83 cm and 118–119 cm, as indicated by the highest occurrence of *Actinocyclus ingens* in the latter sample. The lower Pleistocene *Coscinodiscus elliptopora/Actinocyclus ingens* Zone continues from this level down to the interval between Samples 120-751A-2H-1, 50–51 cm, and 120-751A-2H-2, 20–21 cm, where a short hiatus is indicated by the highest occurrence of *Coscinodiscus kolbei* and *Coscinodiscus vulnificus* is noted. The co-occurrence of these two diatoms suggests the absence of the *C. kolbei/R. barboi* Zone and the upper portion of the *C. vulnificus* Zone, representing more than 0.3 m.y in the late Pliocene (between 1.9 and >2.2 Ma), or a very condensed sequence within the above interval in Core 120-751A-2H.

The upper Pliocene *C. vulnificus* Zone continues from the level of the hiatus down to the highest occurrence of *Coscinodiscus insignis*, which defines the top of the underlying *C. insignis* Zone, in Sample 120-751A-2H-2, 56 cm. This zone continues down to the highest occurrence of *Nitzschia interfrigidaria* in Sample 120-751A-2H-2, 100–102 cm, defining the top of the

underlying *N. interfrigidaria/C. vulnificus* Zone. The *Nitzschia weaveri* Zone is not recognized at this site.

The lowest occurrence of *C. vulnificus* occurs in the interval between Samples 120-751A-2H-2, 100–102 cm, and 120-751A-2H-4, 50 cm, defining the top of the mid-Pliocene *Nitzschia interfrigidaria* Zone. The base of this zone is noted by the lowest occurrence of the nominative species in the interval between Samples 120-751A-3H-1, 44–46 cm, and 120-751A-3H-2, 110–111 cm. The lower Pliocene *Nitzschia angulata* Zone continues down from this level to the lowest occurrence of *N. "angulata"* between Samples 120-751A-3H-4, 51–52 cm, and 120-751A-4H-2, 126 cm. This datum down to the highest occurrence of *Denticulopsis hustedtii* in the interval between Samples 120-751A-4H-5, 132 cm, and 120-751A-4H-6, 89 cm, marks the range of the lower Pliocene *Nitzschia reinholdii* Zone. The lower Pliocene to upper Miocene *Denticulopsis hustedtii* Zone continues below the *N. reinholdii* Zone and is discussed below.

#### Miocene

Sediments recovered from Hole 751A yielded rich lower Miocene to upper Miocene diatom assemblages. Most Neogene diatoms from Hole 751A are characteristic of Southern Ocean assemblages, and standard biostratigraphic zonal schemes were applied with several revisions (see "Explanatory Notes" chapter, this volume). Diatom biostratigraphic zonal assignments are outlined below and summarized in Figure 11 and Table 4.

The top of the upper Miocene *Denticulopsis hustedtii* Zone (4.5–8.0 Ma) occurs between Sample 120-751A-4H-5, 132 cm, and 120-751A-4H-6, 89 cm, and is identified by the highest occurrence of *Denticulopsis hustedtii*.

The highest occurrence of *Denticulopsis dimorpha* marks the base of the *Denticulopsis hustedtii* Zone and the top of the underlying *Denticulopsis hustedtii–Denticulopsis dimorpha* Zone (8.0–11.4 Ma) within the interval between Samples 120-751A-7H-CC and 120-751A-8H-CC. The highest occurrence of *Nitzschia denticuloides* is recognized in Sample 120-751A-8H-CC near the top of this zone. The base of the *D. hustedtii–D. dimorpha* Zone and the top of the underlying middle Miocene *D. dimorpha–N. denticuloides* Zone is identified between Samples 120-751A-10H-CC and 120-751A-11H-CC by the highest consistent occurrence of *N. denticuloides* in the abundant presence of *D. dimorpha*.

The co-occurrence of both dominant *D. dimorpha* and consistent *D. hustedtii* characterizes the middle to upper Miocene diatom assemblages from the *D. dimorpha–N. denticuloides* Zone to the *D. hustedtii–D. dimorpha* Zone. The contact between middle Miocene and upper Miocene lies within the lower part of the *D. hustedtii–D. dimorpha* Zone (Fig. 11).

The lowest occurrence of common *Denticulopsis hustedtii* within the interval between Samples 120-751A-11H-CC and 120-751A-12H-CC defines the base of the middle Miocene *D. dimorpha–N. denticuloides* Zone (11.4–13.8 Ma) and also the top of the underlying *Nitzschia grossepunctata* Zone (13.8–16.0 Ma). At this zonal boundary, the lowest occurrences of both *D. dimorpha* and *D. praedimorpha* are recognized. Common *Denticulopsis lauta* s.l. occur consistently throughout the *D. dimorpha–N. denticuloides* Zone and the overlying *D. hustedtii–D. dimorpha* Zone.

The highest occurrences of *Denticulopsis hyalina*, *D. nicobarica* s.l., and *N. grossepunctata* are detected at the top of the *N. grossepunctata* Zone, suggesting an age of 13.8 Ma between Samples 120-751A-11H-CC and 120-751A-12H-CC. *Actinocyclus ingens* is abundant within this zone and the underlying *D. maccollumii* Zone. The stratigraphic interval between Samples 120-751A-12H-CC and 120-751A-13H-CC contains the lowest occurrence of *N. grossepunctata*, *N. denticuloides*, *Denticulop-*

**Table 4. Miocene diatom zones and biostratigraphic datums, Hole 751A.**

Index species	Between Samples 120-751A-	Age
<i>Denticulopsis hustedtii</i>	4H-5, 132 cm, and 4H-6, 89 cm	4.5 Ma
<i>Denticulopsis hustedtii</i> Partial Range Zone		
highest <i>Denticulopsis dimorpha</i>	7H-CC and 8H-CC	8.0 Ma
highest <i>Denticulopsis lauta</i> s.l.	7H-CC and 8H-CC	8.0 Ma
highest <i>Nitzschia denticuloides</i>	7H-CC and 8H-CC	8.0 Ma
<i>Denticulopsis hustedtii</i> - <i>Denticulopsis dimorpha</i> Concurrent Range Zone		
highest common <i>N. denticuloides</i>	10H-CC and 11H-CC	11.4 Ma
highest <i>D. praedimorpha</i>	10H-CC and 11H-CC	11.4 Ma
<i>Denticuloides dimorpha</i> - <i>Nitzschia denticuloides</i> Concurrent Range Zone		
lowest <i>D. hustedtii</i>	11H-CC and 12H-CC	13.8 Ma
lowest common <i>D. lauta</i> s.l.	11H-CC and 12H-CC	13.8?
lowest <i>Denticulopsis dimorpha</i>	11H-CC and 12H-CC	
lowest <i>D. praedimorpha</i>	11H-CC and 12H-CC	
highest <i>D. hyalina</i>	11H-CC and 12H-CC	
highest <i>N. grossepunctata</i>	11H-CC and 12H-CC	13.8 Ma
highest <i>D. nicobarica</i> s.l.	11H-CC and 12H-CC	
highest abundant <i>A. ingens</i> s.l.	11H-CC and 12H-CC	
<i>Nitzschia grossepunctata</i> Interval Zone		
lowest <i>N. grossepunctata</i>	12H-CC and 13H-CC	16.0 Ma
lowest <i>D. hyalina</i>	12H-CC and 13H-CC	15.0 Ma
lowest <i>N. denticuloides</i>	12H-CC and 13H-CC	(13.9 Ma)
highest <i>D. maccollumii</i>	12H-CC and 13H-CC	(13.4 Ma)
highest <i>C. lewisianus</i>	12H-CC and 13H-CC	(12.7 Ma)
highest <i>Nitzschia</i> sp. 17 Schrader	12H-CC and 13H-CC	(16.0 Ma)
lowest abundant <i>A. ingens</i> s.l.	14H-CC and 15H-CC	(17.0 Ma)
lowest <i>D. lauta</i> s.l.	14H-CC and 15H-CC	
lowest <i>D. praelauta</i>	14H-CC and 15H-CC	
highest <i>D. kanayae</i>	14H-CC and 15H-CC	
highest <i>D. punctata</i>	14H-CC and 15H-CC	
highest <i>N. maleinterpretaria</i>	14H-CC and 15H-CC	(15.6 Ma)
<i>Denticulopsis maccollumii</i> Partial Range Zone		
lowest <i>D. maccollumii</i>	15H-CC and 16H-CC	16.7 Ma
lowest <i>C. lewisianus</i>	15H-CC and 16H-CC	
lowest <i>Nitzschia</i> sp. 17 Schrader	15H-CC and 16H-CC	(17.0 Ma)
lowest <i>D. kanayae</i>	15H-CC and 16H-CC	(17.8 Ma)
lowest <i>D. punctata</i>	15H-CC and 16H-CC	(17.8 Ma)
<i>Nitzschia maleinterpretaria</i> Partial Range Zone		
lowest <i>N. maleinterpretaria</i>	16H-CC and 17H-CC	18.8 Ma
lowest <i>D. nicobarica</i> s.l.	16H-CC and 17H-CC	17.8 Ma
highest <i>Thalassiosira fraga</i>	16H-CC and 17H-CC	
highest <i>Coscinodiscus rhombicus</i>	17H-CC and 18H-CC	
<i>Thalassiosira fraga</i> Partial Range Zone		
lowest <i>Thalassiosira fraga</i>	below 18H-CC	(19.9 Ma)
lowest <i>Coscinodiscus rhombicus</i>	below 18H-CC	

*sis hyalina*, and *Actinocyclus ingens* v. *nodus*. The latter datum approximates the lower Miocene and middle Miocene boundary.

*Denticulopsis maccollumii* Partial Range Zone (16.7 or 17.0? to 16.0 Ma) is newly defined and is based on the continuous occurrence of dominant *D. maccollumii* in this site. The top of the *D. maccollumii* Zone is marked by the lowest occurrence of *N. grossepunctata* and the base by the lowest occurrence of *D. maccollumii*. This new zone corresponds to the upper part of the lower Miocene *Nitzschia maleinterpretaria* Zone of Gombos and Ciesielski (1983). The absence or rare occurrence of *N. maleinterpretaria* near the upper/middle Miocene contact is another reason for proposing this new zone.

Both *Nitzschia* sp. 17 Schrader (1976) and *Coscinodiscus lewisianus* occur consistently throughout the zone. *Denticulopsis kanayae*, *Denticulopsis punctata*, and *N. maleinterpretaria* are

rare in Sample 120-751A-15H-CC representing the lower part of the zone. *Actinocyclus ingens* is abundant and *Denticulopsis lauta* s.l. is rare, but both are consistently present in the upper part of this zone through Samples 120-751A-13H-CC and 120-751A-14H-CC.

Sample 120-751A-16H-CC indicates the *N. maleinterpretaria* Zone (18.8–16.7 Ma), the top of which is defined by the lowest occurrence of *D. maccollumii*. The lowest occurrence of *N. maleinterpretaria* marks the base of this zone. The *N. maleinterpretaria* Zone adopted in Hole 751A corresponds to the lower part of the same named zone defined by Gombos and Ciesielski (1983).

Sediments recovered from the bottom of Hole 751A, through Samples 120-751A-17H-CC and 120-751A-18H-CC, are assigned to the lower Miocene *Thalassiosira fraga* Zone (18.8–19.9 Ma) based on the abundant occurrence of *T. fraga*. Sample 120-751A-18H-CC contains a few specimens of *Coscinodiscus rhombicus*. The lowest occurrence of *T. fraga* defines the base of the *T. fraga* Zone and occurs below the base of Hole 751A, suggesting a maximum age of 19.9 Ma for this hole. The absence of *Bogorovia veniamini* and *Rocella gelida* from Core 120-751A-18H support this age. This zone correlates with the upper part of the *Coscinodiscus rhombicus* Zone of Gombos and Ciesielski (1983).

In summary, diatoms are abundant and well preserved from the lower Miocene through upper Miocene, allowing recognition of standard Southern Ocean zones throughout as well as an attempt to refine several zones.

### Summary

Hole 751A recovered an expanded sequence (166.2 m) of mixed biosiliceous and calcareous ooze of late Pleistocene through middle early Miocene age. Age control provided by siliceous microfossil biostratigraphy for the entire hole and calcareous microfossil biostratigraphy for the lower two-thirds of Hole 751A indicate a sedimentation rate of approximately 3 m/m.y. for the late Pleistocene to late Pliocene and considerably higher rates, increasing from 15 to 20 m/m.y., for the early Pliocene through early Miocene.

Microfossil evidence suggests that four unconformities interrupt the section. Three are identified on biostratigraphic evidence in the middle Miocene (representing ~3.5 m.y. between 16 and 12.5 Ma); upper Miocene (representing ~3 m.y. between 9 and 6 Ma); and upper Pliocene (representing ~0.3 Ma between 1.9 and 2.2 Ma). A fourth unconformity at the Miocene/Pliocene boundary is suggested by magnetostratigraphic analysis and is considered to be minor. All of these unconformities are further discussed in the "Sedimentation Rates" section (this chapter).

Magnetostratigraphic data are of mixed quality, but several key polarity reversals are identified in the early Pliocene to late Miocene (Anomaly Correlatives 3, 3A, 4, and 5) and early Miocene (Anomaly Correlatives 5C through 6) that will enable cross-correlation of biostratigraphic datums between Sites 747, 748, and 751 and the Leg 119 sites, as well as sections in higher and lower latitudes. The co-occurrence of calcareous and siliceous microfossils at all Leg 120 Neogene sections is unique to the southern high latitudes, making these sites important reference sections for cross-calibration between the various groups. This feature is further enhanced by the composite biomagnetostratigraphy that is developing from these three sites.

The alternating abundance of siliceous plankton and calcareous planktonic and benthic faunas and floras and, on a finer scale, changing microfossil assemblage composition within these microfossil groups, indicates either migration of oceanic fronts or changes in physical and chemical properties of the surface water mass that controlled the nature and rate of productivity

over Site 751. Changes in benthic foraminifer assemblage composition and preservation reflect similar changing deep-water environmental conditions as well as surface-water productivity.

Biogeographic data from this site and other Kerguelen Plateau–Antarctic margin sites drilled during Legs 119 and 120 will provide a broad latitudinal transect within which a history of Southern Ocean paleoceanographic and paleobiogeographic change can be delineated. Moreover, the high sedimentation rates at Site 751 in pre-Pliocene, carbonate-rich sediments will enable a high-resolution analysis of oxygen and carbon isotope ratios, providing greater control on the timing and magnitude of paleoclimatic events in the Antarctic region.

### PALEOMAGNETICS

Site 751, located in the central part of the Raggatt Basin on the Southern Kerguelen Plateau (57°43.56' S, 79°48.89' E), provided a good magnetostratigraphic record with comparatively high resolution for about 50% of the Neogene. All 18 cores at Hole 751A were obtained with the APC and were therefore well preserved, except for occasional disturbances at the top or bottom of cores. The magnetic reversal sequence of Cores 120-751A-5H through -8H was identified as the magnetic polarity record of the earliest Pliocene to late Miocene. The next continuous magnetostratigraphic record ranged from Core 120-751A-12H through -18H. This section could be correlated to the standard middle and early Miocene polarity reversal record with the help of paleontologic information (see "Biostratigraphy" section, this chapter).

The natural remanent magnetizations (NRM) of Cores 120-751A-1H through -18H were measured with the cryogenic magnetometer with a 5-cm spacing between measurements (see Fig. 12). The results for the same cores after alternating field (AF) demagnetization at 9 mT are shown in Figure 13. The inclinations obtained from stepwise AF demagnetization of discrete sediment cubes on shore are shown by stars. We used the inclination record after AF demagnetization for identification of anomaly correlatives, since it showed more details in some cases than the NRM record.

Only the second half of the first section of Core 120-751A-1H (0.7–1.5 mbsf) was undisturbed and yielded a normal polarity interval (Fig. 13). Based on a diatom datum (see "Sedimentation Rates" section, this chapter), this normal interval can be placed in the Pleistocene and represents either the Olduvai or Brunhes Polarity Chron. Cores 120-751A-2H and -3H cannot be interpreted because inclinations were too shallow. Core 120-751A-4H (24–33 mbsf) is mainly of reversed polarity, but its inclinations are rather shallow (around +30°). The normal period from 38 mbsf to 40.5 mbsf (Fig. 13) coincides with the best-fitted line through the biostratigraphic markers when it is interpreted as the Thvera Subchron (see "Sedimentation Rates" section, this chapter).

As at the previous sites, we used the time scale of Berggren et al. (1985a, 1985b). The two short normal periods above the Thvera Subchron may be the remaining two normal subchrons of the Gilbert. The two long normal intervals between 43 mbsf and 48 mbsf in Core 120-751A-6H can easily be recognized as Anomaly Correlative 3A when compared to the seafloor-spreading record. The average intensity of magnetization in the cores described above is still relatively high after AF demagnetization and over an order of magnitude above the noise level (0.1 mA/m) of the cryogenic magnetometer. Short drops in intensity often occur at the boundary between sections. These decreases in intensity can be explained by the 10-cm sensing region of the magnetometer, which senses partly beyond the end of a section.

Anomaly Correlatives 4 and 4A are missing because of a hiatus of approximately 2 m.y. in the upper part of Core 120-751A-7H (see "Sedimentation Rates" section, this chapter). Usually

the long normal intervals are considered first when cross-correlating a polarity record to a standard reversal time scale. The long normal period (55–66 mbsf and 68–69 mbsf) in the upper Miocene can almost certainly be identified as part of Anomaly Correlative 5. From Core 120-751A-9H through -11H (71–98 mbsf), the magnetic intensity is very low and mostly below the noise level of the magnetometer (0.1 mA/m). Thus, the measurements from 71 to 98 mbsf are uninterpretable and shore-based measurements on discrete samples are needed to obtain information in this gap.

The normal periods between 98 and 108 mbsf can be tentatively correlated to Anomaly 5A. A hiatus of 2.5 m.y. has been inferred from the sedimentation rate curve at the top of Core 120-751A-13H (see "Sedimentation Rates" section, this chapter) and therefore Chrons 5AA through 5AD are missing. The four normal intervals from 114 to 123 mbsf (Fig. 13) represent the complete Anomaly Correlative 5C. One of the three short reversed periods in 5C is probably due to spurious data. The identification of Anomaly Correlative 5C is substantiated by the simultaneous occurrence of the short planktonic foraminifer Zone M4, which coincides with the lower part of our normal Chron 5C (see "Biostratigraphy" section, this chapter; Berggren, 1985). Consequently, the two short normal intervals (110 mbsf) at the top of Core 120-751A-13H can be correlated to Anomaly 5B if the sedimentation rate between 5B and 5C is low (about 7 m/m.y.).

Whether the three short normal intervals between 125 and 130 mbsf are real remains to be investigated by single-sample measurements. Anomaly Correlative 5D is recognized between 133 and 136 mbsf (Fig. 13). There is a possibility that the lower part of Anomaly Correlative 5D is missing. Another explanation for the relatively short duration of 5D on our record may be a lower sedimentation rate (about 6 m/m.y.) at the time of 5D compared with the average rate of 20 m/m.y. predicted for the early Miocene at Site 751 (see "Sedimentation Rates" section, this chapter). Unfortunately, Core 120-751A-16H (138–147 mbsf) had very low intensity of magnetization and no useful information could be obtained for this core from the measurements on the cryogenic magnetometer. The occurrence of Anomaly Correlative 5E from 152 to about 164 mbsf (Fig. 13) is in agreement with foraminifer and diatom zones and the predicted sedimentation rate (see "Biostratigraphy" and "Sedimentation Rates" sections, this chapter). Although the results from Hole 751A do not represent a complete magnetostratigraphic sequence for the Neogene, they can be cross-correlated with the record of Site 747. The magnetostratigraphies of Sites 747 and 751 complement each other in parts, and they can be combined to produce a nearly complete magnetobiostratigraphy for the Neogene and late Oligocene at high southern latitudes.

### SEDIMENTATION RATES

Sedimentation rates for Site 751 are based on both biostratigraphic and magnetostratigraphic data (Table 5), which were used to construct the age-depth curve shown in Figure 14. In Cores 120-751A-1H to -12H (Pleistocene to middle Miocene), diatom and radiolarian stratigraphy provides most of the available biostratigraphic information, since calcareous microfossils are mostly non-age-diagnostic forms.

Magnetostratigraphic data from this interval are interpretable for Cores 120-751A-5H through -8H, but are uninterpretable in Cores 120-751A-1H to -4H and Cores 120-751A-9H to -11H (see "Biostratigraphy" and "Paleomagnetism" sections, this chapter). For Cores 120-751A-13H through -18H (lower Miocene), biostratigraphic datum levels are provided by planktonic foraminifers, diatoms, and calcareous nannofossils. Magnetostratigraphic data from most of this interval are also of good quality and provide several datum levels.

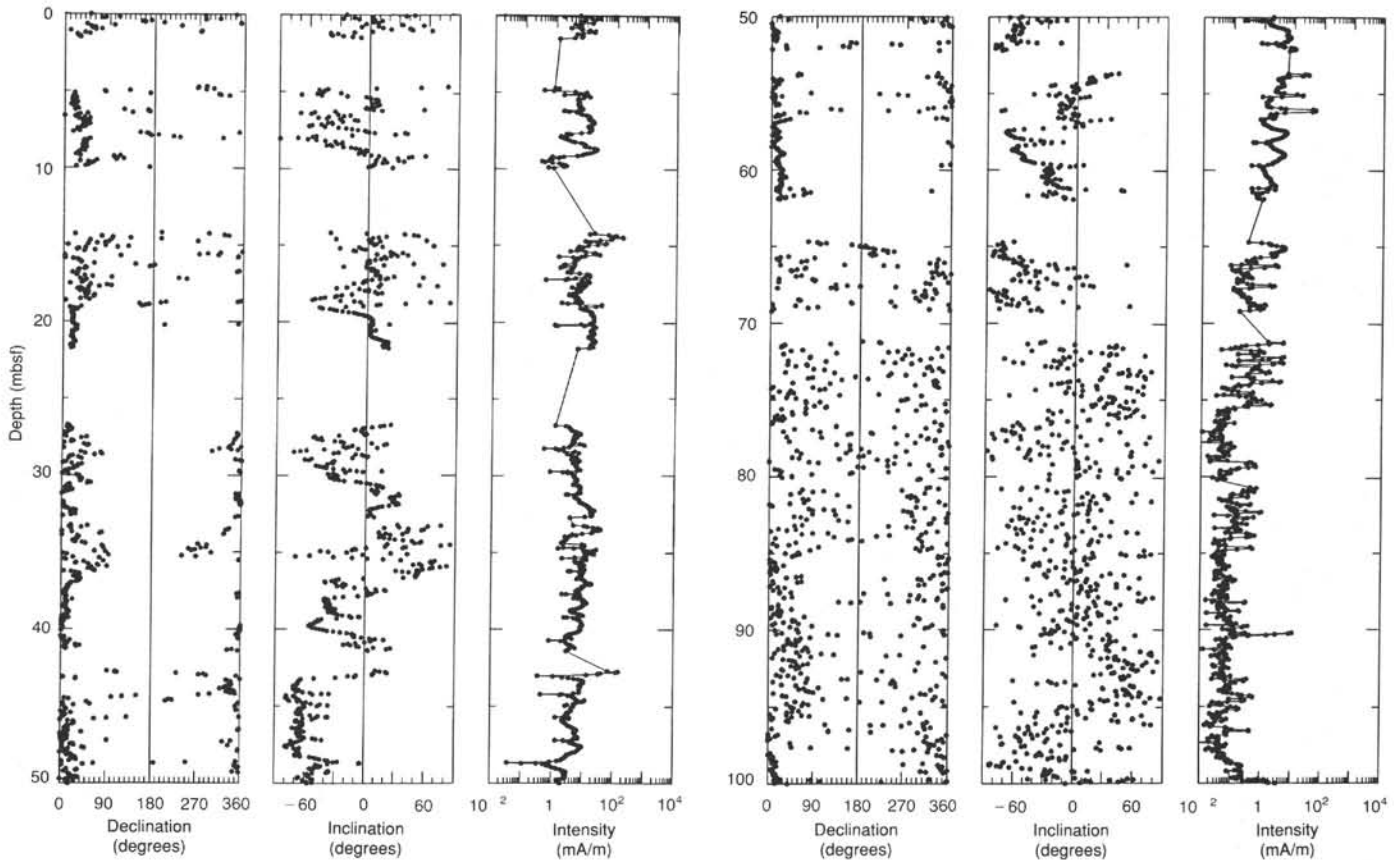


Figure 12. Declination, inclination, and intensity of natural remanent magnetization of Cores 120-751A-1H through -18H. The archive halves were measured at a 5-cm sample spacing with the cryogenic magnetometer.

Two major and two minor hiatuses appear to be present in this section, which otherwise seems to be a relatively continuous record of sedimentation covering almost the entire Neogene. A hiatus between  $\sim 12.1$  Ma and  $\sim 14.8$  Ma is apparent at  $\sim 110$  mbsf (the base of Core 120-751A-12H or the top of Core 120-751A-13H). The hiatus is clearly marked in Figure 14 by several biostratigraphic datum levels in these two cores. A second hiatus is inferred to exist within Core 120-751A-7H, which covers the time interval from  $\sim 6.2$  to  $\sim 9.5$  Ma. The duration of this hiatus is constrained by magnetostratigraphic data that suggests the presence of Chron C5 within the lower part of Core 120-751A-7H; by combined biostratigraphic and magnetostratigraphic data that suggests the presence of Chron 6 in the base of Core 120-751A-6H; and via extrapolation of the age-depth curve segments above and below this level. A short hiatus appears to be present at the Miocene-Pliocene boundary, which has removed most of the lowermost reversed interval of the Gilbert Polarity Chron. This hiatus coincides with the boundary between lithologic Units I and II (see "Lithostratigraphy and Sedimentology" section, this chapter).

Sedimentation rates within the Miocene and Pliocene are estimated to be between 15 and 20 m/m.y. for those time intervals not missing in hiatuses (Fig. 14). Sedimentation rates for the late Pliocene and Pleistocene are much lower—only about 3 m/m.y. (Fig. 14). Based on an extrapolation of the age-depth curve to the base of the hole, the oldest sediment recovered in Site 751 is about 19.5 m.y. old.

Site 751, with its high sedimentation rate, excellent recovery, and well-preserved calcareous and siliceous microfossils, is the best Neogene record of Antarctic Water Mass history yet recov-

ered. It will be a key site in future paleoceanographic studies of the region.

## INORGANIC GEOCHEMISTRY

### Introduction

At Site 751, located in the central part of the Raggatt Basin on the Southern Kerguelen Plateau about 46 nmi west of Site 750, one hole was drilled into Pleistocene to lower Miocene sediments. This site was of particular interest because of its high sedimentation rates in the Neogene (see "Sedimentation Rates" section, this chapter). Furthermore, a high abundance of siliceous ooze, especially within the upper 50 m, and anomalously young and shallow chert layers are characteristic for this hole (see "Lithostratigraphy and Sedimentology" section, this chapter).

Six samples from depths between 17.10 and 162.65 mbsf were obtained from squeezed fluids ranging between 42 and 85 cm<sup>3</sup> in volume. Shipboard analysis of pH, alkalinity, salinity, sulfate, chlorine, magnesium, calcium, and silica were conducted according to the methods described by Gieskes and Peretsman (1986; see also "Explanatory Notes" chapter, this volume). The results of interstitial water (IW) analysis are summarized in Table 6. All concentrations are given in millimoles per liter (mM) except for silica, which is given in micromoles per liter ( $\mu$ M).

### Results

#### Salinity and Chlorinity

The salinity values range from 35.5 to 36.1 g/kg and correspond to chlorine concentrations between 555 and 567 mM (the

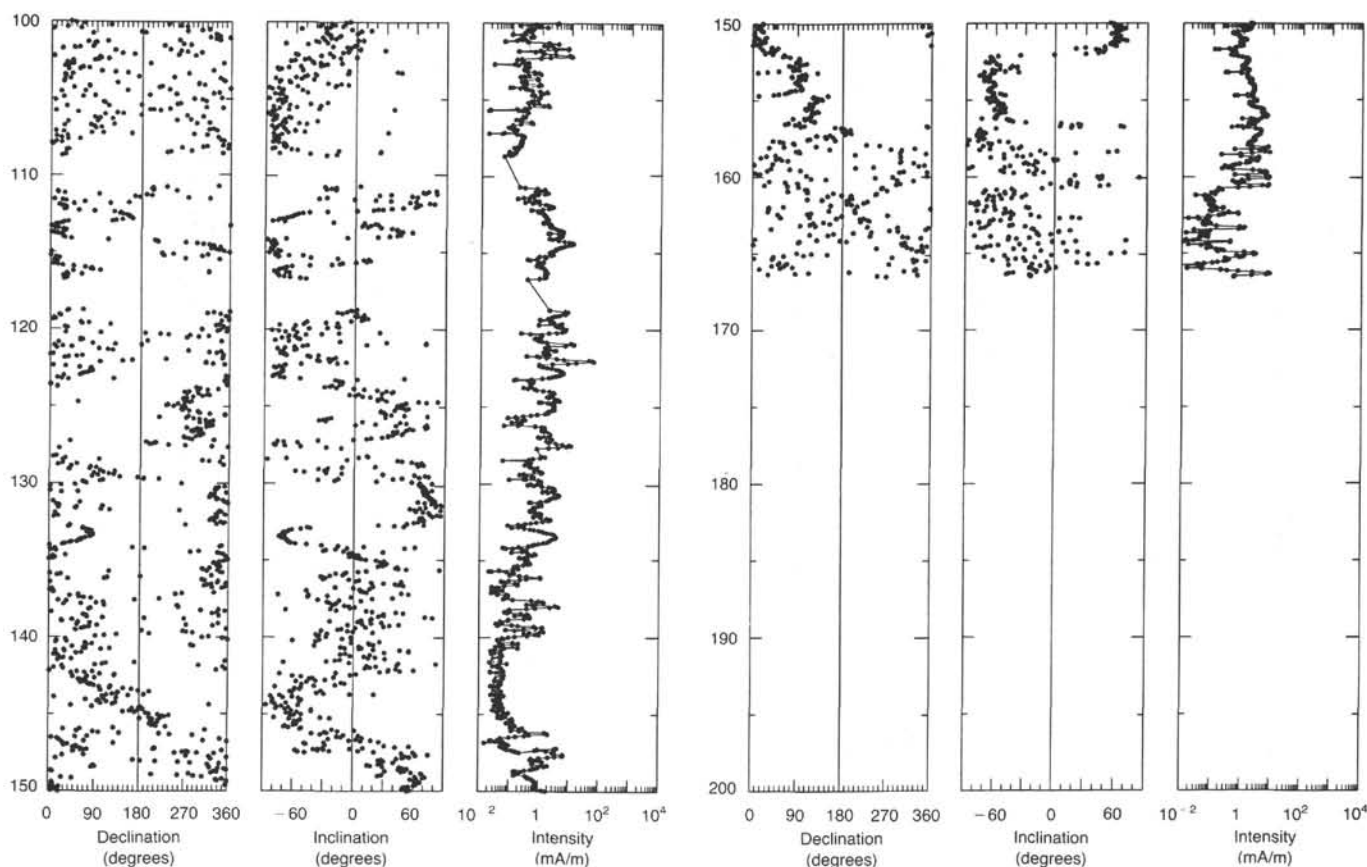


Figure 12 (continued).

uppermost sample yielded 36.3 g/kg in a first run; remeasurement gave a much more likely value of 35.8 g/kg, which agrees with the chlorine data even better, so the first high salinity value appears to have been due to evaporation residue on the refractometer). Salinity and chlorine concentrations increase slightly with depth (Fig. 15). There is no ready explanation for the rather low salinity at 107.15 and 135.65 mbsf (35.5 g/kg).

#### Alkalinity and pH

The lowest alkalinity value (3.053 mM) occurs at the top and the highest alkalinity value (3.521 mM) occurs at the bottom of the IW column (Fig. 15); we observed a slight depth-dependent gradient. The increase in alkalinity, however, is in contrast to the previous sites, where alkalinity decreased with depth due to carbonate precipitation. Concluding from this difference and from the increase in calcium and silica with depth at constant pH, still-active solution processes with no carbonate precipitation and hence increasing  $\text{HCO}_3^-$  concentrations control IW alkalinity in Hole 751A. The pH values (7.50–7.39) do not show significant variations and seem to be buffered by the carbonate and silica systems.

#### Sulfate

Sulfate concentrations range from 28.44 mM at the top to 25.12 mM at the bottom and display an overall decrease with depth (Fig. 15). A sharp drop in alkalinity occurs at 50.15 mbsf and can be correlated with a measurable content of organic carbon (see "Organic Geochemistry" section, this chapter) and some pyrite streaks (see "Lithostratigraphy and Sedimentology" section, this chapter) in the sediments around this depth. Since organic carbon is generally very low (see "Organic Geochemistry" section, this chapter), highly oxidizing conditions prevailed

throughout sedimentation and IW formation except for the interval around 50 mbsf.

#### Magnesium and Calcium

The uppermost sample shows near standard seawater (IAPSO) composition in magnesium (54.16 mM) and calcium (10.79 mM). There is a general increase in calcium (to 15.15 mM) and decrease in magnesium (to 44.48–47.57 mM) with depth (Fig. 15). Conservative cation exchange is assumed to be controlling the increase in calcium and the decrease in magnesium of the IW. A sharp drop in magnesium, which is not matched by a drastic increase in calcium, is observed at 107.15 mbsf and may be related to clay formation and selective magnesium uptake.

#### Silica

Silica concentrations range between 707 and 961  $\mu\text{M}$  and show an overall (but by no means regular) increase with depth (Fig. 15). The steep gradient in dissolved silica within the uppermost 50 mbsf is controlled by the abundance of soluble siliceous diatom skeletons in the sediment and the very silica-undersaturated character of the overlying seawater.

There is no significant sign for silica withdrawal by the chert layer. This is attributed to the very high abundance of still-soluble siliceous material in the sediment. If chert formation is to some extent controlled by processes involving silica from IW, we conclude that formation of chert and thus precipitation of silica is a slower process than dissolution of silica from organic siliceous material.

#### Summary

Salinity and chlorinity display an overall increase with depth and reflect the seawater character of the IW. The carbonate and

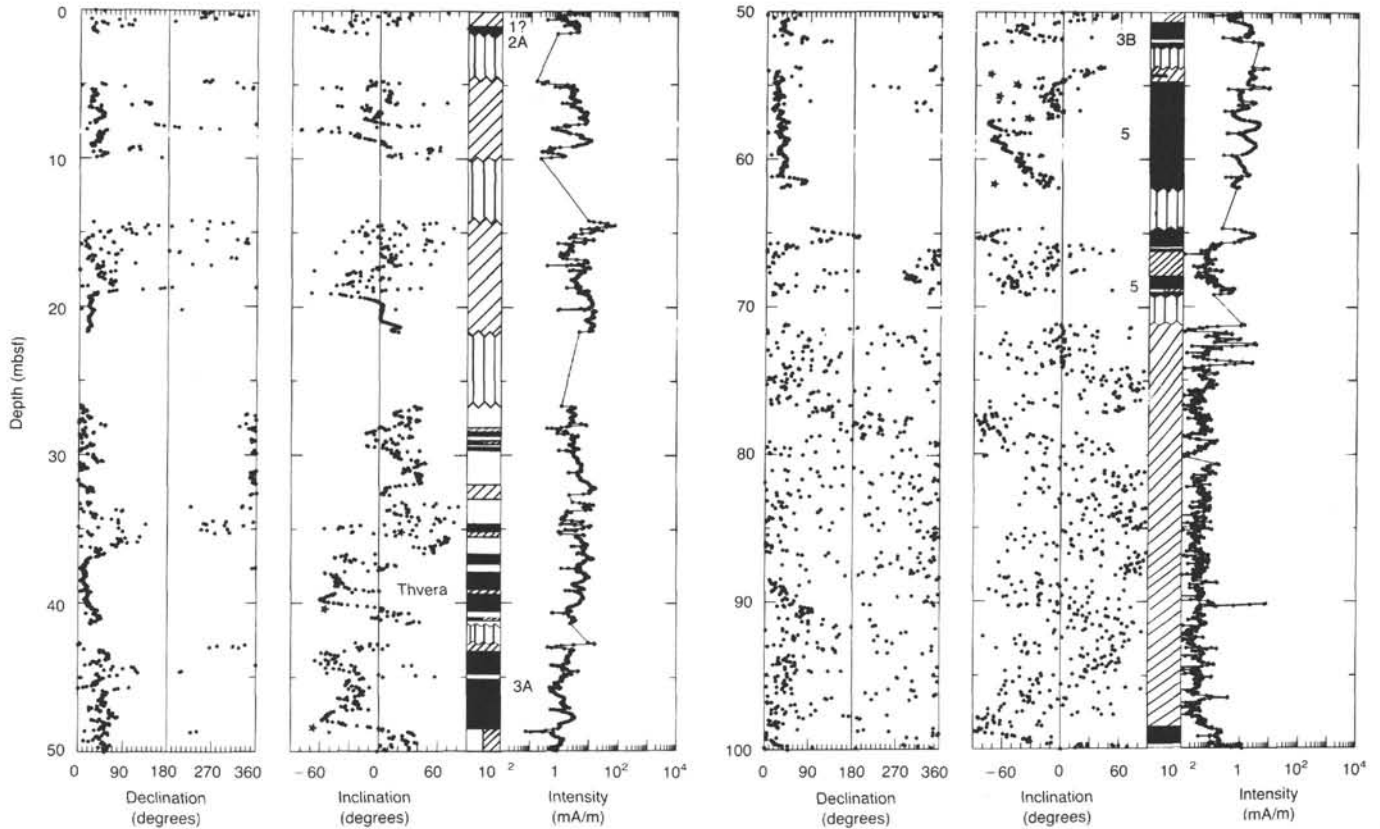


Figure 13. Declination, inclination, and intensity of Cores 120-751A-1H through -18H after demagnetization at 9-mT peak alternating field shown by black dots. The stars represent inclinations, determined from stepwise AF demagnetization of discrete samples. A preliminary identification of normal (black) and reversed (white) polarity chrons is shown to the right of the inclination record. Data gaps are indicated by vertical lines and uninterpretable data by diagonal lines. Polarity chrons, which are based on less reliable data, are indicated by one half appearing as diagonal lines.

silica system buffers pH values around  $7.45 \pm 0.05$ . High sulfate values report oxidizing conditions during sedimentation and diagenesis. Alkalinity, calcium, and silica reflect the ongoing and depth-dependent dissolution of siliceous material and calcium carbonate, whereas magnesium decrease is due to cation exchange with calcium and possibly some clay formation.

The anomalous formation of chert at shallow depths does not seem to influence the IW budget of silica. Either chert formation is independent from silica dissolved in IW or, more likely, silica dissolution is far greater than silica precipitation from IW in the form of chert.

## ORGANIC GEOCHEMISTRY

### Inorganic and Organic Carbon

Inorganic carbon analyses were conducted on a total of 88 samples from Hole 751A. The majority of samples analyzed were physical properties samples taken at one-per-section intervals. Total organic carbon content (TOC) was determined by the difference in total carbon and inorganic carbon. All inorganic and organic carbon results are reported in Table 7 and Figure 16. Analytical methods are outlined in the "Explanatory Notes" chapter (this volume).

The inorganic carbon content expressed as weight percent carbonate shows considerable variability with depth at Site 751. Values range from near 0% in the upper portion of the sequence to greater than 90% toward the bottom of the hole (Fig. 16). The sequence can be divided into two distinct units based on the

carbonate content. The upper 40 m of sediment are characterized by extremely low carbonate contents, generally less than 1%. Scattered within this unit, from 0.7 to 9.0, 19.0 to 21.0, and 29.0 to 31.0 mbsf, are discrete intervals of higher carbonate contents.

The low-carbonate intervals consist mainly of diatoms whereas the high-carbonate intervals contain a mixture of diatoms and planktonic foraminifers. Samples from the lower unit (41.0–165.0 mbsf) yield relatively higher carbonate contents from 40% to 90%. The variability reflects changes in the relative concentrations of siliceous and calcareous microfossils, which in turn may reflect changing surface-water conditions during the Miocene glacial/interglacial fluctuations. The transition zone between the low- and high-carbonate units corresponds with the position of the Miocene/Pliocene boundary as determined by diatom biostratigraphy (see "Biostratigraphy" section, this chapter).

Despite the relatively high Neogene sedimentation rates estimated for this location (see "Sedimentation Rates" section, this chapter), total organic carbon contents at Site 751 are low, with maximum TOC values less than 0.4%. This indicates that these sediments were deposited in a well-oxygenated environment. There is no clear relationship between TOC content, lithology, and/or sedimentation rates.

### Hydrocarbon Gases

Headspace analyses were conducted on a routine basis with sampling of every third core. Gases were extracted from sediment samples by head-space techniques. An outline of analyti-

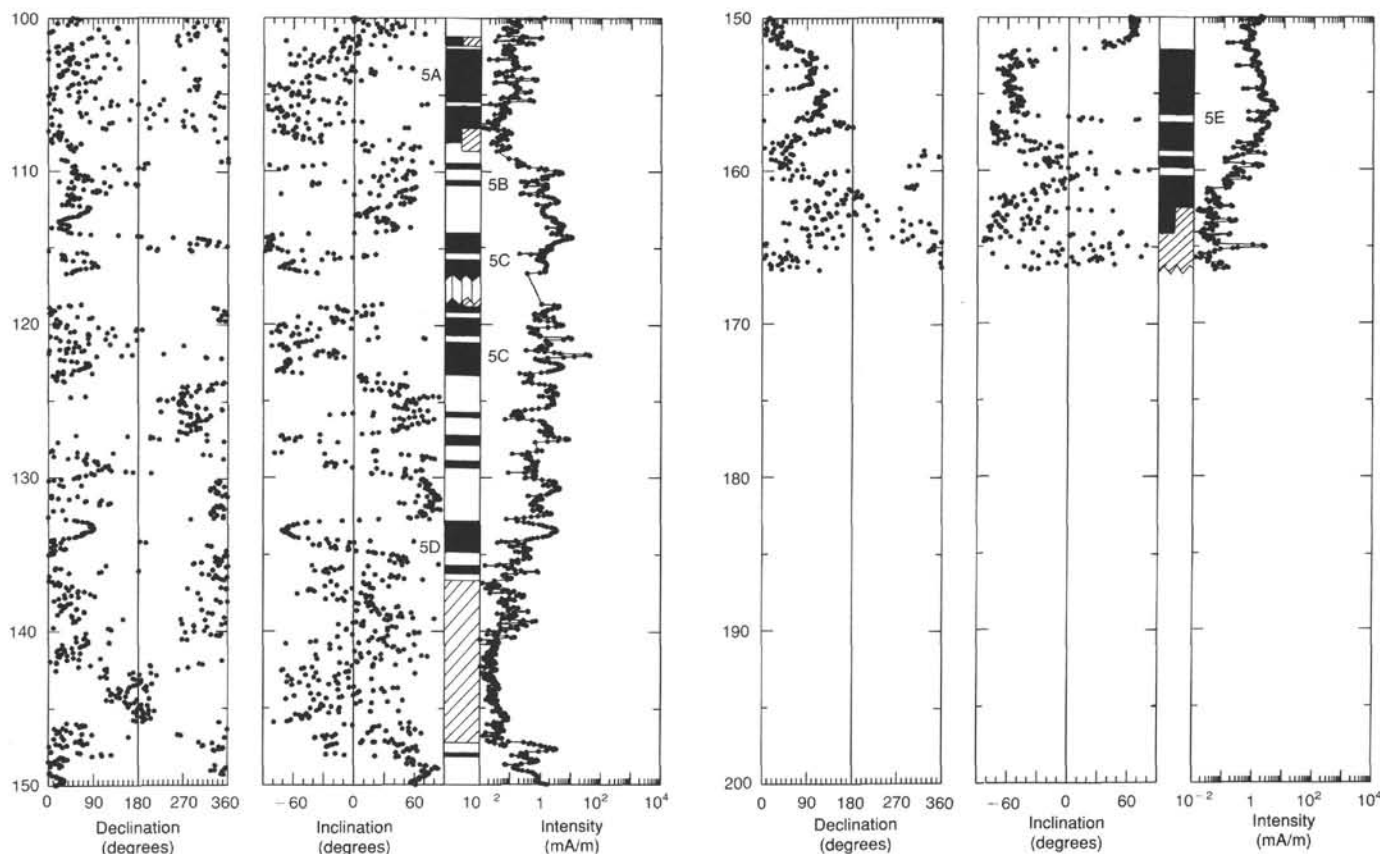


Figure 13 (continued).

cal procedures is provided in the "Explanatory Notes" chapter (this volume).

Concentrations of  $C_1$  through  $C_7$  gases at Site 571 were below the detectable limit on board ship. These results are consistent with the low TOC values reported above.

## PHYSICAL PROPERTIES

### Introduction

Site 751 was located at a critical position in the Raggatt Basin on the Southern Kerguelen Plateau at a water depth of 1633.8 m (from sea level). A single APC hole was continuously cored to a total depth of 166.2 mbsf. The physical properties program was designed (1) to provide high-resolution (50-cm sample spacing) profiles of index properties that would aid in an interpretation of the Neogene history of pelagic sedimentation at this high-latitude location and (2) to determine whether variations in these profiles can be used as a tool to investigate cyclicality in the lithologic record at this site.

The sample spacing for this study was carefully chosen to supplement the high-resolution research activities planned by members of the Leg 120 Shipboard Scientific Party and to act as a pilot study for assessing the possible magnitude and frequency of the sedimentary response to climatic periodicity, or Milankovitch-type orbital forcing, at this site.

The potential use of fine-scale changes in physical properties as a tool for extracting paleoceanographic information and/or for interpreting past depositional environments has been suggested by several DSDP and ODP shipboard investigators since the advent of the hydraulic piston corer (e.g., Mayer, 1981). The volume of samples required for high-resolution work, and the time necessary to process them accurately, has normally been an

impediment to this kind of high-resolution study of physical properties, although workers in regions of relatively high sedimentation rates have interpreted sample spacings of one per section as "high resolution" (Site 704, Leg 114; Ciesielski, Kristofferson et al., 1988).

The sensitive environmental location, the generally high sedimentation rates (averaging  $\sim 20$  m/m.y.), and the relatively shallow total depth of penetration at Hole 751A ( $< 170$  m) provided the opportunity to test the concept of using physical properties profiles to extract the climatic and paleoceanographic information preserved in the sedimentary record. Although the sample spacing of three per section used in this study is still inadequate for detailed environmental studies on time scales of thousands of years, it should provide the basic framework necessary for beginning to investigate the regional (or possibly global) Neogene paleoceanographic signal in the marine record of the Southern Kerguelen Plateau. Continuous measurements on whole-round cores before splitting may provide additional information for these types of studies.

The physical properties determined included (1) index properties (wet- and dry-bulk density, grain density, water content, and porosity) (see Fig. 17 and Table 8); (2) compressional wave velocity (see Fig. 18 and Table 9); (3) vane shear strength (see Figs. 19 and 20 and Table 10); (4) carbonate content (see Figs. 18 and 20 and Table 7); and (5) continuous measurements of bulk density and  $P$ -wave velocity using the gamma ray attenuation porosity evaluator (GRAPE) and  $P$ -wave logger (PWL) (see Figs. 21, 22, and 23). These data are compiled in both tabular and graphic form. The methods employed in the measurement of the physical properties obtained during Leg 120 are described in the "Explanatory Notes" chapter (this volume). A more detailed discussion of these measurements can be found in Lambe and Whitman (1969) and Boyce (1976, 1977).

Table 5. Biostratigraphic data used in Figure 14.

#	Depth (mbsf)	Age (Ma)	Name
F1	109.2	12.1	B <i>N. nympa</i>
F2	118.7–128.2	16.8	B <i>G. miozea</i>
F3	118.7–128.2	17.6	T <i>C. dissimilis</i>
F4	137.7–147.2	17.6	B <i>G. zealandica</i>
F5	147.2–156.7	19.0	B <i>G. praescitula</i>
N1	109.2–109.7	11.6	T <i>R. floridana</i>
N2	109.2–118.7	16.2	T <i>H. ampliapertura</i>
N3	4.7–14.2	3.5	T <i>R. pseudoumbilica</i>
DA	0.83–1.18	0.2	T <i>A. ingens</i>
DB	5.2–6.4	2.2	T <i>C. vulnificus</i>
DC	6.4–6.8	2.45	T <i>C. insignis</i>
DD	6.8–7.2	2.8	T <i>N. interfrigidaria</i>
DE	7.2–10.0	3.1	T <i>N. praeinterfrigidaria</i>
DF	18.0–19.2	3.8	B <i>C. kolbei</i>
DG	19.2–25.5	4.1	B <i>N. angulata</i>
DI	39.8–40.2	5.5–6.0	T <i>C. i. triangularis</i> , <i>N. mirabilis</i> , etc.
DK	109.2–118.7	15.0	B <i>D. hyalina</i>
D1	31.6–32.5	>4.5	T <i>D. hustedtii</i>
D2	61.7–71.2	10.0	T common <i>D. dimorpha</i>
D3	90.2–99.7	11.8	T common <i>D. denticuloides</i>
D4	99.7–109.2	13.8	B common <i>D. hustedtii</i> T <i>N. grossepunctata</i>
D5	99.7–109.2	12.5	B <i>D. dimorpha</i> , <i>D. praedimorpha</i>
D6	109.2–118.7	16.0	B <i>N. grossepunctata</i>
D7	137.7–147.2	16.7	B <i>D. maccollumii</i>
D8	147.2–156.7	18.8	B <i>N. maleinterpretaria</i>
R1	1.5–2.56	1.2	LAD <i>A. cylindrica</i>
R2	5.68–7.18	1.6	LAD <i>C. pliocenica</i>
R3	5.68–7.18	1.9	LAD <i>E. calvertense</i>
R4	5.68–7.18	2.4	LAD <i>H. vema</i>
R5	7.18–8.68	2.4	LAD <i>D. spongiosa</i>
R6	7.18–8.68	2.6	FAD <i>C. davisiana</i>
R7	18.18–19.68	3.2	LAD <i>P. titan</i>
R8	27.68–29.18	4.2	FAD <i>H. vema</i>
R9	37.18–38.68	4.4	LCO <i>L. grande</i>
R10	42.7–45.18	5.4	LAD <i>C. spongothorax</i>
R11	65.68–68.68	9	FAD multishell <i>Collo. sp.</i>
R12	71.2–76.68	9.7	FAD <i>E. pseudoinflatum</i>
R13	84.68–90.2	10.4	LAD <i>A. golownin</i>
R14	98.68–99.7	12.3	FAD <i>C. spongothorax</i>
R15	109.2–111.68	13.4	FAD <i>A. golownini</i>
R16	>166.2	23	FAD <i>C. tetrapera</i>
M1	54.4–57.2	8.92	T 5
M3	114.0	16.22	T 5C
M4	123.2	16.98	B 5C
M5	132.7	17.57	T 5D
M6	152.1	18.56	T 5E
M7	36.7	4.57	T Gilbert "c"
M8	40.2	4.77	B Gilbert "c"
M9	42.6	5.35	T 3A
M10	48.5	5.89	B 3A
M11	50.6	6.37	T Chron 6N
M12	109.55	14.8	T 5B
M13	108.	12.1	B 5A

Note: Events in column 1 are numbered within each fossil group (F = planktonic foraminifer, N = calcareous nannofossil, D = diatom, and R = radiolarian). Paleomagnetic reversal boundaries are designated by M. B = Bottom of datum range and T = top of datum range. For sources of age and depth information, see "Explanatory Notes" chapter (this volume) and "Biostratigraphy" and "Paleomagnetism" sections (this chapter). FAD = first appearance datum; LAD = last appearance datum.

### Index Properties

Index properties measured at Site 751 were determined from gravimetric data using a Penta pycnometer and a Scientec balance. Samples were dried using a Labconco freeze-dry apparatus. Values of wet- and dry-bulk density, grain density, water content, and porosity were determined for each sample. These

results are summarized in Table 8 and Figure 17. Additional carbonate samples were analyzed to supplement the profile generated by the Leg 120 organic geochemist (see "Organic Geochemistry" section, this chapter). These additional samples helped increase the resolution of the carbonate profile between 80 and 130 mbsf and aided in our interpretation of the physical properties results. A lack of time prevented carbonate analysis on all of the index properties samples.

The fluctuations in index properties are largely the result of the changing dominance of calcareous (grain density = 2.65–2.75 g/cm<sup>3</sup>) or siliceous (grain density = 2.00–2.40 g/cm<sup>3</sup>) microfossil skeletons in this pelagic environment. The relative shifts in carbonate/siliceous productivity and/or preservation are evident in the fine-scale variation in index properties downhole. Changes in carbonate content are largely mirrored by fluctuations in the percentage of biogenic silica in the cores.

The major lithologic boundary at Site 751 was located at ~40 mbsf where there was a dramatic shift from siliceous-dominated (lithologic Unit I) to calcareous-dominated (lithologic Unit II) sediment (see "Lithostratigraphy and Sedimentology" section, this chapter). The profiles of wet- and dry-bulk density and grain density all show the same relative shift to increasing values. The magnitude of this change is between 0.4 and 0.6 g/cm<sup>3</sup> for all three density measurements. A decrease in porosity (85.5%–65.8%) and water content (70.7%–43.7%) over the interval from 38.0 to ~44.0 mbsf corresponds to this lithologic boundary. Biostratigraphic evidence places the Miocene/Pliocene boundary somewhere between 40 and 55 mbsf across this lithologic change. There are many small-scale shifts in the dominant sedimentary components below this major shift.

Biostratigraphic and geochemical analysis should significantly contribute to our knowledge of the timing and duration of these fluctuations as well as to their possible paleoceanographic significance. Of particular note is the decrease in water content and porosity accompanied by an increase in grain and wet- and dry-bulk densities at ~109–110 mbsf, which corresponds to a biostratigraphic proposed hiatus of 3.5 m.y. at this same depth (see "Biostratigraphy" section, this chapter). The physical properties specialists on Leg 114 described similar changes in physical properties when documenting proposed hiatuses at Sites 699 and 701.

### Compressional Wave Velocity

Compressional wave velocity was determined by continuous and discrete methods (Table 9). Continuous values of *P*-wave velocity were obtained using the PWL, which consists of transducers mounted on the GRAPE unit, whereas discrete *P*-wave velocities were obtained using the Hamilton Frame Velocimeter. The Hamilton Frame was used to measure discrete samples from the working half of the core. The methods used for obtaining these measurements are discussed in the "Explanatory Notes" chapter (this volume). The direction of propagation is generally perpendicular to the split face of the core, although some samples are tested at other orientations, using the Hamilton Frame, to investigate anisotropy in various lithologies.

Compressional wave velocities were generally between 1500 and 1600 m/s in Hole 751A (Fig. 18). A lower Pliocene porcellanite, cored at the base of Core 120-751A-2H, gave a velocity of 3100 m/s. The presence of porcellanite at this shallow depth is anomalous. This type of porcellanite has previously been identified in an *Eltanin* core from the Kerguelen Plateau (Wise and Weaver, 1974), and from the Maud Rise in the Weddell Sea during Leg 113 (Barker and Kennett, 1988). The increase in velocity for the porcellanite is accompanied by an increased wet-bulk density to 1.81 g/cm<sup>3</sup>. Velocity values below the porcellanite horizon are generally of the same magnitude as above, averaging 1550–1585 m/s.

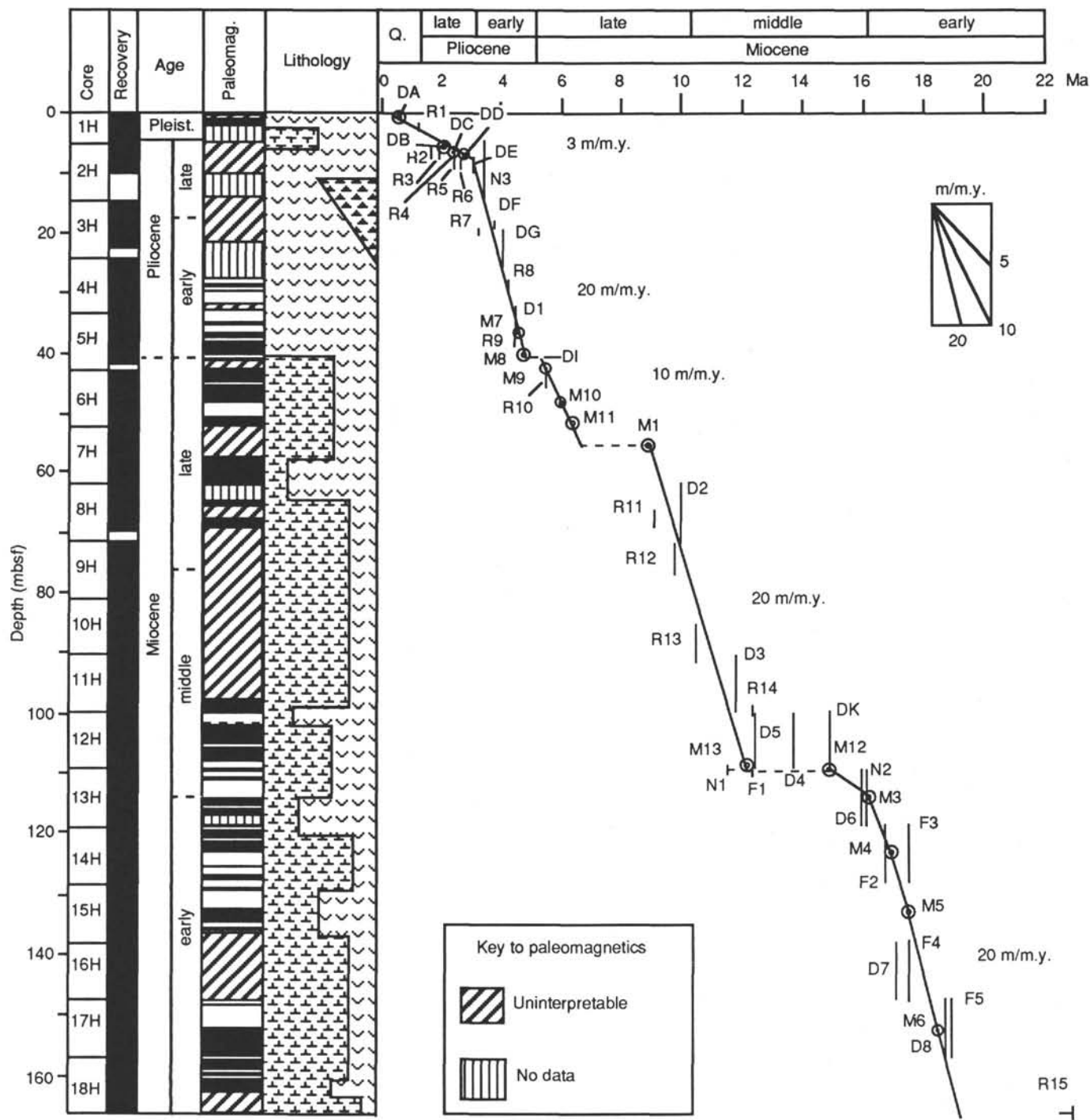


Figure 14. Age vs. depth curve for Site 751, showing sedimentation rates. Age was determined as described in the text. The biostratigraphic data is from "Biostratigraphy" section (this chapter), the paleomagnetic data from "Paleomagnetism" section (this chapter). For an explanation of the lithologic column symbols, see "Lithostratigraphy and Sedimentology" section (this chapter) and "Explanatory Notes" chapter (this volume). The time scale (horizontal axis) is explained in "Explanatory Notes" chapter (this volume). Biostratigraphic and magnetostratigraphic datum levels (e.g., "N12," "F6," "M3," etc.) are from Table 5, which gives age, depth, and name of each datum. Depth uncertainty in the placement of datum levels is shown by vertical lines, uncertainty in age calibration by horizontal lines, and uncertainties in both depth and age by hollow boxes. Bull's-eye symbols are used for datum levels with depth and/or age uncertainties too small to be visible on plot. Solid line segments of age-depth curve denote continuous sedimentation; dashed lines denote hiatuses. The average rate of sedimentation is shown for major segments of the age-depth curve between hiatuses. For additional details and discussion, see text.

**Table 6. Interstitial water chemical data, Site 751.**

Core, section, interval (cm)	Depth (mbsf)	Vol. (cm <sup>3</sup> )	pH	Alk. (mM)	Sal. (g/kg)	Mg <sup>2+</sup> (mM)	Ca <sup>2+</sup> (mM)	Cl <sup>-</sup> (mM)	SO <sub>4</sub> <sup>2-</sup> (mM)	SiO <sub>2</sub> (μm)	Mg <sup>2+</sup> /Ca <sup>2+</sup>
120-751A-											
3H-2, 140-150	17.10	85	7.50	3.053	35.8	54.16	10.79	555.00	28.44	707	5.02
6H-5, 145-150	50.15	45	7.45	3.079	36.0	50.01	13.03	559.00	26.38	852	3.84
9H-4, 145-150	77.15	46	7.49	3.275	36.1	51.53	11.98	563.00	27.08	835	4.30
12H-5, 145-150	107.15	50	7.39	3.495	35.5	44.48	13.83	557.00	26.33	913	3.22
15H-5, 145-150	135.65	42	7.43	3.240	35.5	47.88	14.27	564.00	25.06	872	3.36
18H-4, 145-150	162.65	45	7.44	3.521	36.0	47.57	15.15	567.00	25.12	961	3.14

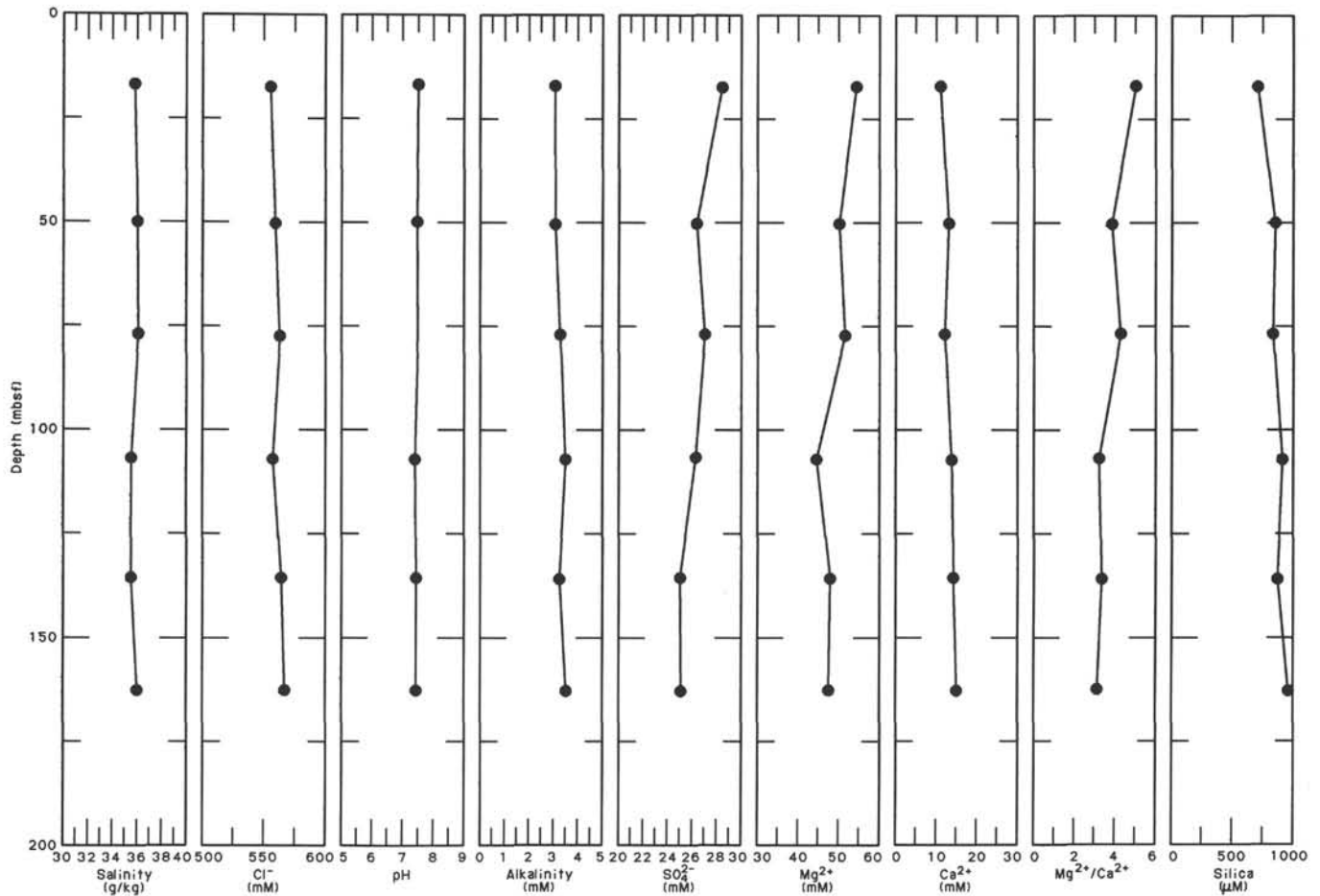


Figure 15. Summary of interstitial water analyses, Site 751, as a function of depth.

A small velocity inversion is seen below 40 mbsf (Table 9). This decrease in velocity to average values of ~1540 m/s coincides with the change from dominantly siliceous sediment containing opaline microfossil skeletons to sediment that is dominantly calcareous. The transition to lithologic Unit II shows a corresponding increase in wet-bulk density to ~1.6 g/cm<sup>3</sup> (see Fig. 18) and a decrease in porosity and water content. Velocity values downhole exhibit a large degree of scatter due to changes in relative concentrations of carbonate and silica (see Fig. 18).

Zones of higher velocity values generally correlate with low carbonate contents and corresponding high siliceous concentrations. This relationship of high velocity with low carbonate content is controlled by the density differences between siliceous and carbonate components and the tendency of siliceous microfossil skeletons to form a strong interlocking sediment fabric.

The frequency of discrete velocity measurements decreased downhole (below ~55 mbsf) due to the demands of processing other samples in a timely fashion.

### Undrained Shear Strength

Undrained shear strength ( $S_u$ ) was measured using a Wykeham Farrance Motorized Vane shear device. The shear strengths determined for Unit I and II are generally less than 30 kPa to ~100 mbsf. There is some scatter in the shear strengths at 30-40 and 50 mbsf, respectively. These fluctuations are likely due to small changes in water content. The overall trend that is revealed in the data is one of increasing shear strength with decreasing wet-bulk density and increasing water content. This is an anomalous situation that has been observed in other regions of siliceous sedimentation. An explanation for this phenome-

**Table 7. Total carbon, inorganic carbon and organic carbon, and weight percent calcium carbonate of samples from Hole 751A.**

Core, section, interval (cm)	Depth (mbsf)	Total carbon (%)	Inorganic carbon (%)	Organic carbon (%)	CaCO <sub>3</sub> (%)
120-751A-					
1H-1, 70-72	0.70	1.56	1.32	0.24	11.0
1H-2, 48-50	1.98		1.83		15.2
1H-3, 30-32	3.30		8.56		71.3
2H-2, 70-72	6.90	3.74	3.74	0	31.2
2H-3, 70-72	8.40		4.23		35.2
2H-4, 30-32	9.50		0.17		1.4
3H-1, 70-72	14.90		0.08		0.7
3H-2, 70-72	16.40	0.16	0.05	0.11	0.4
3H-3, 70-72	17.90		0.10		0.8
3H-4, 70-72	19.40		1.57		13.1
3H-5, 70-72	20.90		1.34		11.2
4H-2, 110-112	26.30	0.14	0.01	0.13	0.1
4H-3, 67-69	27.37		0.02		0.2
4H-4, 67-69	28.87		0.03		0.3
4H-5, 67-69	30.37		2.84		23.7
4H-6, 70-72	31.90	0.09	0.02	0.07	0.2
5H-1, 70-72	33.90		0.02		0.2
5H-2, 70-72	35.40		0.01		0.1
5H-3, 70-72	36.90		0.01		0.1
5H-4, 70-72	38.40	0.10	0.01	0.09	0.1
5H-5, 70-72	39.90		0.01		0.1
5H-6, 30-32	41.00		8.94		74.5
6H-1, 70-72	43.40		8.05		67.1
6H-2, 70-72	44.90	7.60	7.22	0.38	60.1
6H-3, 70-72	46.40		8.55		71.2
6H-4, 70-72	47.90		8.97		74.7
6H-5, 70-72	49.40		8.19		68.2
6H-6, 70-72	50.90	8.08	7.69	0.39	64.1
7H-2, 70-72	54.40		9.47		78.9
7H-3, 70-72	55.90		10.02		83.5
7H-4, 70-72	57.40		9.79		81.6
7H-5, 70-72	58.90	9.29	8.95	0.34	74.6
7H-6, 70-72	60.40		10.28		85.6
7H-7, 30-32	61.50		9.19		76.6
8H-3, 70-72	65.40		8.31		69.2
8H-4, 70-72	66.90	5.15	5.04	0.11	42.0
8H-5, 70-72	68.40		5.08		42.3
9H-1, 70-72	71.90		8.29		69.1
9H-2, 70-72	73.40	6.20	6.13	0.07	51.1
9H-3, 70-72	74.90		6.66		55.0
9H-4, 70-72	76.40		9.58		79.8
9H-5, 70-72	77.90		9.20		76.6
9H-6, 70-72	79.40		8.33		69.4
9H-7, 70-72	80.90	8.69	8.38	0.31	69.8
10H-1, 70-72	81.40		9.60		80.0
10H-2, 70-72	82.90		9.51		79.2
10H-3, 70-72	84.40		10.15		84.6
10H-4, 70-72	85.90	8.94	8.73	0.21	72.7
10H-5, 70-72	87.40		9.62		80.1
11H-1, 70-72	90.90		9.61		80.1
11H-2, 70-72	92.40		10.32		86.0
11H-3, 70-72	93.90	10.56	10.47	0.09	87.2
11H-4, 70-72	95.40		9.30		77.5
11H-5, 70-72	96.90		9.63		80.2
11H-6, 70-72	98.40		8.68		72.3
12H-1, 70-72	100.40	5.20	5.15	0.05	42.9
12H-2, 70-72	101.90		5.61		46.7
12H-3, 70-72	103.40		8.08		67.3
12H-4, 70-72	104.90		7.89		65.7
12H-5, 70-72	106.40	8.44	8.35	0.09	69.6
12H-6, 70-72	107.90		7.03		58.6
13H-1, 70-72	109.90		8.95		74.6
13H-2, 70-72	111.40		7.02		58.5
13H-3, 70-72	112.90		10.03		83.6
13H-4, 70-72	114.40		5.44		45.3
13H-5, 70-72	115.90		10.93		91.1
14H-3, 70-72	122.40		10.03		83.6
14H-4, 70-72	123.90	10.82	10.50	0.32	87.5
14H-5, 70-72	125.40		8.51		70.9
14H-7, 70-72	128.40		7.35		61.2
15H-2, 87-89	130.57		8.56		71.3
15H-3, 70-72	131.90	8.89	8.89	0	74.1
15H-4, 70-72	133.40		10.16		84.6

**Table 7 (continued).**

Core, section, interval (cm)	Depth (mbsf)	Total carbon (%)	Inorganic carbon (%)	Organic carbon (%)	CaCO <sub>3</sub> (%)
120-751A- (Cont.)					
15H-5, 70-72	134.90		10.19		84.9
15H-6, 70-72	136.40		10.25		85.4
16H-1, 70-72	138.40	10.47	10.32	0.15	86.0
16H-2, 70-72	139.90		10.27		85.6
16H-3, 70-72	141.40		11.02		91.8
16H-4, 70-72	142.90		10.83		90.2
16H-5, 70-72	144.40	10.92	10.92	0	91.0
16H-6, 70-72	145.90		10.51		87.6
17H-2, 70-72	149.40		10.58		88.1
17H-5, 70-72	153.90		10.61		88.4
17H-6, 70-72	155.40	9.77	9.71	0.06	80.9
18H-1, 70-72	157.40		9.37		78.1
18H-2, 70-72	158.90		10.10		84.1
18H-3, 70-72	160.40		11.15		92.9
18H-4, 70-72	161.90		9.71		80.9

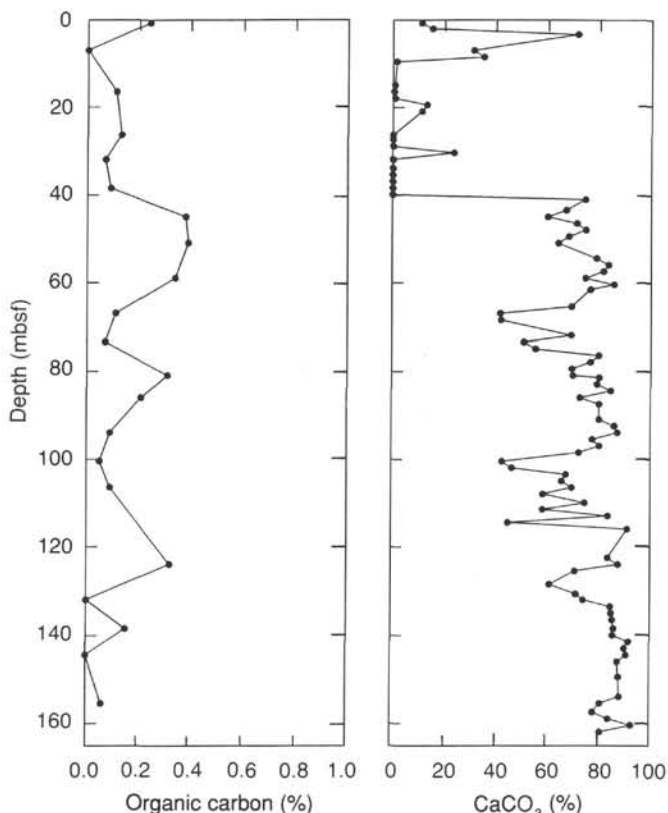


**Figure 16. Total organic carbon and carbonate contents plotted vs. depth, Site 751.**

non seems to be the ability of mixed siliceous and nannofossil oozes to develop a strong sedimentary fabric that resists shearing stresses (Bryant et al., 1981).

Abrupt increases in shear strength are noted at 98.96 and 114.5 mbsf where wet-bulk density values decrease significantly (see Fig. 19 and Table 10). The large increase in undrained shear strength at 114.5 mbsf seems to correspond with the stratigraphic location of a sedimentary hiatus (~3.5 m.y.) proposed by the initial magnetostratigraphic and biostratigraphic results at Site

Table 8. Index properties data, Site 751.

Core, section, interval (cm)	Depth (mbsf)	Water content (%)	Porosity (%)	Wet-bulk density (g/cm <sup>3</sup> )	Dry-bulk density (g/cm <sup>3</sup> )	Grain density (g/cm <sup>3</sup> )
120-751A-						
1H-1, 30	0.30	73.36	86.15	1.21	0.32	2.24
1H-1, 70	0.70	64.66	78.67	1.27	0.45	2.01
1H-1, 115	1.15	71.49	85.16	1.24	0.35	2.28
1H-2, 30	1.80	71.94	83.05	1.19	0.33	1.89
1H-2, 48	1.98	60.94	76.98	1.30	0.51	2.15
1H-3, 30	3.30	48.88	70.98	1.49	0.76	2.58
2H-1, 115	5.85	54.92	75.11	1.41	0.64	2.50
2H-2, 30	6.50	64.69	80.16	1.27	0.45	2.21
2H-2, 70	6.90	66.17	82.75	1.30	0.44	2.45
2H-2, 115	7.35	58.03	74.66	1.35	0.57	2.14
2H-3, 30	8.00	78.65	89.44	1.18	0.25	2.27
2H-3, 70	8.40	60.57	76.24	1.32	0.52	2.09
2H-3, 115	8.85	75.18	87.67	1.17	0.29	2.33
2H-4, 30	9.50	81.84	91.50	1.12	0.20	2.34
3H-1, 20	14.40	20.18	35.11	1.81	1.45	2.17
3H-1, 70	14.90	72.79	86.11	1.22	0.33	2.30
3H-1, 115	15.35	75.25	86.80	1.21	0.30	2.14
3H-2, 30	16.00	69.84	81.44	1.21	0.37	1.88
3H-2, 70	16.40	69.29	83.87	1.24	0.38	2.30
3H-2, 115	16.85	69.83	83.56	1.25	0.38	2.19
3H-3, 70	17.90	68.15	77.77	1.17	0.37	1.61
3H-3, 115	18.35	69.40	84.35	1.25	0.38	2.37
3H-4, 30	19.00	65.21	77.93	1.23	0.43	1.88
3H-4, 70	19.40	67.78	82.55	1.25	0.40	2.24
3H-4, 115	19.85	70.85	83.12	1.21	0.35	2.01
3H-5, 30	20.50	72.04	83.53	1.17	0.33	1.95
3H-5, 70	20.90	70.04	83.95	1.23	0.37	2.23
3H-5, 115	21.35	72.28	83.90	1.22	0.34	1.98
4H-2, 110	26.30	69.14	83.79	1.25	0.39	2.30
4H-3, 30	27.00	77.68	87.19	1.19	0.27	1.92
4H-3, 67	27.37	77.81	87.88	1.15	0.26	2.03
4H-3, 113	27.83	68.29	82.38	1.24	0.39	2.16
4H-4, 30	28.50	74.77	87.23	1.21	0.31	2.29
4H-4, 67	28.87	68.94	83.86	1.24	0.38	2.34
4H-4, 112	29.32	65.25	79.84	1.26	0.44	2.11
4H-5, 30	30.00	68.44	83.76	1.26	0.40	2.37
4H-5, 67	30.37	60.18	78.41	1.29	0.51	2.41
4H-5, 113	30.83	73.05	88.10	1.28	0.35	2.72
4H-6, 30	31.50	69.08	82.49	1.23	0.38	2.10
4H-6, 70	31.90	68.23	81.59	1.25	0.40	2.05
4H-6, 113	32.33	74.97	85.32	1.18	0.29	1.91
5H-1, 30	33.50	70.82	83.58	1.20	0.35	2.08
5H-1, 70	33.90	81.57	90.57	1.17	0.22	2.12
5H-1, 115	34.35	72.03	86.71	1.23	0.34	2.52
5H-2, 30	35.00	74.83	86.87	1.20	0.30	2.20
5H-2, 70	35.40	68.18	82.13	1.23	0.39	2.14
5H-2, 115	35.85	68.55	83.60	1.30	0.41	2.34
5H-3, 30	36.50	68.39	83.16	1.24	0.39	2.28
5H-3, 70	36.90	69.24	81.79	1.22	0.37	1.98
5H-3, 115	37.35	67.16	81.27	1.24	0.41	2.12
5H-4, 30	38.00	70.65	85.51	1.24	0.36	2.44
5H-4, 70	38.40	65.91	81.88	1.29	0.44	2.34
5H-4, 115	38.85	64.47	79.21	1.26	0.45	2.10
5H-5, 30	39.50	61.86	77.92	1.30	0.50	2.18
5H-5, 70	39.90	56.81	71.91	1.27	0.55	1.95
5H-5, 115	40.35	48.00	69.37	1.49	0.77	2.48
5H-6, 30	41.00	44.86	67.14	1.57	0.87	2.54
6H-1, 70	43.40	43.73	66.46	1.57	0.89	2.58
6H-1, 115	43.85	43.12	65.82	1.62	0.92	2.57
6H-2, 30	44.50	47.13	68.85	1.50	0.80	2.50
6H-2, 70	44.90	48.02	70.83	1.52	0.79	2.65
6H-2, 115	45.35	42.47	66.23	1.61	0.92	2.69
6H-3, 30	46.00	43.02	65.87	1.55	0.89	2.58
6H-3, 70	46.40	44.06	65.76	1.59	0.89	2.46
6H-3, 115	46.85	45.38	66.08	1.48	0.81	2.37
6H-4, 30	47.50	43.98	67.00	1.56	0.87	2.61
6H-4, 70	47.90	43.54	65.98	1.57	0.89	2.54
6H-4, 115	48.35	42.16	65.52	1.60	0.93	2.64
6H-5, 30	49.00	40.20	63.40	1.62	0.97	2.61
6H-5, 70	49.40	46.29	67.84	1.51	0.81	2.47
6H-5, 115	49.85	47.59	69.43	1.50	0.79	2.52
6H-6, 30	50.50	46.12	68.12	1.54	0.83	2.52
6H-6, 70	50.90	47.62	69.45	1.52	0.80	2.52
6H-6, 115	51.35	43.34	66.33	1.65	0.94	2.60
6H-7, 30	52.00	45.84	69.41	1.51	0.82	2.71
7H-2, 30	54.00	42.74	64.93	1.59	0.91	2.51
7H-2, 70	54.40	43.96	68.19	1.62	0.91	2.76
7H-2, 115	54.85	41.18	64.55	1.65	0.97	2.63
7H-3, 30	55.50	40.61	64.78	1.66	0.99	2.72
7H-3, 70	55.90	39.63	62.91	1.63	0.98	2.61
7H-3, 115	56.35	37.05	59.91	1.69	1.06	2.57
7H-4, 30	57.00	40.76	63.20	1.63	0.97	2.52
7H-4, 70	57.40	42.27	67.10	1.66	0.96	2.82
7H-4, 115	57.85	41.91	65.06	1.67	0.97	2.61

Table 8 (continued).

Core, section, interval (cm)	Depth (mbsf)	Water content (%)	Porosity (%)	Wet-bulk density (g/cm <sup>3</sup> )	Dry-bulk density (g/cm <sup>3</sup> )	Grain density (g/cm <sup>3</sup> )
120-751A- (Cont.)						
7H-5, 30	58.50	42.82	66.33	1.59	0.91	2.66
7H-5, 70	58.90	43.63	65.00	1.55	0.87	2.42
7H-5, 115	59.35	41.39	63.83	1.61	0.94	2.53
7H-6, 30	60.00	37.88	62.72	1.70	1.05	2.79
7H-6, 70	60.40	35.76	60.02	1.76	1.13	2.73
7H-6, 115	60.85	46.20	68.07	1.52	0.82	2.51
7H-7, 30	61.50	46.84	68.31	1.51	0.80	2.47
8H-3, 30	65.00	52.62	72.84	1.47	0.70	2.43
8H-3, 70	65.40	49.09	70.92	1.49	0.76	2.55
8H-3, 115	65.85	50.47	71.71	1.49	0.74	2.51
8H-4, 30	66.50	49.46	70.36	1.46	0.74	2.45
8H-4, 70	66.90	56.95	74.75	1.37	0.59	2.25
8H-4, 115	67.35	51.81	72.14	1.46	0.70	2.43
8H-5, 30	68.00	53.93	71.49	1.38	0.64	2.15
8H-5, 70	68.40	54.98	73.24	1.40	0.63	2.25
8H-5, 115	68.85	51.12	71.32	1.54	0.75	2.40
8H-6, 30	69.50	53.62	73.55	1.43	0.67	2.42
9H-1, 30	71.50	52.96	74.24	1.44	0.68	2.58
9H-1, 70	71.90	49.02	71.39	1.48	0.75	2.62
9H-1, 115	72.35	48.83	70.12	1.47	0.75	2.48
9H-2, 30	73.00	50.78	71.48	1.47	0.72	2.45
9H-2, 70	73.40	54.81	74.17	1.43	0.65	2.38
9H-2, 115	73.85	52.81	71.99	1.44	0.68	2.31
9H-3, 30	74.50	54.21	73.96	1.39	0.64	2.42
9H-3, 70	74.90	51.49	71.03	1.45	0.70	2.33
9H-3, 115	75.35	47.18	69.06	1.54	0.81	2.52
9H-4, 30	76.00	47.84	70.60	1.53	0.80	2.65
9H-4, 70	76.40	40.21	63.18	1.66	0.99	2.58
9H-4, 115	76.85	42.23	65.81	1.59	0.92	2.66
9H-5, 30	77.50	42.85	65.36	1.58	0.90	2.54
9H-5, 70	77.90	44.26	67.27	1.58	0.88	2.62
9H-5, 115	78.35	44.43	66.25	1.58	0.88	2.48
9H-6, 30	79.00	48.12	70.46	1.54	0.80	2.60
9H-6, 70	79.40	46.31	68.97	1.51	0.81	2.60
9H-6, 115	79.85	47.30	68.90	1.53	0.81	2.49
9H-7, 30	80.50	0.89	3.85	1.54	1.52	4.57
9H-7, 70	80.90	46.37	70.08	1.56	0.84	2.74
10H-1, 70	81.40	41.31	63.55	1.65	0.97	2.50
10H-1, 115	81.85	42.60	65.99	1.60	0.92	2.64
10H-2, 30	82.50	41.82	64.94	1.61	0.94	2.61
10H-2, 70	82.90	45.36	68.23	1.61	0.88	2.61
10H-2, 115	83.35	43.37	66.84	1.57	0.89	2.66
10H-3, 30	84.00	42.42	65.88	1.58	0.91	2.65
10H-3, 70	84.40	38.17	61.36	1.68	1.04	2.60
10H-3, 115	84.85	40.12	64.36	1.64	0.98	2.73
10H-4, 30	85.50	45.88	67.46	1.55	0.84	2.47
10H-4, 70	85.90	46.89	68.95	1.53	0.81	2.54
10H-4, 115	86.35	43.14	67.15	1.60	0.91	2.73
10H-5, 30	87.00	41.75	65.35	1.64	0.95	2.66
10H-5, 70	87.40	44.52	67.55	1.57	0.87	2.62
10H-5, 115	87.85	39.98	63.02	1.63	0.98	2.59
10H-6, 30	88.50	42.60	66.07	1.63	0.94	2.65
10H-6, 70	88.90	44.97	68.61	1.57	0.87	2.70
10H-6, 115	89.35	41.12	62.20	1.56	0.92	2.38
10H-7, 30	90.00	41.53	65.73	1.61	0.94	2.73
11H-1, 30	90.50	43.23	66.66	1.60	0.91	2.66
11H-1, 70	90.90	44.08	67.40	1.60	0.89	2.65
11H-1, 115	91.35	38.11	61.29	1.67	1.03	2.60
11H-2, 30	92.00	38.98	63.25	1.71	1.04	2.73
11H-2, 70	92.40	39.63	62.78	1.65	1.00	2.60
11H-2, 115	92.85	37.17	59.88	1.71	1.07	2.55
11H-3, 30	93.50	37.98	63.05	1.72	1.07	2.82
11H-3, 70	93.90	39.40	63.48	1.64	0.99	2.71
11H-3, 115	94.35	37.79	60.65	1.66	1.03	2.57
11H-4, 30	95.00	42.43	66.04	1.63	0.94	2.67
11H-4, 70	95.40	42.27	64.94	1.61	0.93	2.56
11H-4, 115	95.85	45.89	68.80	1.56	0.84	2.63
11H-4, 135	96.05	54.15	72.68	1.40	0.64	2.27
11H-5, 30	96.50	47.71	68.04	1.48	0.77	2.35
11H-5, 70	96.90	42.27	64.64	1.58	0.91	2.52
11H-5, 115	97.35	41.42	64.46	1.63	0.95	2.59
11H-6, 30	98.00	48.07	68.48	1.50	0.78	2.37
11H-6, 70	98.40	45.65	67.78	1.54	0.84	2.53
11H-6, 115	98.85	47.76	68.99			

Table 8 (continued).

Core, section, interval (cm)	Depth (mbsf)	Water content (%)	Porosity (%)	Wet-bulk density (g/cm <sup>3</sup> )	Dry-bulk density (g/cm <sup>3</sup> )	Grain density (g/cm <sup>3</sup> )
120-751A- (Cont.)						
12H-4, 30	104.50	41.78	64.32	1.60	0.93	2.54
12H-4, 70	104.90	40.62	63.14	1.65	0.98	2.53
12H-4, 115	105.35	40.29	63.36	1.65	0.98	2.59
12H-5, 30	106.00	40.78	63.29	1.61	0.95	2.53
12H-5, 70	106.40	39.60	63.02	1.67	1.01	2.63
12H-5, 115	106.85	45.20	66.94	1.54	0.84	2.48
12H-6, 30	107.50	46.03	67.82	1.55	0.83	2.50
12H-6, 70	107.90	43.73	65.50	1.59	0.89	2.47
12H-6, 115	108.35	45.95	67.75	1.47	0.79	2.50
12H-7, 30	109.00	53.81	73.15	1.39	0.64	2.35
13H-1, 70	109.90	41.68	68.67	1.74	1.02	3.11
13H-1, 115	110.35	13.80	30.39	1.13	0.98	2.77
13H-2, 30	111.00	38.25	61.93	1.70	1.05	2.66
13H-2, 70	111.40	48.11	70.00	1.55	0.80	2.54
13H-2, 115	111.85	38.51	61.33	1.69	1.04	2.56
13H-3, 30	112.50	33.59	57.80	1.82	1.21	2.74
13H-3, 70	112.90	34.74	59.71	1.83	1.19	2.82
13H-3, 115	113.35	34.93	58.72	1.77	1.15	2.69
13H-4, 30	114.00	35.99	59.85	1.74	1.11	2.69
13H-4, 70	114.40	51.15	71.59	1.46	0.71	2.43
13H-4, 115	114.85	65.60	77.35	1.24	0.43	1.78
13H-5, 30	115.50	33.89	57.74	1.82	1.20	2.70
13H-5, 70	115.90	36.18	59.44	1.76	1.12	2.62
13H-6, 30	117.00	34.82	60.39	1.84	1.20	2.89
14H-1, 130	120.00	56.81	74.24	1.37	0.59	2.20
14H-2, 30	120.50	36.25	59.69	1.72	1.10	2.64
14H-2, 70	120.90	35.22	59.30	1.74	1.12	2.71
14H-2, 115	121.35	36.65	61.04	1.75	1.11	2.74
14H-3, 30	122.00	34.71	59.36	1.77	1.16	2.78
14H-3, 70	122.40	37.51	61.45	1.68	1.05	2.69
14H-3, 130	123.00	35.51	58.80	1.73	1.12	2.63
14H-4, 30	123.50	34.58	59.44	1.78	1.16	2.81
14H-4, 70	123.90	38.03	61.91	1.71	1.06	2.68
14H-4, 115	124.35	37.85	62.00	1.68	1.05	2.71
14H-5, 30	125.00	35.90	58.09	1.70	1.09	2.51
14H-5, 70	125.40	40.80	63.26	1.62	0.96	2.53
14H-5, 130	126.00	43.44	66.72	1.62	0.91	2.64
14H-6, 30	126.50	45.85	69.25	1.55	0.84	2.69
14H-6, 70	126.90	46.37	70.50	1.55	0.83	2.79
14H-7, 30	128.00	51.51	72.61	1.48	0.72	2.52
14H-7, 70	128.40	45.00	67.17	1.55	0.85	2.53
15H-1, 30	128.50	45.16	65.75	1.54	0.85	2.55
15H-1, 70	128.90	42.94	65.68	1.58	0.90	2.57
15H-1, 115	129.35	43.48	66.69	1.60	0.90	2.63
15H-2, 30	130.00	39.28	62.49	1.64	1.00	2.61
15H-2, 87	130.57	37.99	61.29	1.67	1.03	2.62
15H-2, 115	130.85	41.80	65.97	1.65	0.96	2.73
15H-3, 30	131.50	42.55	66.11	1.62	0.93	2.66
15H-3, 70	131.90	41.31	64.29	1.60	0.94	2.59
15H-3, 115	132.35	40.44	64.69	1.63	0.97	2.73
15H-4, 30	133.00	40.55	63.59	1.65	0.98	2.59
15H-4, 70	133.40	39.75	63.41	1.66	1.00	2.66
15H-4, 115	133.85	36.37	60.57	1.76	1.12	2.72
15H-5, 30	134.50	40.21	63.91	1.65	0.99	2.67
15H-5, 70	134.90	40.39	63.75	1.63	0.97	2.63
15H-5, 115	135.35	38.97	63.71	1.68	1.03	2.78
15H-6, 30	136.00	37.23	60.66	1.72	1.08	2.63
15H-6, 70	136.40	39.14	61.74	1.66	1.01	2.54
15H-6, 115	136.85	38.86	62.65	1.68	1.03	2.67
16H-1, 30	138.00	40.40	65.24	1.69	1.01	2.80
16H-1, 70	138.40	40.36	64.66	1.67	1.00	2.74
16H-1, 115	138.85	41.37	64.46	1.62	0.95	2.60
16H-2, 30	139.50	38.84	61.54	1.65	1.01	2.55
16H-2, 70	139.90	41.93	63.98	1.60	0.93	2.49
16H-2, 115	140.35	37.50	61.62	1.68	1.05	2.71
16H-3, 30	141.00	37.65	60.48	1.69	1.05	2.57
16H-3, 70	141.40	38.29	62.57	1.73	1.07	2.73
16H-3, 115	141.85	37.60	60.86	1.71	1.07	2.61
16H-4, 30	142.50	37.26	61.24	1.72	1.08	2.69
16H-4, 70	142.90	37.77	62.30	1.72	1.07	2.76
16H-4, 115	143.35	36.22	59.57	1.74	1.11	2.63
16H-5, 30	144.00	37.14	63.21	1.76	1.10	2.95
16H-5, 70	144.40	40.25	63.18	1.68	1.00	2.58
16H-5, 115	144.85	36.72	60.77	1.71	1.08	2.70
16H-6, 30	145.50	37.38	61.34	1.70	1.07	2.69
16H-6, 70	145.90	38.66	62.67	1.71	1.05	2.70
16H-6, 115	146.35	36.97	61.16	1.72	1.09	2.72
16H-7, 30	147.00	37.90	60.14	1.67	1.04	2.50
16H-7, 70	147.40	37.97	61.77	1.70	1.06	2.67
17H-1, 30	147.50	38.31	62.73	1.72	1.06	2.74
17H-2, 30	149.00	36.62	60.72	1.72	1.09	2.71
17H-2, 70	149.40	38.55	62.20	1.68	1.03	2.66
17H-2, 115	149.85	38.21	62.53	1.72	1.06	2.73
17H-3, 30	150.50	41.88	64.74	1.59	0.93	2.58

Table 8 (continued).

Core, section, interval (cm)	Depth (mbsf)	Water content (%)	Porosity (%)	Wet-bulk density (g/cm <sup>3</sup> )	Dry-bulk density (g/cm <sup>3</sup> )	Grain density (g/cm <sup>3</sup> )
120-751A- (Cont.)						
17H-3, 70	150.90	41.02	64.97	1.66	0.98	2.70
17H-3, 115	151.35	40.63	64.02	1.61	0.96	2.63
17H-4, 115	152.85	44.67	67.46	1.56	0.86	2.60
17H-5, 30	153.50	40.31	64.48	1.67	1.00	2.72
17H-5, 70	153.90	38.80	62.87	1.69	1.03	2.70
17H-5, 115	154.35	37.45	60.28	1.71	1.07	2.57
17H-6, 30	155.00	43.90	66.93	1.61	0.90	2.61
17H-6, 70	155.40	42.83	67.43	1.64	0.94	2.80
17H-6, 115	155.85	42.38	64.18	1.65	0.95	2.46
17H-7, 30	156.50	40.06	62.04	1.65	0.99	2.47
18H-1, 30	157.00	43.65	68.18	1.63	0.92	2.80
18H-1, 70	157.40	43.49	66.76	1.59	0.90	2.64
18H-1, 115	157.85	43.12	66.19	1.58	0.90	2.61
18H-2, 30	158.50	44.25	66.06	1.61	0.90	2.48
18H-2, 70	158.90	42.72	65.11	1.62	0.93	2.53
18H-2, 115	159.35	41.07	64.80	1.67	0.99	2.67
18H-3, 30	160.00	40.79	65.20	1.67	0.99	2.75
18H-3, 70	160.40	37.97	62.15	1.74	1.08	2.72
18H-3, 115	160.85	45.57	68.48	1.56	0.85	2.62
18H-4, 30	161.50	39.52	61.68	1.66	1.00	2.49
18H-4, 70	161.90	40.83	64.41	1.67	0.99	2.65
18H-4, 115	162.35	38.59	62.32	1.67	1.02	2.66
18H-5, 30	163.00	39.46	62.91	1.66	1.01	2.63
18H-5, 70	163.40	48.75	70.77	1.51	0.77	2.57
18H-5, 115	163.85	39.42	62.56	1.66	1.01	2.60
18H-6, 30	164.50	45.17	67.42	1.60	0.88	2.54

751 (see "Biostratigraphy" and "Paleomagnetism" sections, this chapter). Carbonate content decreases abruptly at the approximate depths of major shear strength increases (see Fig. 20). These decreases in carbonate content seem to correlate with increases in water content (see Fig. 20). This pattern may correspond to erosion, the dissolution and nondeposition of carbonate sediments, or their dilution by increasing amounts of siliceous microfossils at these depth intervals.

Keller and Barron (1987) have discussed the paleodepth distribution of Miocene and early Pliocene hiatuses as they reflect surface productivity patterns and the distribution of deep and intermediate water masses. The examination of microfossil assemblage changes across these zones of increased shear strength, when combined with other post-cruise work, should help define the paleoceanographic conditions responsible for causing these abrupt changes.

#### GRAPE and P-Wave Logger

The GRAPE and PWL provide a semicontinuous record of wet-bulk density and compressional wave velocity, respectively. These two instruments take closely spaced measurements, parallel to bedding, through the plastic core liner of the whole-round APC core sections. Continuous measurements are compared with discrete measurements of wet-bulk density and compressional wave velocity, respectively, to evaluate the accuracy of the results (see Figs. 21 and 22).

Compressional wave velocities measured from discrete samples are consistently higher than the continuous values obtained from the PWL. Discrete gravimetric bulk densities are generally lower than the corresponding continuous GRAPE measurements. The discrepancy in the GRAPE values may correspond to the low grain density of siliceous oozes (2.02 g/cm<sup>3</sup>), which are much less than the 2.75 g/cm<sup>3</sup> value assumed in the GRAPE calculations. These profiles will require post-cruise adjustments to remove this systematic error.

The amount of information contained in these continuous profiles is potentially useful for high-resolution studies. The resolution of the continuous GRAPE and PWL measurements, for the interval from 50 to 150 mbsf, is on the order of about 2

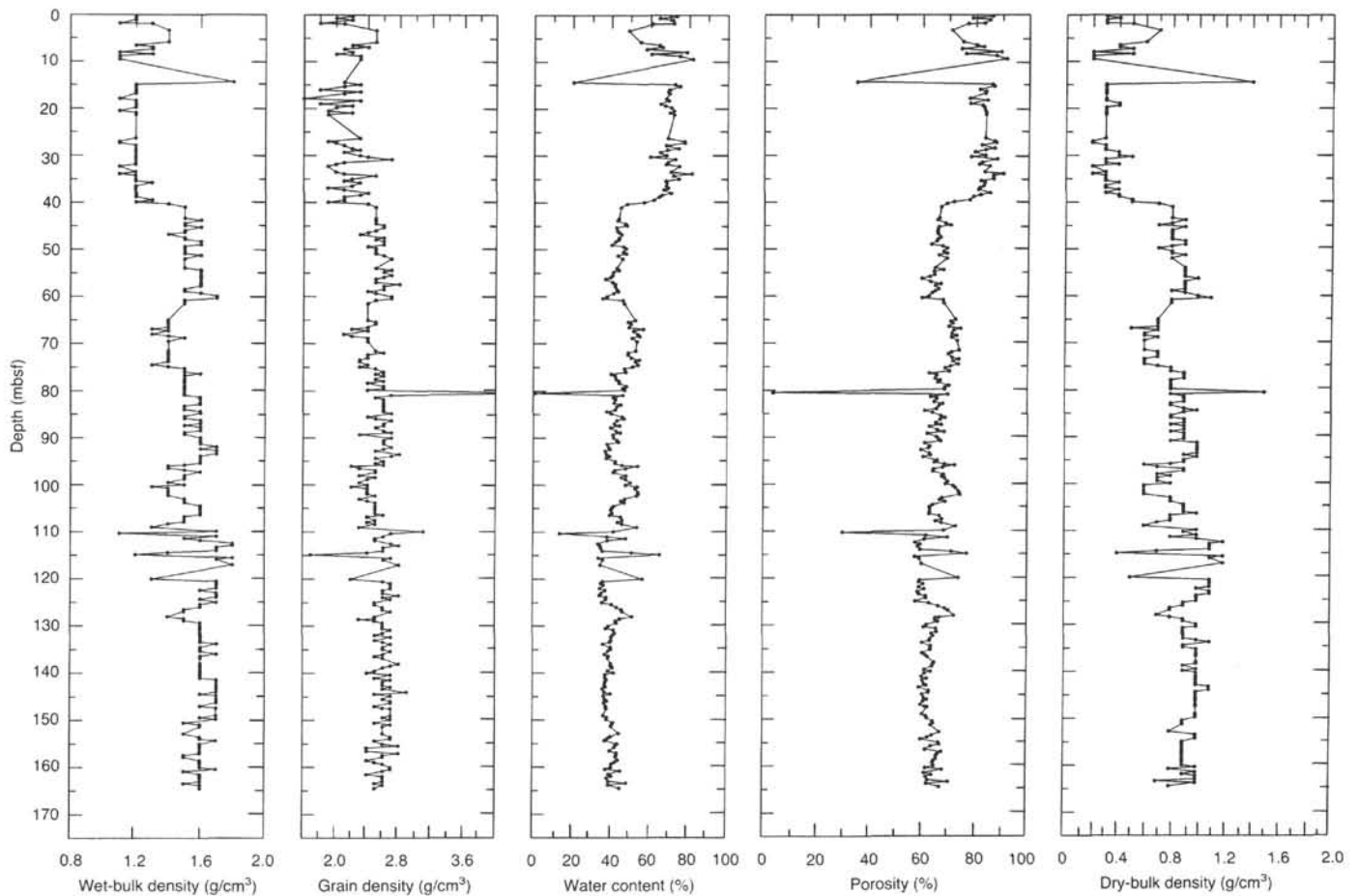


Figure 17. Downhole changes in index properties (wet-bulk density, grain density, water content, porosity, and dry-bulk density) at Site 751.

cm/data point for recovered APC core sections (see Fig. 23). Gaps in the PWL data set may result from poor contact between the sonic transducers and the core liner, incomplete filling of the core liner with sediment, or from missing core sections in the continuous sequence.

### Conclusions

The physical properties program at Site 751 resulted in a high-resolution sequence of discrete and continuous measurements that should provide detailed information for paleoceanographic and climatic studies. The periodic changes from siliceous- to calcareous-dominated lithologies are evident in fluctuations in index properties, undrained shear strength, and sonic velocities.

If one accepts that fluctuations in water masses, paleoproductivity, microfossil preservation, and climate are recorded by the downhole changes in physical properties, then this record should contain valuable information regarding the dynamic history of pelagic sedimentation on the Southern Kerguelen Plateau. Post-cruise analysis of this data set, when combined with the results of biostratigraphic, geochemical, and sedimentologic information, will contribute to an integrated, coherent picture of Neogene events as recorded at this site.

### SEISMIC STRATIGRAPHY

The basement at Site 751 in the central part of the Raggatt Basin (Figs. 2 and 7) is characterized by a weakly defined reflector, which can be traced at 1.76 s TWT below seafloor. At Site

751 the seismic profile (MD47-05) is dominated by a major reflector at a depth of 0.88 s TWT below seafloor, which corresponds to the boundary between Sequences P2 and P1; this reflector separates the upper and lower megasequences (see "Site Geophysics" section, this chapter).

The upper megasequence contains two clear reflectors: from top to bottom the first lies at 0.24 s TWT and corresponds to the boundary between Sequences NQ1 and PN1; the second, at 0.37 s TWT, corresponds to the boundary between Sequences PN1 and P2. Other reflectors at 0.99, 1.11, and 1.52 s TWT in the lower megasequence were mostly deduced from seismic stratigraphy studies and will not be discussed in this section since drilling was restricted to the Neogene sedimentary section.

Site 751 was continuously cored down to a depth of 166.2 mbsf. Two lithologic units were distinguished (see "Lithostratigraphy and Sedimentology" section, this chapter). Unit I consists of 40.1 m of upper Pleistocene to lower Pliocene diatom ooze with minor components of IRD, volcanic ash, and porcellanitic chert. Unit II consists of 126.1 m of upper to lower Miocene siliceous diatom ooze alternating with calcareous nannofossil ooze. The index physical properties and compressional wave velocity values show clear changes at a depth of about 40 mbsf at the boundary between the two units.

The mean velocity for lithologic Unit I is 1.56 km/s and 1.54 km/s for lithologic Unit II. The corresponding seismic data do not indicate a correlation of the lithologic subdivision or identified hiatuses with specific reflectors. The interpreted seismic section (*Marion Dufresne* MD47-05) at Site 751 is given in Figure 24.

**Table 9. Compressional wave velocity measured using the Hamilton Frame, Site 751.**

Core, section interval (cm)	Depth (mbsf)	DIR	Velocity (m/s)
120-751A-			
1H-1, 30	0.30	C	1536.3
1H-1, 70	0.70	C	1538.7
1H-1, 115	1.15	C	1551.3
1H-2, 30	1.80	C	1568.8
1H-2, 48	1.98	C	1575.1
1H-3, 30	3.30	C	1575.3
2H-1, 115	5.85	C	1573.9
2H-2, 30	6.50	C	1553.3
2H-2, 70	6.90	C	1531.0
2H-2, 115	7.35	C	1537.8
2H-3, 30	8.00	C	1528.8
2H-3, 70	8.40	C	1510.4
2H-3, 115	8.85	C	1542.4
2H-4, 30	9.50	C	1536.1
3H-1, 20	14.40	C	3111.6
3H-1, 70	14.90	C	1550.7
3H-1, 115	15.35	C	1560.5
3H-2, 30	16.00	C	1574.3
3H-2, 70	16.40	C	1567.7
3H-2, 115	16.85	A	1559.1
3H-3, 115	18.35	A	1531.8
3H-4, 30	19.00	C	1567.3
3H-4, 70	19.40	C	1583.4
3H-4, 115	19.85	C	1572.6
3H-5, 30	20.50	C	1545.8
3H-5, 70	20.90	C	1571.8
3H-5, 115	21.35	C	1572.7
4H-2, 111	26.31	C	1564.2
4H-3, 31	27.01	C	1604.3
4H-3, 68	27.38	C	1568.3
4H-3, 114	27.84	A	1562.7
4H-4, 31	28.51	C	1585.1
4H-4, 68	28.88	C	1582.9
4H-4, 113	29.33	C	1540.3
4H-5, 31	30.01	C	1595.5
4H-5, 68	30.38	C	1551.8
4H-5, 114	30.84	C	1575.0
4H-6, 31	31.51	C	1583.7
4H-6, 71	31.91	A	1557.3
4H-6, 114	32.34	C	1586.3
5H-1, 30	33.50	C	1546.9
5H-1, 70	33.90	C	1525.2
5H-1, 115	34.35	C	1552.5
5H-2, 30	35.00	C	1523.7
5H-2, 70	35.40	C	1566.8
5H-2, 115	35.85	A	1540.9
5H-3, 30	36.50	C	1588.9
5H-3, 70	36.90	C	1565.9
5H-3, 115	37.35	C	1587.6
5H-4, 30	38.00	C	1596.3
5H-4, 70	38.40	C	1590.8
5H-4, 115	38.85	C	1587.0
5H-5, 30	39.50	C	1578.2
5H-5, 70	39.90	C	1612.7
5H-5, 115	40.35	C	1587.2
5H-6, 30	41.00	C	1578.1
6H-1, 70	43.40	C	1549.6
6H-1, 115	43.85	C	1571.7
6H-2, 30	44.50	C	1570.4
6H-2, 70	44.90	C	1606.1
6H-2, 115	45.35	C	1569.2
6H-3, 30	46.00	C	1568.8
6H-3, 70	46.40	C	1540.4
6H-3, 115	46.85	C	1542.9
6H-4, 30	47.50	C	1564.9
6H-4, 70	47.90	C	1541.8
6H-4, 115	48.35	C	1552.4
6H-5, 30	49.00	C	1563.6
6H-5, 70	49.40	C	1561.9
6H-5, 115	49.85	C	1547.9
6H-6, 30	50.50	C	1553.8
6H-6, 70	50.90	C	1561.0
6H-6, 115	51.35	C	1545.6
6H-7, 30	52.00	C	1550.1

**Table 9 (continued).**

Core, section interval (cm)	Depth (mbsf)	DIR	Velocity (m/s)
120-751A- (cont.)			
7H-2, 70	54.40	C	1546.6
7H-4, 70	57.40	C	1522.4
7H-6, 70	60.40	C	1557.1
8H-3, 70	65.40	C	1533.6
8H-5, 70	68.40	C	1560.0
9H-2, 70	73.40	C	1538.6
9H-4, 70	76.40	C	1553.4
9H-6, 30	79.00	C	1533.1
10H-2, 70	82.90	C	1529.2
10H-2, 70	82.90	C	1534.2
10H-4, 70	85.90	C	1490.4
10H-6, 70	88.90	C	1527.8
11H-2, 115	92.85	A	1529.1
11H-4, 115	95.85	C	1553.8
11H-4, 135	96.05	A	1489.5
11H-4, 135	96.05	C	1504.8
11H-6, 70	98.40	C	1531.1
11H-6, 70	98.40	C	1531.1
11H-6, 115	98.85	A	1525.6
11H-6, 115	98.85	C	1507.8
11H-7, 30	99.50	C	1554.9
12H-1, 70	100.40	C	1568.5
12H-3, 70	103.40	C	1545.6
12H-5, 70	106.40	C	1563.5
13H-2, 70	111.40	C	1569.9
13H-4, 70	114.40	C	1597.1
14H-1, 130	120.00	C	1545.2
14H-3, 130	123.00	C	1520.8
14H-5, 130	126.00	C	1552.0
15H-2, 87	130.57	C	1522.7
15H-3, 70	131.90	C	1505.3
15H-4, 115	133.85	C	1528.7
15H-6, 30	136.00	C	1531.0
16H-2, 30	139.50	C	1522.4
16H-5, 115	144.85	C	1527.9
16H-6, 31	145.51	C	1525.5
17H-2, 116	149.86	C	1535.2
17H-5, 116	154.36	C	1548.4
17H-6, 116	155.86	C	1558.2
18H-2, 70	158.90	C	1562.3
18H-4, 70	161.90	C	1546.8
18H-6, 30	164.50	C	1563.3

Note: DIR = direction of propagation, A = perpendicular to bedding, and C = perpendicular to split face of core.

From the compressional wave velocity measurements, we anticipated that the first reflector at 0.24 s TWT, which corresponds to the boundary between Sequences NQ1 and PN1, would lie just below the bottom of the hole at about 185 m. Sequence NQ1 is characterized by high-amplitude reflectors with high continuity. The sequence is flat lying, thins progressively, and finally disappears in all directions by toplap along the bottom-water reflector.

The sedimentary section cored at Site 751 is much too short and cannot aid in deciphering the evolutionary history of the Southern Kerguelen Plateau. Two hiatuses in sedimentation (from 6 to 9 Ma and from 12.5 to 16 Ma) are recorded between the present and the early Miocene. The interstratification of siliceous and calcareous sediments with high sedimentation rates (15–20 m/m.y.) during most of the Miocene and the observed hiatuses are related to the high-amplitude reflectors that characterize the upper part of the seismic section close to the site. The low sedimentation rate of 3 m/m.y., recorded at this location in the central part of the Raggatt Basin during the Pliocene and Pleistocene, may be related to the main erosional event, which

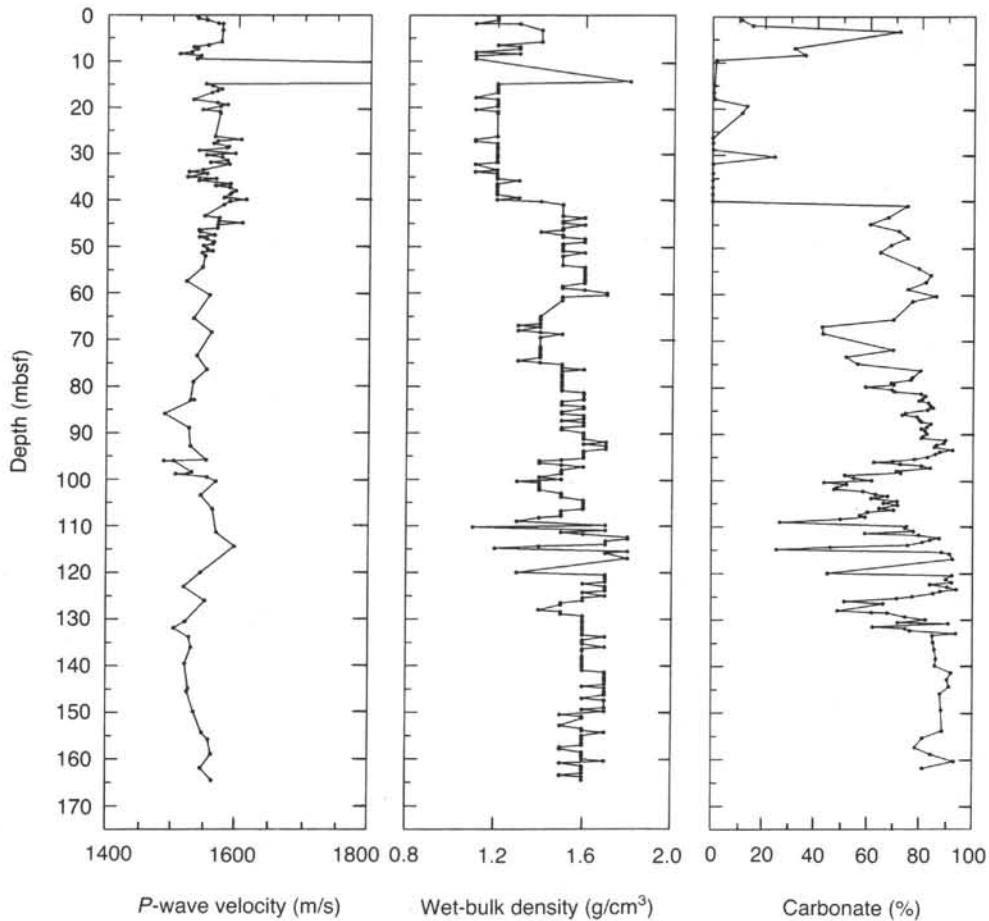


Figure 18. Comparison of compressional wave velocity (as measured with the Hamilton Frame), gravimetric wet-bulk density, and carbonate content, Site 751.

affects Sequences NQ1, PN1, and P2 all over the Southern Kerguelen Plateau.

### SUMMARY AND CONCLUSIONS

Site 751 (proposed Site SKP-2C; 57°43.56'S; 79°48.89'E; water depth, 1633.8 m) is located in the central part of the Raggatt Basin on the Southern Kerguelen Plateau. We chose this site with the intention of recovering a high-resolution Neogene and Paleogene stratigraphic section deposited above the calcium carbonate compensation depth and well south of the present-day Polar Front, which lies 900 km to the north. This site is a key component of a latitudinal paleoceanography transect across the plateau. The *Marion Dufresne* MCS line MD47-05 shows a thick sedimentary cover of at least 2500 m at this locality. Due to time constraints imposed by an unexpected mid-cruise round-trip between the Kerguelen Plateau and Fremantle, Australia, drilling at Site 751 was limited to the Neogene objective, which covers a seismic sequence of 0.24 s TWT.

A 166.2-m-thick section of upper Pleistocene through middle lower Miocene mixed biosiliceous and calcareous ooze was cored by the APC with 98% recovery. An unusual finding was an exceptionally young (early Pliocene age) porcellanite bed encountered in Core 120-751A-2H. Operations in high seas were ended when the APC piston rod failed during pullout, leaving the core barrel and the last core stuck in the hole.

The following lithologic units were recognized at Site 751:

Unit I: depth, 0–40.1 mbsf; upper Pleistocene (>0.2 Ma) to lower Pliocene; diatom ooze with minor ice-rafted debris, foraminifers, volcanic ash, and porcellanite.

The carbonate content in this unit ranges from 0% to 70%, whereas foraminifer abundance ranges from ~3%–25% near the top to rare near the bottom of the unit. Ice-rafted debris is scattered in minor abundance throughout the unit, mostly as sand-size specks. The predominantly milky white porcellanite, disturbed by drilling, fills the top 44 cm of Core 120-751A-3H and contains some burrowlike casts. Two vitric ash layers are present in the lower Pliocene sediments.

Unit II: depth, 40.1–166.2 mbsf; upper Miocene to lower Miocene; diatom nannofossil ooze.

Although nannofossils predominate, diatoms occur in equal or greater abundance in many intervals; foraminifers, radiolarians, and silicoflagellates are rare or appear in trace amounts. Faint green centimeter-scale laminae enriched in diatoms occur between 88 and 104 mbsf.

The lower Pliocene through lower Miocene represents an expanded section with sedimentation rates from 15 to 20 m/m.y., whereas much lower rates of about 3 m/m.y. characterize the abbreviated upper Pliocene–Pleistocene section. Beneath the ubiquitous erosional surface at the top, as many as four hiatuses have been detected within this part of the section. The most extensive of these can be correlated across the Raggatt Basin and spans the interval from about 12.1 to 14.8 Ma in the middle Mi-

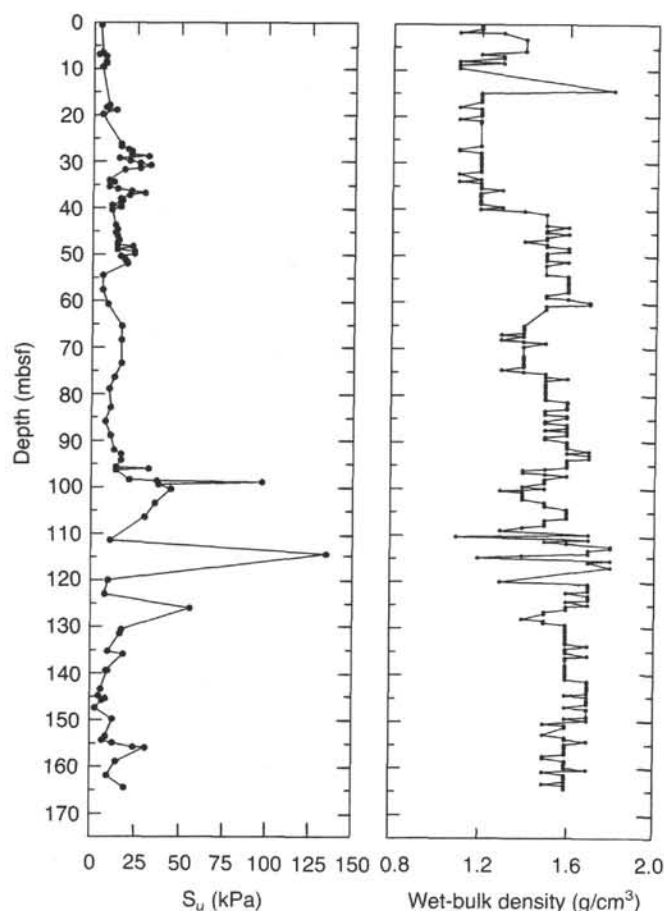


Figure 19. Undrained shear strength measured using the Wykeham-Farrance Motorized Vane device compared with gravimetric wet-bulk density at Site 751.

ocene. A second represents about 3.5 m.y. between 9.5 and 6.2 Ma in the late Miocene. A third short hiatus represents about 0.4 m.y. between 4.8 and 5.2 Ma, whereas a fourth spans an interval of some 0.3 m.y. between 1.9 and 2.2 Ma in the late Pliocene. Magnetostratigraphic data are of mixed quality, but key polarity reversals are identified in the lower Pliocene to upper Miocene (Anomaly Correlatives 3, 3A, 4, and 5) and lower Miocene (Anomaly Correlatives 5C through 6).

High biogenic silica contents in lithologic Unit I yielded low bulk densities and high porosity values relative to Unit II. Compressional wave velocity values, however, were generally higher above 45 mbsf than below this level in the nannofossil ooze (1560 m/s above vs. 1535 m/s below). The corresponding seismic data do not indicate a correlation of lithologic subdivisions or identified hiatuses with specific reflectors. From the compressional wave velocity measurements, however, it is anticipated that the first reflector at 0.24 s TWT lies just below the bottom of the hole at about 185 m and may correspond to the Oligocene/Miocene contact. If so, sedimentation rates would suggest that a disconformity could be expected at this point.

The hiatuses and low sedimentation rate recorded for the Pliocene-Pleistocene at this location in the central Raggatt Basin may be related to erosion that has affected Seismic Sequences NQ1, PN1, and P2 all over the Southern Kerguelen Plateau. Intermittent erosion from the late Miocene to the present is widespread on plateaus and similar promontories at this latitude that lie in the path of the Antarctic Circumpolar Current, which has

Table 10. Undrained shear strength ( $S_u$ ) measured with the Wykeham-Farrance Vane device, Site 751.

Core, section, interval (cm)	Depth (mbsf)	$S_u$ (kPa)
120-751A-		
1H-1, 60.0	0.60	4.3
2H-2, 30.0	6.50	5.0
2H-2, 74.0	6.94	3.9
2H-2, 115.0	7.35	7.9
2H-3, 70.0	8.40	7.0
2H-3, 91.0	8.61	7.9
2H-3, 115.0	8.85	7.2
2H-4, 30.0	9.50	5.0
3H-3, 67.0	17.87	9.1
3H-3, 110.0	18.30	7.0
3H-3, 135.0	18.55	8.1
3H-4, 26.0	18.96	13.7
3H-4, 110.0	19.80	5.0
4H-2, 107.0	26.27	16.1
4H-3, 16.0	26.86	16.1
4H-3, 70.0	27.40	20.2
4H-3, 110.0	27.80	22.9
4H-4, 30.0	28.50	22.0
4H-4, 70.0	28.90	32.1
4H-4, 115.0	29.35	15.6
4H-5, 26.0	29.96	21.6
4H-5, 76.0	30.46	27.1
4H-5, 110.0	30.80	33.5
4H-6, 35.0	31.55	27.5
4H-6, 65.0	31.85	18.4
5H-1, 80.0	34.00	9.2
5H-1, 120.0	34.40	12.8
5H-2, 76.0	35.46	9.6
5H-2, 125.0	35.95	14.2
5H-3, 24.0	36.44	22.9
5H-3, 65.0	36.85	30.3
5H-3, 110.0	37.30	21.6
5H-4, 34.0	38.04	16.1
5H-4, 78.0	38.48	17.9
5H-4, 112.0	38.82	16.5
5H-5, 22.0	39.42	11.5
5H-5, 65.0	39.85	16.1
5H-5, 126.0	40.46	11.5
6H-1, 106.0	43.76	13.3
6H-2, 40.0	44.60	14.7
6H-2, 110.0	45.30	13.3
6H-3, 36.0	46.06	14.7
6H-3, 125.0	46.95	15.1
6H-4, 35.0	47.55	14.7
6H-4, 75.0	47.95	14.2
6H-4, 110.0	48.30	23.4
6H-5, 25.0	48.95	14.7
6H-5, 75.0	49.45	24.8
6H-5, 125.0	49.95	24.3
6H-6, 25.0	50.45	16.5
6H-6, 75.0	50.95	18.8
6H-6, 125.0	51.45	19.3
6H-7, 39.0	52.09	20.2
7H-2, 81.0	54.51	6.9
7H-4, 92.0	57.62	6.9
7H-6, 108.0	60.78	9.2
8H-3, 75.0	65.45	17.9
8H-5, 75.0	68.45	17.0
9H-2, 75.0	73.45	17.9
9H-4, 75.0	76.45	13.8
9H-6, 25.0	78.95	10.6
10H-2, 75.0	82.95	11.0
10H-4, 75.0	85.95	8.7
10H-6, 75.0	88.95	11.0
11H-2, 32.0	92.02	13.3
11H-2, 125.0	92.95	17.4
11H-3, 106.0	94.26	17.4
11H-4, 109.0	95.79	14.7
11H-4, 130.0	96.00	33.0
11H-5, 19.0	96.39	14.7
11H-6, 75.0	98.45	22.0
11H-6, 90.0	98.60	38.5

Table 10 (continued).

Core, section, interval (cm)	Depth (mbsf)	S <sub>u</sub> (kPa)
120-751A- (cont.)		
11H-6, 126.0	98.96	98.6
11H-7, 20.0	99.40	39.4
12H-1, 75.0	100.45	46.8
12H-3, 75.0	103.45	37.9
12H-5, 75.0	106.45	31.9
13H-2, 75.0	111.45	11.9
13H-4, 75.0	114.45	135.1
14H-1, 135.0	120.05	10.4
14H-3, 135.0	123.05	8.2
14H-5, 135.0	126.05	57.2
15H-2, 90.0	130.60	18.8
15H-3, 30.0	131.50	17.2
15H-5, 115.0	135.35	10.3
15H-6, 21.0	135.91	19.3
16H-2, 21.0	139.41	9.1
16H-2, 25.0	139.45	10.1
16H-4, 120.0	143.40	6.2
16H-5, 118.0	144.88	5.6
16H-6, 25.0	145.45	9.9
16H-6, 68.0	145.88	7.0
16H-7, 72.0	147.42	3.3
17H-2, 110.0	149.80	13.0
17H-5, 30.0	153.50	9.5
17H-5, 110.0	154.30	7.4
17H-6, 28.0	154.98	13.0
17H-6, 118.0	155.88	25.0
17H-6, 122.0	155.92	32.1
18H-2, 75.0	158.95	15.1
18H-4, 75.0	161.95	10.6
18H-6, 35.0	164.55	20.6

been an especially vigorous current since Antarctica first became fully glaciated during the late Miocene. The effect of this current, especially of its Circumpolar Deep Water component, on such features as the Falkland Plateau has been discussed by Ciesielski and Wise (1977), Ciesielski et al. (1982), and Wise et al. (1985), among others. The role that Antarctic glaciations may have played in modulating the strength of this current is a topic of current research and debate.

The relatively high carbonate contents and high sedimentation rates for the Miocene at this site and the co-occurrence of siliceous and calcareous microfossil groups are unique for the high southern latitudes. These features will make this and other Leg 120 sites on the Kerguelen Plateau important reference sections for stable isotope and biomagnetostratigraphic studies. Changing microfossil assemblage compositions within each group indicate repeated migrations of major water mass boundaries over the site and should provide important paleobiogeographic and paleoceanographic records for this region. The most striking features of this record are the rapid meter-scale alternations in microfossil assemblage characteristics and physical and sedimentologic properties, which indicate that this site may be capturing some of the high-frequency paleoclimatic variability documented in Neogene sequences in other parts of the world's oceans.

## REFERENCES

- Barker, P. F., Kennett, J. P., et al., 1988. *Proc. ODP, Init. Repts.*, 113: College Station, TX (Ocean Drilling Program).
- Barron, J. A., Larsen, B., et al., 1989. *Proc. ODP, Init. Repts.*, 119: College Station, TX (Ocean Drilling Program).
- Berggren, W. A., Aubry, M.-P., and Hamilton, W. N., 1983. Neogene magnetobiostratigraphy of Deep Sea Drilling Project Site 516 (Rio Grande Rise, South Atlantic). *In* Barker, P. F., Dalziel, I.W.D., et al., *Init. Repts. DSDP*, 72: Washington (U.S. Government Printing Office), 676-713.
- Berggren, W. A., Kent, D. V., Flynn, J. J., and Van Couvering, J.A., 1985a. Cenozoic geochronology. *Geol. Soc. Am. Bull.*, 96:1407-1418.
- Berggren, W. A., Kent, D. V., and Van Couvering, J. A., 1985b. The Neogene: Part 2, Neogene geochronology and chronostratigraphy. *In* Snelling, N. J. (Ed.), *The Chronology of the Geological Record*. Geol. Soc. Mem. (London), 10:211-260.
- Boyce, R. E., 1976. Definitions and laboratory techniques of compressional sound velocity parameters and wet-water content, wet-bulk density, and porosity parameters by gravimetric and gamma ray attenuation techniques. *In* Schlanger, S. O., Jackson, E. D., et al., *Init. Repts. DSDP*, 33: Washington (U.S. Govt. Printing Office), 931-955.
- \_\_\_\_\_, 1977. Deep Sea Drilling Project procedures for shear strength measurement of clayey sediment using modified Wykeham-Farrance laboratory vane apparatus. *In* Barker, P. F., Dalziel, I.W.D., et al., *Init. Repts. DSDP*, 36: Washington (U.S. Govt. Printing Office), 1059-1068.
- Bryant, W. R., Bennett, R. H., and Katherman, C. F., 1981. Shear strength, consolidation, porosity, and permeability of oceanic sediments. *In* Emiliani, C. (Ed.), *The Sea* (Vol. 7): New York (Wiley), 1555-1615.
- Chen, P.-H., 1975. Antarctic radiolaria. *In* Hayes, D. E., Frakes, L. A., et al., *Init. Repts. DSDP*, 28: Washington (U.S. Govt. Printing Office), 437-513.
- Ciesielski, P. F., Kristofferson, Y., et al., 1988. *Proc. ODP, Init. Repts.*, 114: College Station, TX (Ocean Drilling Program).
- Ciesielski, P. F., Ledbetter, M. T., and Ellwood, B. B., 1982. The development of Antarctic glaciation and the Neogene paleoenvironment of the Maurice Ewing Bank. *Mar. Geol.*, 46:1-51.
- Ciesielski, P. F., and Wise, S. W., Jr., 1977. Geologic history of the Maurice Ewing Bank of the Falkland Plateau (southwest Atlantic sector of the Southern Ocean) based on piston and drill cores. *Mar. Geol.*, 25:175-207.
- Coffin, M. F., Munsch, M., Colwell, J. B., Schlich, R., Davies, H. L., and Li, Z. G., in press. Seismic stratigraphy of the Raggatt Basin, Southern Kerguelen Plateau: tectonic and paleoceanographic implications. *Geol. Soc. Am. Bull.*
- Colwell, J. B., Coffin, M. F., Pigram, C. J., Davies, H. L., Stagg, H.M.J., and Hill, P. J., 1988. Seismic stratigraphy and evolution of the Raggatt Basin, Southern Kerguelen Plateau. *Mar. Pet. Geol.*, 5: 75-81.
- Gieskes, J. M., and Peretsman, G., 1986. Water chemistry procedures on SEDCO 471—some comments. *ODP Tech. Note*, No. 5.
- Gombos, A. M., Jr., and Ciesielski, P. F., 1983. Late Eocene to early Miocene diatoms from the southwest Atlantic. *In* Ludwig, W. J., Krashennikov, V. A., et al., *Init. Repts. DSDP*, 71, Pt. 2: Washington (U.S. Govt. Printing Office), 583-634.
- Houtz, R. E., Hayes, D. E., and Markl, R. G., 1977. Kerguelen Plateau bathymetry, sediment distribution and crustal structure. *Mar. Geol.*, 25:95-130.
- Keller, G., and Barron, J. A., 1987. Paleodepth distribution of Neogene deep-sea hiatuses. *Paleoceanography*, 2:697-713.
- Lambe, T. W., and Whitman, R. V., 1969. *Soil Mechanics*: New York (Wiley).
- Leclaire, L., Bassias, Y., Denis-Clochchiatti, M., Davies, H., Gautier, I., Gensous, B., Giannesini, P. J., Patriat, P., Segoufin, J., Tesson, M., and Wannesson, J., 1987a. Lower Cretaceous basalts and sediments from the Kerguelen Plateau. *Geo-Mar. Lett.*, 7:169-176.
- Leclaire, L., Denis-Clochchiatti, M., Davies, H., Gautier, I., Gensous, B., Giannesini, P. J., Morand, F., Patriat, P., Segoufin, J., Tesson, M., and Wannesson, J., 1987b. Nature et âge du Plateau de Kerguelen-Heard, secteur sud. Résultats préliminaires de la campagne "N.A.S.K.A.-MD48". *C. R. Acad. Sci., Ser. 2*, 304:23-28.
- Mayer, L. A., 1981. Physical properties of sediment recovered on Deep Sea Drilling Project Leg 68 with the hydraulic piston corer. *In* Prell, W. L., Gardner, J. V., et al., *Init. Repts. DSDP*, 68: Washington (U.S. Govt. Printing Office), 365-382.
- Miller, K., Kahn, M. J., Aubry, M.-P., Berggren, W. A., Kent, D. V., and Melillo, A., 1985. Oligocene to Miocene bio-, magneto-, and isotope stratigraphy of the western North Atlantic. *Geology*, 13: 257-261.
- Schlich, R., 1975. Structure et âge de l'océan Indien occidental. *Mem. Hors Ser. Soc. Geol. Fr.*, 6:1-103.

- \_\_\_\_\_, 1982. The Indian Ocean: aseismic ridges, spreading centers, and oceanic basins. In Nairn, A.E.M., and Stehli, F. G. (Eds.), *The Ocean Basins and Margins: The Indian Ocean* (Vol. 6): New York (Plenum Press), 51-147.
- Schlich, R., Coffin, M. F., Munsch, M., Stagg, H.M.J., Li, Z. G., and Reville, K., 1987. *Bathymetric Chart of the Kerguelen Plateau*. [Jointly edited by Bureau of Mineral Resources, Geology and Geophysics, Canberra, Australia; Institut de Physique du Globe, Strasbourg, France; and Territoires des Terres Australes et Antarctiques Françaises, Paris, France.]
- Schlich, R., Munsch, M., Boulanger, D., Cantin, B., Coffin, M. F., Durand, J., Humler, E., Li, Z. G., Savary, J., Schaming, M., and Tissot, J. D., 1988. Résultats préliminaires de la campagne océanographique de sismique réflexion multitraces MD47 dans le domaine sud du plateau de Kerguelen. *C. R. Acad. Sci., Ser. 2*, 305:635-642.
- Schrader, H.-J., 1976. Cenozoic planktonic diatom biostratigraphy of the southern Pacific Ocean. In Hollister, C. D., Craddock, C., et al., *Init. Repts. DSDP*, 35: Washington (U.S. Govt. Printing Office), 605-671.
- Schroder, C. J., 1986. Deep-water arenaceous foraminifera in the north-west Atlantic Ocean. *Can. Tech. Rept. Hydrogr. Ocean Sci.*, No. 71.
- Tjalsma, R. C., 1974. Cenozoic foraminifera from the South Atlantic, DSDP Leg 36. In Barker, P. F., Dalziel, I.W.D., et al., *Init. Repts. DSDP*, 36: Washington (U.S. Govt. Printing Office), 493-517.
- Weaver, F. M., and Wise, S. W., Jr., 1973. Early diagenesis of a deep-sea bedded chert. *U.S. Antarctic J.*, 8:298-300.
- Wise, S. W., Jr., Gombos, A. M., and Muza, J. P., 1985. Cenozoic evolution of polar water masses, southwest Atlantic Ocean. In Hsü, K. J., and Weissert, J. H. (Eds.), *South Atlantic Paleooceanography*: Cambridge (Cambridge Univ. Press), 283-324.
- Wise, S. W., Jr., and Weaver, F. M., 1974. Certification of oceanic sediments. In Hsü, K. J. (Ed.), *Pelagic Sedimentation on Land and under the Sea*. Spec. Publ. Int. Assoc. Sediment., 1:301-326.

MS 120A-113

**NOTE: All core descriptions forms ("barrel sheets") and core photographs have been printed on coated paper and bound as Section 3 near the back of the book, beginning on page 377.**

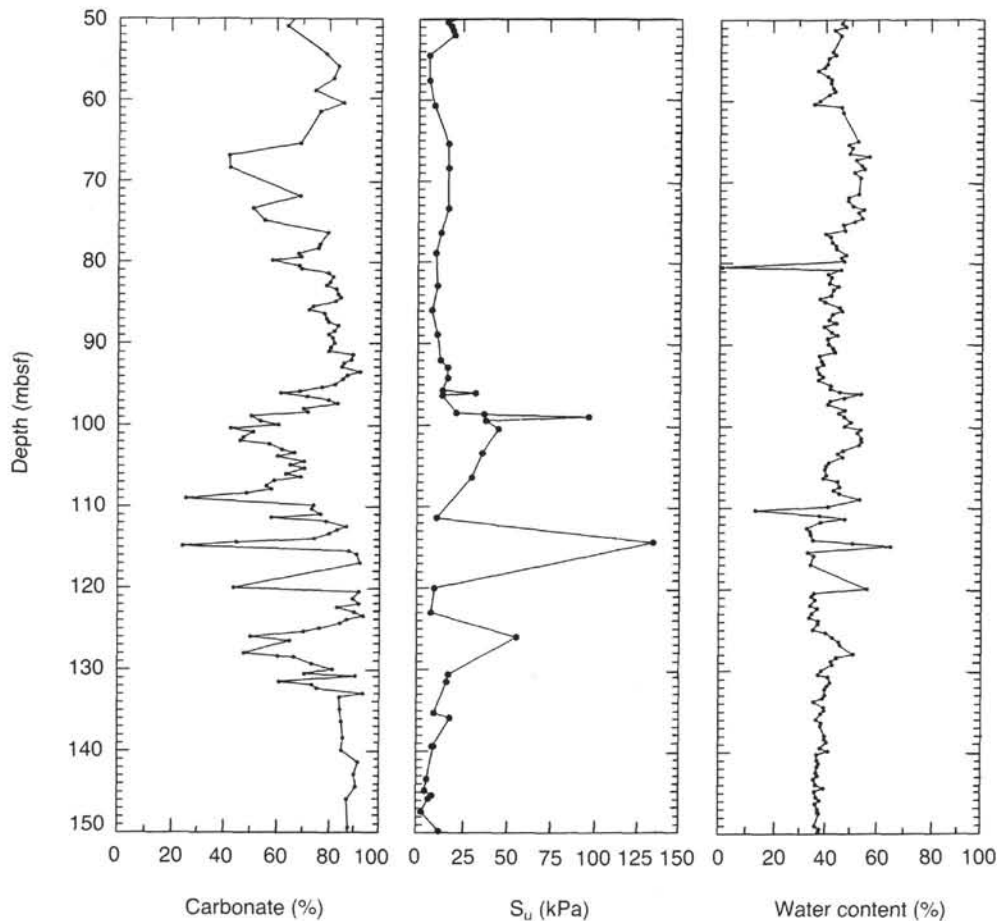


Figure 20. Comparison between carbonate content, undrained shear strength ( $S_u$ ), and water content at Site 751 (50-150 mbsf).

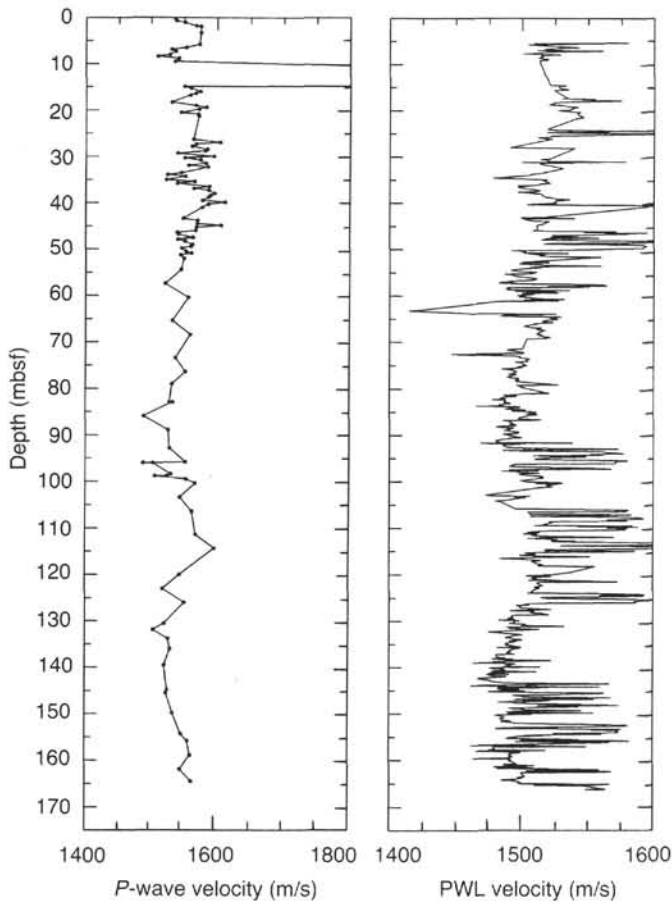


Figure 21. Comparison of discrete and continuous compressional wave velocity measurements at Site 751.

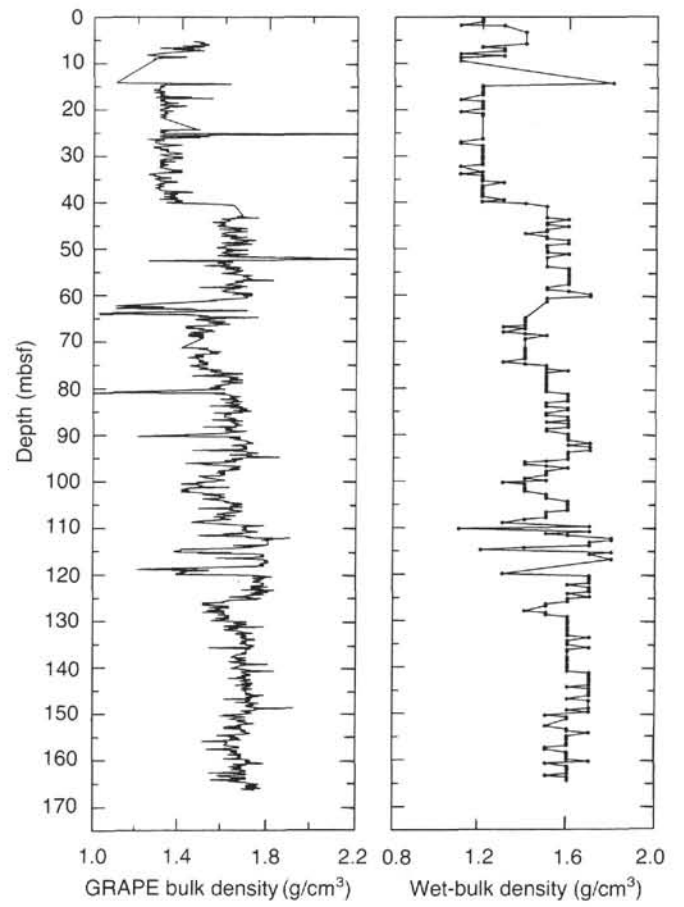


Figure 22. Comparison of GRAPE bulk density and gravimetric wet-bulk density profiles at Site 751.

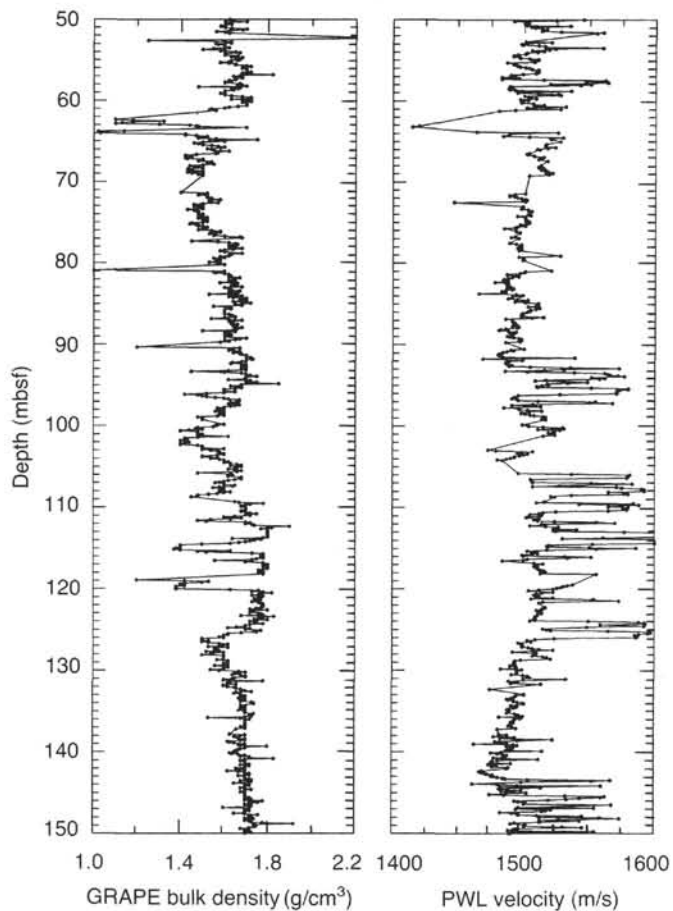


Figure 23. Downhole profiles of GRAPE bulk density and PWL compressional wave velocity at Site 751 (50–150 mbsf).

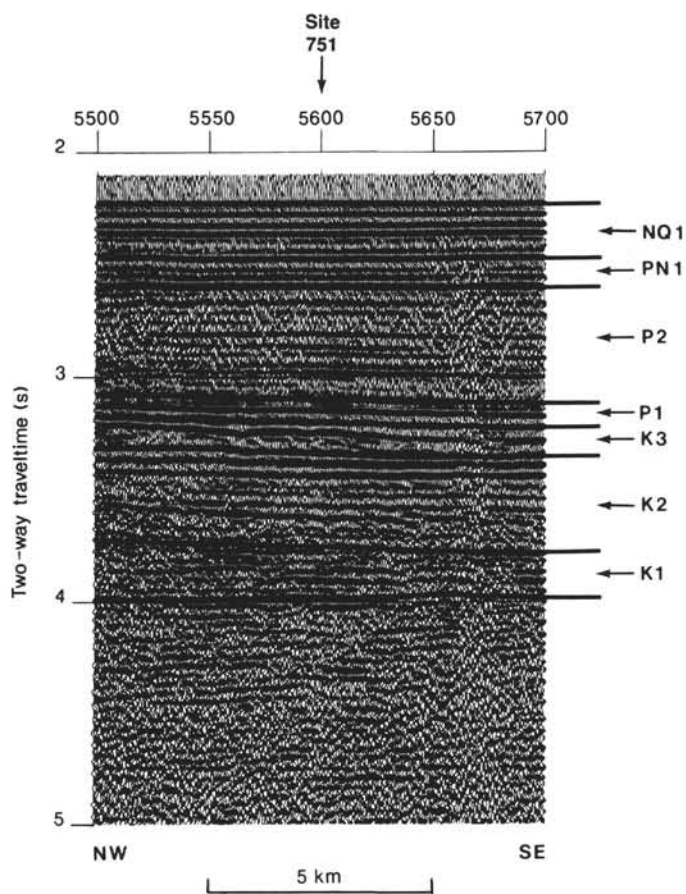


Figure 24. Interpretation of the *Marion Dufresne* (MD47-05) seismic reflection profile at Site 751. The uninterpreted seismic section is shown on Figure 7.